

Voltage Relaxation Methods for State of Charge, and State of Health Estimation in Lithium-Ion Batteries

by

David B. L. Theuerkauf

Submitted in partial fulfilment of the requirements
for the degree of Master of Applied Science

at

Dalhousie University
Halifax, Nova Scotia
August 24th 2022

© Copyright by David B. L. Theuerkauf, 2022

Table of contents

List of tables.....	4
List of figures	5
Abstract	7
List of abbreviations and symbols used	8
Acknowledgements.....	10
Chapter 1 Introduction	12
Chapter 2 Background	17
2.1. The lithium ion cell.....	17
2.1.1 Construction.....	17
2.1.2 Positive electrode	20
2.1.3 Electrolyte	22
2.1.1 Negative electrode	22
2.1.2 Solid electrolyte interphase.....	24
2.2. Performance metrics	25
2.3. State of charge estimation.....	28
2.3.1 Coulomb counting.....	28
2.3.2 Open circuit voltage.....	29
2.4. Degradation of the lithium ion cell.....	30
2.4.1 Effects on performance	30
2.4.2 Degradation causes, mechanisms, and modes	31
2.4.3 Degradation considerations.....	32
2.5. Single cycle battery models.....	32
2.5.1 Electrical models.....	33
2.5.2 Electrochemical models	34
2.5.3 Mathematical models	37
2.6. Voltage relaxation.....	38
Chapter 3 Literature review	43
3.1. Equivalent circuit model for VR	43
3.2. Electrochemical model for VR investigation	45
3.3. Mathematical model for VR investigation	46
3.4. Outcomes of literature review	47

3.4.1	Motivation for thesis objectives.....	47
3.4.2	Model architecture decision.....	48
Chapter 4	Methods.....	49
4.1.	Lithium ion cells.....	49
4.2.	Battery testing system.....	51
4.3.	Test set up.....	54
4.4.	Test schedules for first study	56
4.4.1	Reference performance test.....	56
4.4.2	Three hour voltage relaxation at 10% SOC increments.....	57
4.4.3	Twenty four hour voltage relaxation.....	58
4.5.	Test schedules for second study	58
4.5.1	Reference performance test.....	58
4.5.2	Voltage relaxation test	59
4.5.3	Degradation test	59
4.6.	Data capture.....	60
4.7.	Mathematical analysis of voltage relaxation	62
4.7.1	Novel battery model architecture and coefficient determination.....	62
4.7.2	Assessing model inaccuracy impacts on SOC and SOH	64
4.7.3	Assessing correlation of variables	66
Chapter 5	Investigation of Voltage Relaxation for Cell Parameterization	68
5.1.	Purpose	68
5.2.	Results and discussion.....	69
5.2.1	VR magnitude vs SOC.....	69
5.2.2	VR shape and SS-OCV	71
5.2.3	Model complexity	73
5.2.4	Quantifying inaccuracy impacts on SOC and SOH.....	76
5.3.	Outcome.....	77
Chapter 6	Investigation of degradation via voltage relaxation	79
6.1.	Purpose	79
6.2.	Degradation results	80
6.2.1	Capacity degradation	80
6.2.2	IR degradation.....	83
6.3.	VR results	85

6.3.1	NCA	87
6.3.2	NMC	91
6.3.3	LFP	95
6.4.	Outcomes	97
Chapter 7 Conclusions & Recommendations		99
7.1.	Outcomes from thesis objectives	99
7.2.	Findings from research questions	100
7.3.	Recommendations	100
References		102
Appendix A	Batteries journal copyright agreement	107
	Copyright and Licensing.....	107
	Reproducing Published Material from other Publishers.....	107
Appendix B	Copyright Permission.....	108
Appendix C	Cell specification sheets	111
	NCA 111	
	NMC 112	
	LFP 113	
Appendix D	Fluke 289 Calibration Sheets	114
Appendix E	Arbin Calibration Sheets	120
Appendix F	MATLAB scripts.....	124

List of tables

Table 1: Specifications of cells	50
Table 2: Arbin BT2000 specifications	51
Table 3: Reference performance test schedule	56
Table 4: Three hour voltage relaxation test schedule	57
Table 5: Twenty-four hour VR test schedule.....	58
Table 6: Internal resistance test schedule.....	58
Table 7: Degradation test schedule	59
Table 8: SOC error for various complexity of RC equivalent circuit model.....	76
Table 9: EST and RMSD for each tested chemistry and number of RC circuits in the model.....	77
Table 10: SOH for each chemistry and test set.....	80
Table 11: Results of Correlation and R^2 of VR magnitude and degradation characteristics for NCA batteries	91
Table 12: Correlation and R^2 analysis of time constants for NMC	92
Table 13: Results of Correlation and R^2 of VR magnitude and degradation characteristics for NMC batteries	94
Table 14: Correlation and R^2 of LFP VR results	97

List of figures

Figure 1: Basic cylindrical structure construction method provided from Mitch Gregory.	13
Figure 2: Example of typical degradation plots to evaluate SOH and IR growth	14
Figure 3: Cylindrical cell LIBs scaling from cells to modules to packs	15
Figure 4: Graphical representation of internal view of a lithium ion cell [9]	17
Figure 5: Full and half cell voltages vs capacity for a lithium ion battery	19
Figure 6: Example Li concentration throughout the cell on discharge	20
Figure 7: Reduction potential of various elements versus lithium reproduced with permission from [10].....	21
Figure 8: Voltage profile of a graphitic negative electrode with staging effect graphics adapted from [11]	23
Figure 9: Schematic of charge and discharge of a lithium ion battery from the perspectives of the anode and cathode. (Not real curve shapes.) Reproduced from [12].....	24
Figure 10: SEI formation reproduced from [13].....	25
Figure 11: Performance metrics graphic.....	26
Figure 12: Degradation mechanism flow chart reproduced from [18]	31
Figure 13: Equivalent circuit model of a lithium ion battery.....	34
Figure 14: Example of electrochemical model from first principles to final simulation adapted from [24].....	36
Figure 15: KiBaM graphic showing fluid equivalent battery system	37
Figure 16: Discrete Time Markov Chain of an LIB reproduced from [26]	38
Figure 17: Voltage relaxation curve labeled with points of interest, data for this curve taken from tests performed in this thesis	39
Figure 18: Curve Shape of VR shown to compare single exponential error	40
Figure 19: Voltage relaxation pictured in an electrode.....	41
Figure 20: photograph of NCA, NMC, and LFP cells used in the studies.	49
Figure 21: Calibration results of the Arbin II	52
Figure 22: Test set up for a single cell.....	54
Figure 23: 3 parallel cells test set up as a diagram (top) and photograph (bottom).....	55
Figure 24: Data flow from BTS to MATLAB analysis and summary of results.....	61
Figure 25: Standard equivalent circuit model and proposed VR-ECM of an LIB with its response to open circuit conditions	62

Figure 26: Pseudo OCV vs SOC with inset showing SOC error determination.....	66
Figure 27: Importance of correlation and R^2 for useful relationship	67
Figure 28: VR from operational profile as a function of SOC with values post discharge current shown in gray and values post charge current shown in red.....	70
Figure 29: Twenty-four Hour Relaxation shown on a linear and logarithmic scale of NMC, NCA, and LFP chemistries	72
Figure 30: Equivalent circuit model curve fit for models employing 1, 3, or 5 RC circuits, along with the overall RMSD error for models ranging from 1-6 RC circuits ...	74
Figure 31: Impact of each RC circuit in a model on the VR profile for NMC batteries for 3, 4, and 5 RC circuit models	75
Figure 32: Degradation plot of Capacity vs cycles and SOH vs cycles.....	81
Figure 33: Final RPT of the NCA battery where failure due to thermal runaway occurred.....	82
Figure 34: IR degradation results of NCA batteries for charge and discharge	83
Figure 35: IR growth on charge and discharge for NMC battery	84
Figure 36: IR growth on charge and discharge for LFP battery	84
Figure 37: VR tests for NCA cells at 100% SOH and 54.4%	86
Figure 38: Different sorting of VR results to show features, exemplified from NCA results	87
Figure 39: Modeled time constants for each RC circuit for NCA battery	88
Figure 40: VR magnitude for each RC circuit of NCA battery	89
Figure 41: VR Magnitude of NCA cells vs SOC for all tests	90
Figure 42: VR magnitude of NCA cells vs. SOH and IR	90
Figure 43: NMC time constants	92
Figure 44: NMC VR Magnitude	94
Figure 45: LFP modeled time constants	95
Figure 46: VR magnitude for LFP	96

Abstract

Lithium ion batteries are the dominant technology for energy storage, and only projected to grow as Electric Vehicles gain higher adoption rates. Monitoring of the state of charge and the degradation metrics (state of health and internal resistance growth) in lithium-ion batteries without destructive investigation is an important and difficult task. For this reason, an in-situ monitoring technique could be a useful method to determine state of charge and degradation metrics. Voltage relaxation is a method that could be such a monitoring technique.

Voltage relaxation is the process by which operational voltage changes to a steady-state open-circuit voltage after current stops flowing in a battery. There are two important metrics with voltage relaxation: magnitude and curve shape. Magnitude is amount of voltage that is relaxed, where curve shape describes how it approaches steady-state open-circuit voltage.

Two studies were performed on three popular chemistries of lithium ion-batteries with the purpose of: (1) finding a battery model to accurately curve fit voltage relaxation; (2) finding the relationships between degradation metrics and voltage relaxation metrics; (3) determine methodologies for evaluation of state of charge, state of health, and internal resistance from voltage relaxation.

A new model was adapted from the equivalent circuit model. It can estimate state of charge within 0.5% for nickel based chemistries and 2.27% for the Lithium iron phosphate (LFP) chemistry while achieving acceptable curve fit error. The studies showed that for nickel based chemistries the magnitude of voltage relaxation is a function of state of charge and has a useful relationship to degradation metrics. This means that if state of charge is known, or determined, degradation metrics can be estimated from a voltage relaxation period. Methodologies were created and trialed that used these relationships to determine the state of charge, state of health and IR from voltage relaxation periods with considerations for practical applications. Voltage relaxation in LFP batteries is a function of state of charge, but insufficient degradation was achieved to analyze degradation metrics. For this reason, further studies should include full cycle life of LFP batteries to find these relationships and determine the sensitivity required of voltage relaxation analysis of degradation metrics.

List of abbreviations and symbols used

Acronyms and abbreviations

Ah-CycEq	Amp hour cycle equivalents
BMS	Battery Management system
BOL	Beginning of life
BTS	Battery testing system
CC	Constant Current
CV	Constant Voltage
D-AhT	Discharge amp hour throughput
dV/dQ	incremental voltage incremental current
ECM	Equivalent circuit model
EOL	End of life
EST	Estimated settling time
EV	Electric Vehicle
FSR	Full scale range
IR	Internal resistance
KiBaM	Kinetic battery model
LEDC	Lithium Ethylene dicarbonate
LFP	Lithium iron phosphate
LIBS	Lithium ion battery
LMO	lithium manganese oxide
NCA	Nickel cobalt aluminium
NMC	nickel manganese cobalt
OCV	open circuit voltage
PDE	partial differential equation
RMSD	Root mean square deviation
RMSE	Root mean square error
RPT	Reference performance test
SEI	Solid electrolyte interphase
SOC	state of charge
SOH	State of health
SS-OCV	Steady state open circuit voltage
VR	voltage relaxation
VR-ECM	voltage relaxation equivalent circuit model

Symbols and constants (Units)

C	Capacitance of an RC pair in the ECM (F)
D	Number of datapoints in a data set
d	Index of the datapoint being evaluated
E_{cell}^0	Electrochemical potential of a cell (V)
E_{NE}^0	Electrochemical potential of a negative electrode (V)
E_{PE}^0	Electrochemical potential of a positive electrode (V)

R	Resistance of an RC pair in the ECM (Ω)
RMSD%	Root mean squared deviation in percentage (%)
n	Arbitrary number to indicate position in set
t	Time (s)
$V_n(\text{ECM})$	Initial voltage of an RC pair in ECM (V)
$V_n(\text{VR-ECM})$	Final voltage of an RC pair in the VR-ECM (V)
$V_{RC,n}$	The function which dictates voltage for an RC pair in the ECM (V)
V_s	Voltage of the SOC dependant voltage source in the ECM (V)
V_{terminal}	Terminal voltage of a battery (V)
\hat{V}	Expected voltage used for error analysis (V)
$VR_{\text{magnitude}}$	Voltage relaxation magnitude (V)
x	An arbitrary value from dataset x
\bar{x}	The mean of dataset x
y	An arbitrary value from dataset y
\bar{y}	The mean of dataset y
Greek letters	
Ω	Resistance (Ω)
τ	Time constant or coefficient for RC pair in the ECM (1/s)
Chemical Nomenclature	
Al	Aluminum
C	Carbon
Co	Cobalt
F	Fluorine
Fe	Iron
Li	Lithium
Mn	Manganese
O	Oxygen
P	Phosphorous

Acknowledgements

The first and most important person to acknowledge in the completion of this thesis is Dr. Lukas Swan. Without his guidance, expertise, and uncanny ability to say the most motivating words with perfect timing this thesis would not exist. He has been a role model as both an engineer and person, that I hope to compare to one day. His obsessive drive for improvement and high standards of quality has raised my capabilities over my two years in this lab. He has shown me not only how to be direct and concise with professional communication, but to be personable as well. I look back at the work we did together with a profound pride that I was able to take part in it.

I would like to thank Jaza Energy for the funding and experience I gained from working with them through a MITACs scholarship. They, as a company, embody why I started engineering and continue to pursue it: A simple goal of helping each other. Without their financial aid and professional development, I would have been unable to complete this thesis to the quality I have.

I would like to acknowledge the members of the renewable energy storage lab that I got to meet and grow with. The diverse mindsets of this superb group of people always challenged me to think differently and critically. The group truly feels like you can depend on each other for an honest assessment, be that personal or professional.

In particular, Bryan Ellis and Mitch Gregory have been exceptionally beneficial to my time in the lab. From motivating me to be in the gym for a morning workout, to destressing over lunch, to having the best arguments about inconsequential things. I could count on them to improve my day. These are friendships that I will cherish looking back at this time.

I would like to thank my family and friends who supported me each in their own way. I am lucky to have people in my life who check in, call, or visit me because they care about me. These people are who prepared and motivated me most for the hardest parts of these past two years.

Finally thank you for reading this thesis, whomever it may be.

Through this thesis process there are certain contributions that should be addressed.

1 – NSERC: NSERC provided the discovery grant that provided funding for my stipend during my 2 year thesis.

2 – MITACS and Jaza Energy: Partnering with Jaza Energy we were awarded a MITACS accelerate grant to perform research on sub-Saharan off-grid solar powered installation of LIBs. This provided additional income for the lab and increased my stipend.

3 – Mitch Gregory: Mitch Gregory was a fellow RESL member who provided the real pictures of cell deconstruction used in Figure 1.

Chapter 1 Introduction

Lithium-ion batteries (LIBs) are an established and growing technology with useful applications in diverse fields. According to the International Renewable Energy Agency, manufacturing capacity of LIBs for energy storage is set to quadruple from 2021 to 2025 from 625 GWh to 2500 GWh [1]. With a valuation of roughly 50 billion USD [2] they are a cornerstone of the energy storage market. For energy storage technologies LIBs have consistently produced over 80% of all capacity since 2015, usually accounting for over 90% [2]. One major factor is their top of class energy density, related to both volume and mass. They regularly achieve between 150 – 200 Wh/kg and 250 – 350 Wh/L [3]. This is significantly higher than any other rechargeable battery technology. Their decrease in cost over the past 20 years only adds to the motivation to use the technology. In 2000 the price was roughly 3,400 USD/kWh, while in 2019 the price was 156 USD/kWh. This is still set to lower as the technology continues to mature [4]. For these reasons LIBs are often the only reasonable choice for many applications.

There are 3 mass market construction methods for LIBs: pouch, cylindrical, and prismatic. All cell construction methods operate under the same principles with sizing, capacity rating and thermal management being the main differences. In this thesis only cylindrical cells are used. For a cylindrical cell, the contents are rolled into a spiral called a jelly roll and put into a rigid metal cylindrical casing as shown in Figure 1. This casing acts as the negative terminal, with a cap that acts as the positive terminal for the cell.

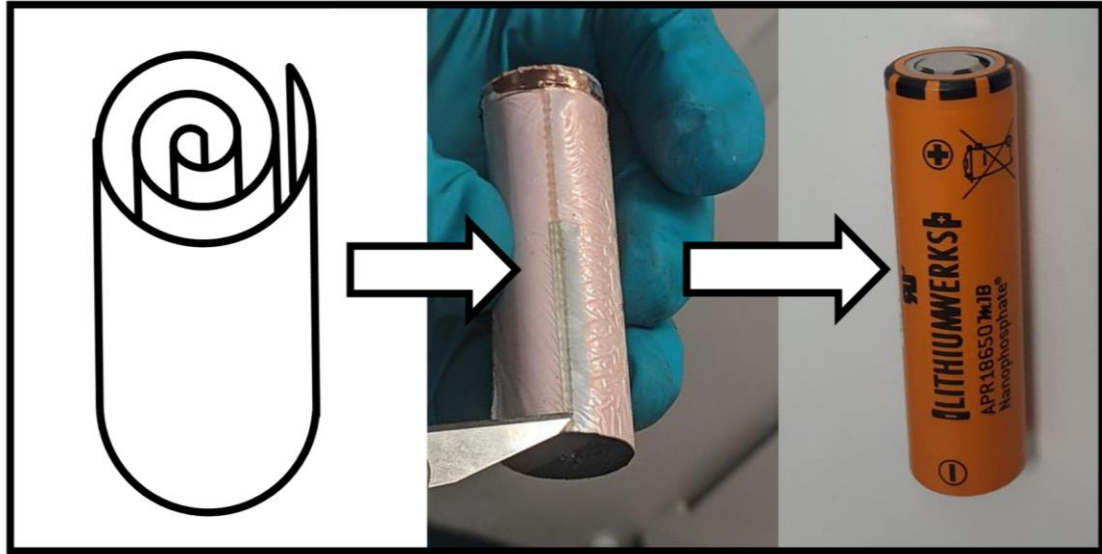


Figure 1: Basic cylindrical structure construction method provided from Mitch Gregory.

Once constructed, the cell can not be taken apart without rendering the battery inoperable. Meaning that all monitoring of the cell must come from external measurements such as temperature, or electrical properties such as voltage. This limitation is the one of the motivating factors for the work performed in this thesis, using an in-situ method to determine metrics for an LIB.

Two important metrics for LIBs are State of charge (SOC) and State of health (SOH). SOC is a cycle-based metric for how much useful capacity is remaining until the battery can not output energy. SOH is a lifetime-based metric for the current total capacity of the battery compared to its highest achieved total capacity. Therefore, a battery that is rated at 1 Ah which can deliver 0.95 Ah is at 95% SOH. SOC is a cycle based metric where SOH is a lifetime based metric. As the battery wears through cycling and calendar ageing the maximum capacity will decrease, thus lowering the SOH; this is one of the effects of degradation.

Degradation is the process by which the capacity of the battery decreases over time and the internal resistance (IR) grows. Lower capacity means the battery has less useful energy. Higher IR results in more heat generation, lower efficiency, and lower power capability. These degradation metrics can be used as health indications of the battery. SOH is more commonly monitored than IR growth as energy out is often the most useful property of the

battery. For different applications the SOH value that is considered end of life (EOL) can vary. Most commonly, and specifically for electric vehicles (EVs), the value of 80% SOH is used [5] [6]. SOH is important to view against the cycle count of the battery to determine how quickly it is degrading. When batteries are used in real world applications, they are rarely cycled consistently between 100% and 0% SOC. Therefore, number of charge and discharge cycles is a poor metric as it is specific to the operation of the battery. SOH should be compared to equivalent cycles based on nominal capacity (Ah-CycEq), how many times has the rated capacity been discharged from the battery. There is always a negative correlation between SOH and Ah-CycEq. This is shown next to an example of IR growth as a degradation metric in Figure 2.

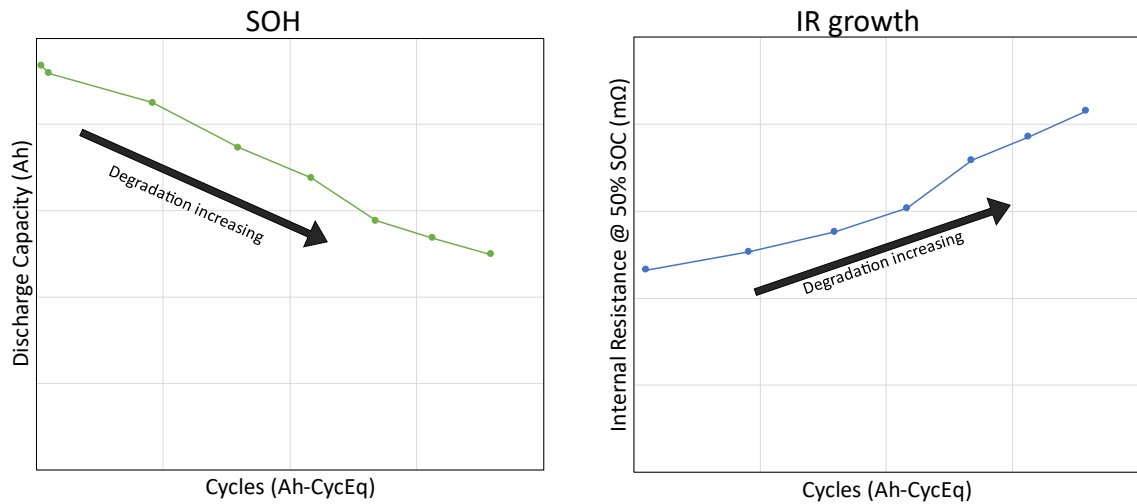


Figure 2: Example of typical degradation plots to evaluate SOH and IR growth

Measuring maximum capacity requires a 1.5 day test, and IR requires a specialized charge and discharge control. These are not always feasible to achieve in applications where operational time is maximized and cost is minimized. Therefore, finding a method to determine degradation metrics with a simple procedure is valuable.

Another issue that is facing LIBs is how they scale as more storage is required. To gain higher capacity, voltage or power output, cells must be stacked in parallel and series. This is different than some other energy storage technologies such as pumped hydro, and Vanadium redox flow batteries [7] which can increase capacity by increasing the size of the storage mechanism. This difference explains the tiered structure of battery packs.

Individual cells are put into parallel and series groups called modules. Then modules are organized into series groups called packs as pictured in Figure 3.

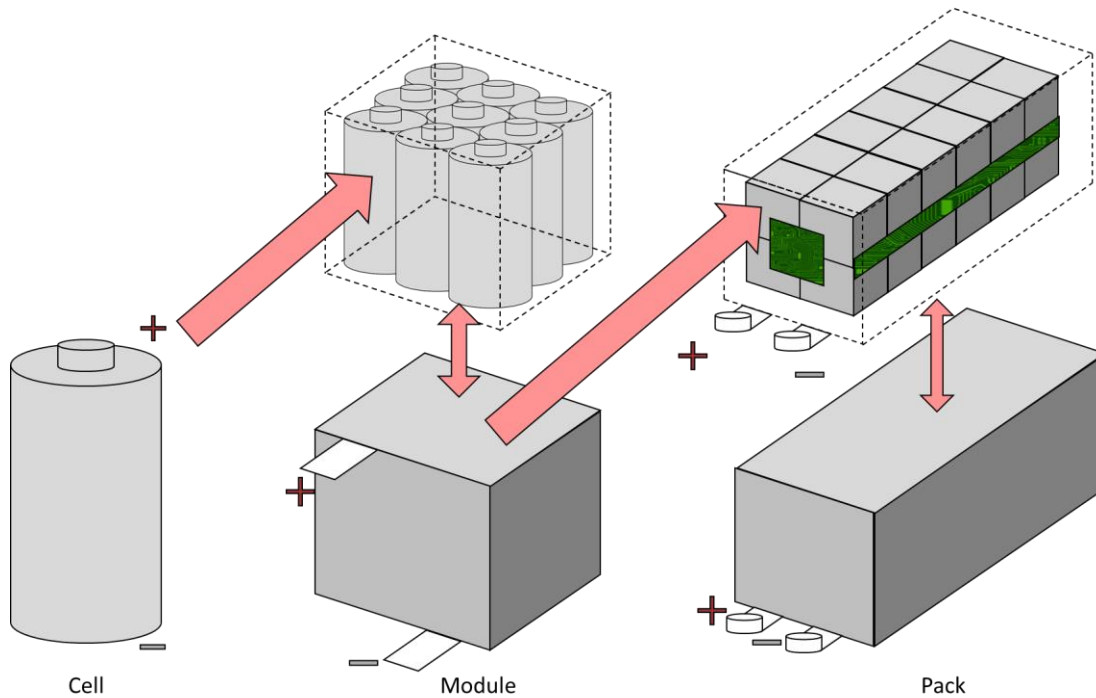


Figure 3: Cylindrical cell LIBs scaling from cells to modules to packs

This organization paired with the safety requirements of the LIB make monitoring an individual cell for failure a difficult task. Each pack requires a battery management system (BMS) that monitors each of the operational metrics for the pack and safety parameters for the modules. The BMS is required to monitor the SOC and SOH. One method that has been proposed to determine these metrics is voltage relaxation.

Voltage relaxation (VR) is the process that occurs to the voltage of the battery after current stops flowing, where it relaxes to a steady-state open circuit voltage (SS-OCV) from an operational voltage. VR is commonly used as a replacement for slow rate testing to find initial characteristics of batteries. Using a correlation between SS-OCV and SOC, VR can be used to estimate SOC. It has also been shown to predict the degradation processes taking place in batteries [8]. VR can be used to show the SOH of the battery and could potentially give insight into IR growth as well. VR takes a long time to reach SS-OCV, 5 hours or longer depending on the chemistry of the battery. To shorten this period, battery models can be used to predict SS-OCV, and VR curve shape.

In this thesis VR is studied as a method for SOC determination and SOH estimation. The following research questions were created to guide the studies:

1. How does the VR magnitude and curve shape change as a function of SOC value?
2. What period of time is necessary for the battery to be considered fully rested at SS-OCV?
3. For estimating SOC, how complex must a model be, and how short can the VR period be, to accurately determine SS-OCV?
4. For estimating SOH, how complex must a model be, and how short can the VR period be, at a sensitive SOC position to accurately capture VR magnitude and curve shape?
5. Do time constants of VR curve shape change as a function of degradation metrics (SOH & IR growth) with a relationship that is useful to predict degradation metrics?
6. Does VR magnitude change as a function of degradation metrics with a relationship that is useful to predict degradation metrics?

The questions then inform the thesis objectives that were created:

1. Determine a battery model that can accurately curve fit VR so that it can be evaluated quantitatively.
2. Determine a methodology for estimating SOC from a VR period to the highest accuracy possible.
3. Determine a methodology for evaluating degradation metrics (SOH and IR growth) from a VR period.
4. Find relationships between VR metrics (magnitude and curve shape) and degradation metrics.

Chapter 2 Background

2.1. The lithium ion cell

2.1.1 Construction

There are 3 primary components to the lithium ion cell, these are the negative electrode (Anode), the electrolyte, and the positive electrode (cathode). There are also 4, non-active, secondary components, the solid electrolyte interphase (SEI), separator, and current collectors, without which the cell could not function. Figure 4 shows how the primary components are arranged. Chapter 2.1.1 to 2.1.1 will describe the relevant components for degradation and VR comprehension.

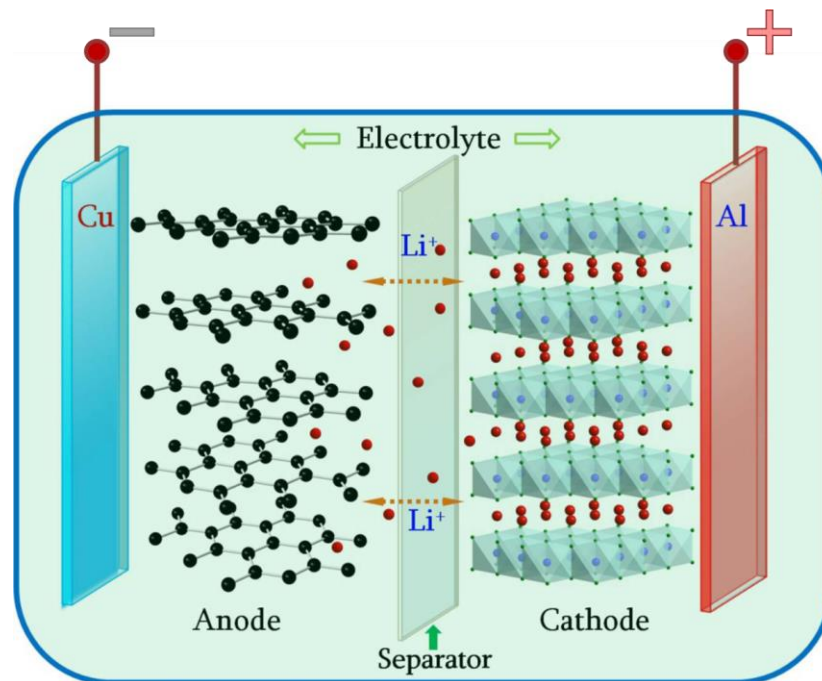
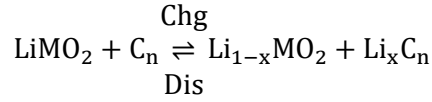


Figure 4: Graphical representation of internal view of a lithium ion cell [9]

The basic function of the cell relies on the mass transfer of lithium ions between the electrodes and intercalation. Intercalation is a chemical process by which a foreign ion or molecule can be inserted between sheets of a host lattice material to create a semi-stable structure. Intercalation facilitates the half reactions, which take place in each electrode, typically creating the following full reaction, Eq [1].

Eq [1]: Complete cell reaction of a lithium ion battery



Where MO_2 is the mixed metal oxide of the positive electrode. In the case of certain positive electrodes such as Lithium Iron Phosphate (LFP), this would be an altered reaction with PO_4 in place of the MO_2 . In the full cell reaction, a lithium ion is traveling from one electrode to another. During this process the lithium ion must pass through the SEI, the electrolyte on either side of the semi-permeable separator, through said separator, and finally intercalates into the opposite electrode. For the positive electrode the charge from the lithium ion receives a balancing electron from the current collector, which reduces the metal's oxidation state creating the positive half reaction. For the negative electrode the balancing electron from the current collector, reduces the lithium ion creating the negative half reaction. The current collector is connected to the electrode and allows for travel of electrons to an external circuit.

The open circuit voltage (OCV) of the cell is determined by the reduction potential of the positive electrode and the negative electrode with Eq [2].

Eq [2]: Potential of the cell

$$E_{\text{Cell}}^0 = E_{\text{PE}}^0 - E_{\text{NE}}^0$$

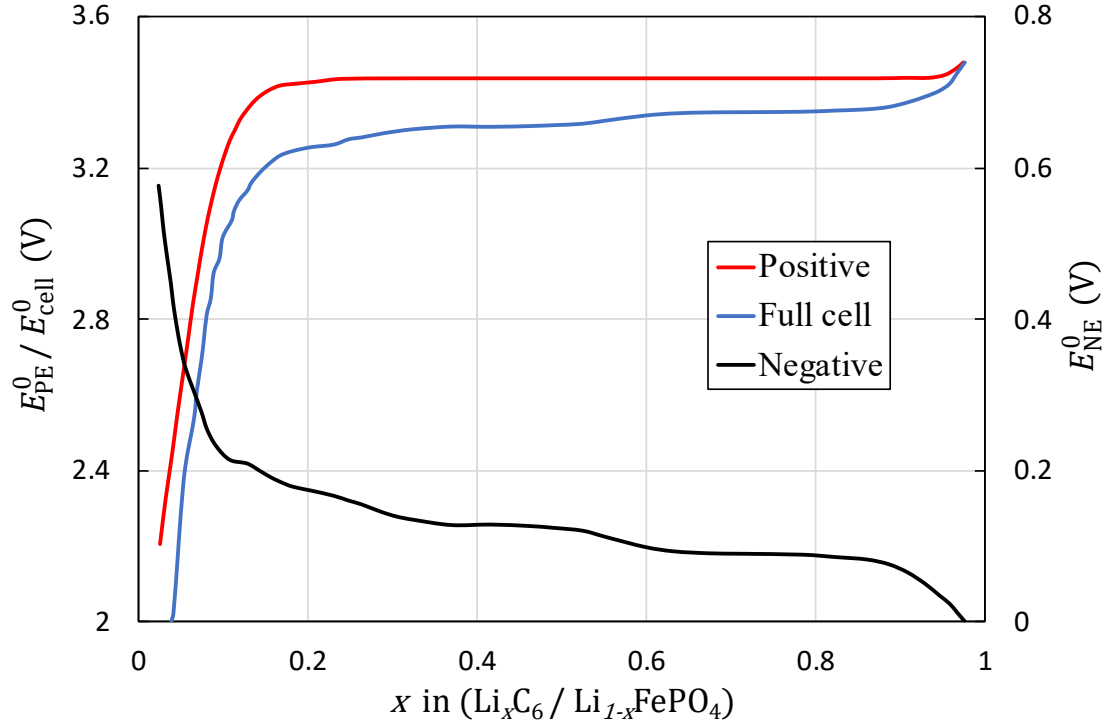


Figure 5: Full and half cell voltages vs capacity for a lithium ion battery

Where E_{PE}^0 and E_{NE}^0 relates to the potential of the positive and negative electrode respectively. Figure 5 shows that these values of E_{PE}^0 and E_{NE}^0 change as a function of x , which is the ratio of lithium intercalated into the negative electrode. This variable is analogous to SOC, but not equivalent as x will never reach 0 or 1. The potential of the cell will always be lower than the positive curve as achieving a voltage lower than the baseline is chemically impossible for this architecture. The underlying electrochemical mechanism behind these curve shapes is the lithium concentration at the surface of the electrodes.

The concentration of lithium in the electrodes is the most important behaviour of LIBs to understand VR of a cell. As current passes through a cell this forms a concentration gradient though both electrodes and electrolyte. This gradient is different for each component but is related to each other as they must be roughly equal at the interfaces. Picturing each electrode as a cylinder the 1 dimensional gradient is the concentration of lithium from the center to the surface. Figure 6 shows this is different from the electrolyte which is the concentration from one electrode to the other.

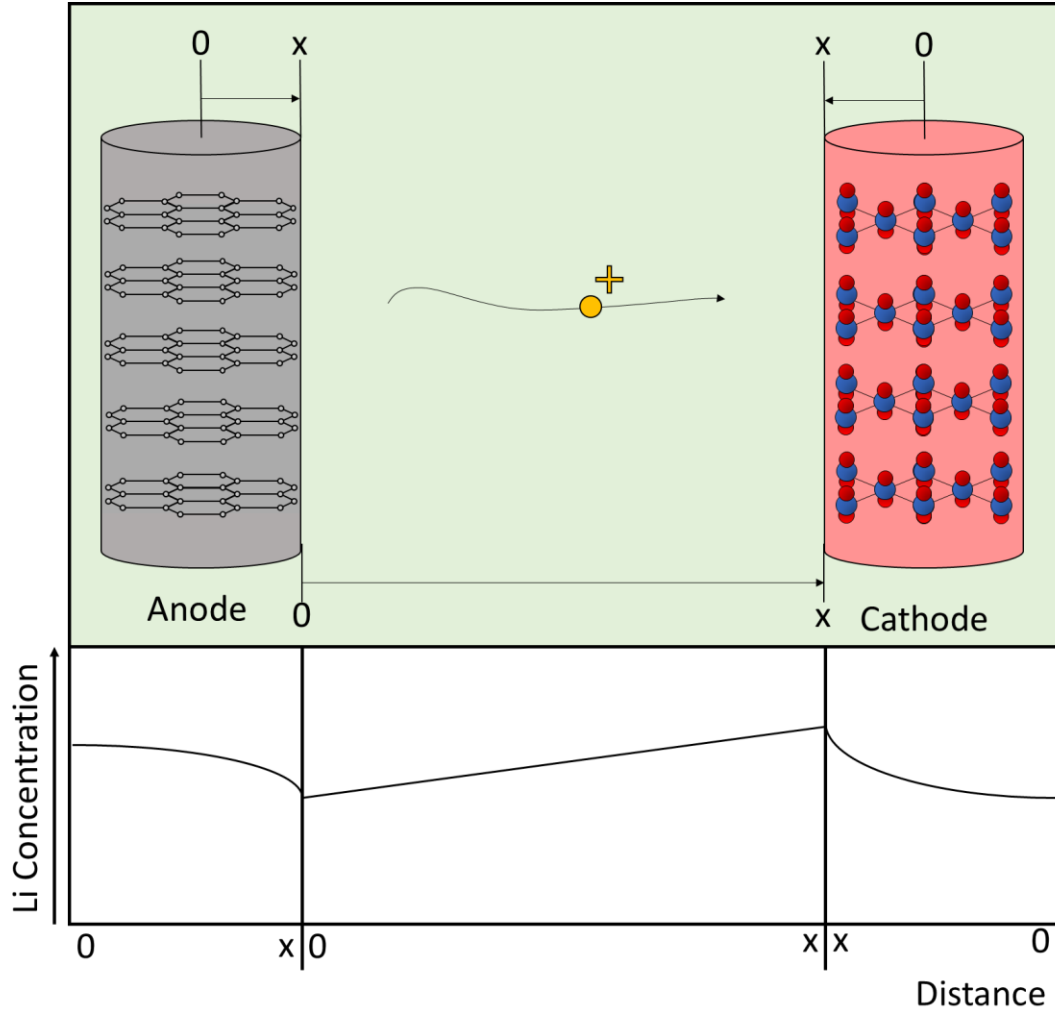


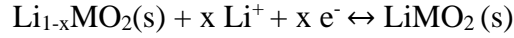
Figure 6: Example Li concentration throughout the cell on discharge

These gradients are highly dependent on the current passing through the cell, and the health of the cell. A high current will create a larger gradient. These gradients take a number of coulombs to pass through the cell for them to be fully expressed. This means that different current rates will result in different time for gradient stabilization [17].

2.1.2 Positive electrode

The positive electrode, also called the positive active material or cathode, is where the positive half reaction occurs. This is different than the negative electrode in that the reduction pair is a different metal than lithium as can be seen in the half reaction Eq [3].

Eq [3]: Positive half reaction in the lithium ion cell



The positive half reaction has M being the oxidizing metal same as the full reaction. Depending on the positive electrode material there is a difference in the potential of the half reaction. For example, LFP cells reduce the Iron from Fe^{3+} to Fe^{2+} and have a potential of roughly 3.5 V vs Li/Li^+ . Figure 7 shows the reduction potential for various common potential positive electrode materials.

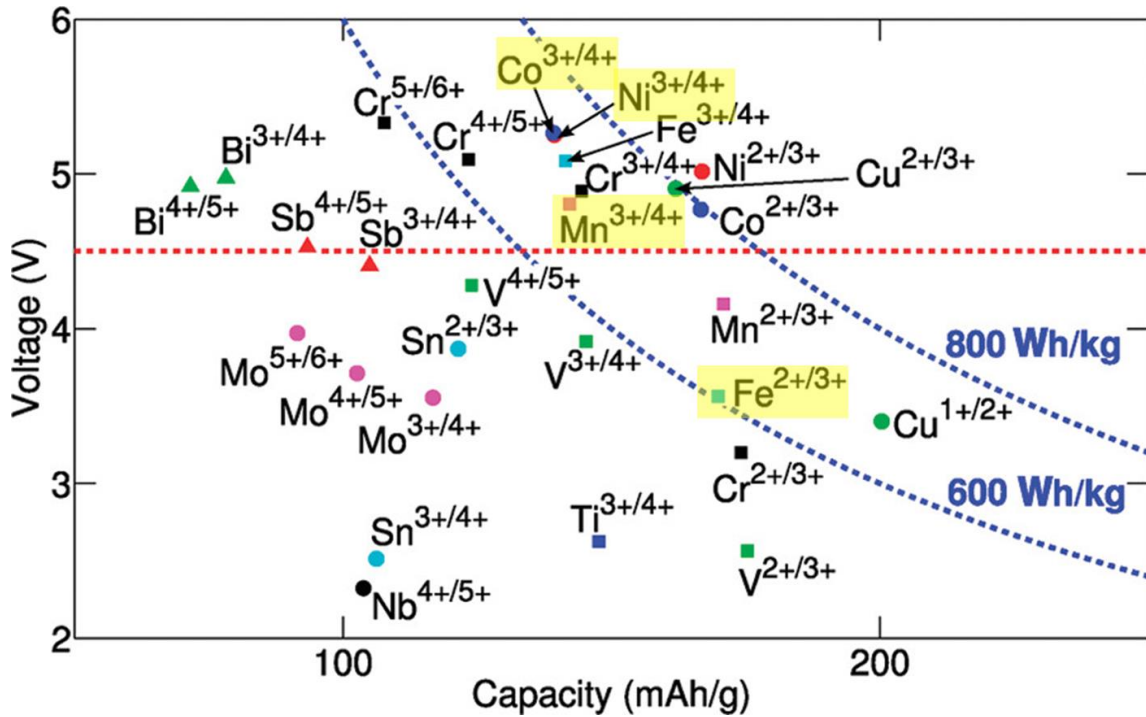


Figure 7: Reduction potential of various elements versus lithium reproduced with permission from [10]

From this graph the ideal positive electrode material would be a material with the highest specific capacity (mAh/g), how much energy can be stored per unit mass, and the highest potential. This explains some of the dominant chemistries that can be observed in the market which are highlighted. Nickel Manganese Cobalt (NMC) and Nickel Cobalt Aluminum (NCA) cells have a high voltage and specific capacity, and this can be seen in the figure. This graph also shows that LFP cells have lower capacity and voltage which when placed into the LiFePO_4 configuration as this increases atomic mass thus lowering

the specific capacity, while keeping the same voltage potential of $\text{Fe}^{2+/3+}$. The effect would be pushing the point further left as LiFePO_4 is heavier than LiFeO_2 .

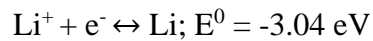
2.1.3 Electrolyte

The electrolyte is a key component of the lithium ion cell as it facilitates the mass transport of lithium ions from the one electrode to the other. To accomplish this, the electrolyte is usually a high molarity aqueous salt solution with different additives. The specific solution must be stable for the operation of the cell. When looking at the voltage range for this solution it must be relatively large, approximately 4.2 V in NMC cells for example. This selection is made more difficult with the varied temperatures where it needs to stably perform. The lowest temperatures being lower than -20°C and the highest being above 60°C . This makes selecting the electrolyte a balancing act of good thermal and electrochemical stability while not losing performance and keeping cost low. One final aspect of electrolyte selection is the formation and long term evolution of the SEI.

2.1.1 Negative electrode

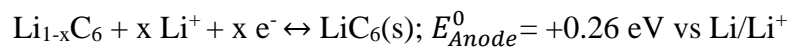
The negative electrode, also called the negative active material or anode, is where the negative half reaction occurs in the lithium ion cell. Lithium ions are reduced from a $1+$ state to a neutral state, as shown in Eq [4].

Eq [4]: Redox reaction of a lithium ion



This redox reaction is the basis for the potential in lithium ion cells. It is common to reference other voltages in the context of the cell as eV vs Li/Li^+ . Often it is done without mention and simply referred to with V as was done in Figure 5. This shows the relative potential to this reduction which gives an easier to interpret number for the voltage of the final cell. Therefore, the lowest potential in the cell is the reduction of lithium, which is 0. To facilitate this reaction carbon sheets are used to host the lithium via intercalation, which gives the half reaction for the cell of:

Eq [5]: Negative half reaction of a lithium ion cell



One of the main benefits of using graphite is the low potential of the intercalation. The lithium is stored between each sheet of graphite. Each possible location in the stack of graphite that this can occur is called an intercalation site. As the lithium occupies a site it applies mechanical stress to the lattice, making the non occupied sites entrances compress. This paired with the positive charge of lithium ions repelling other lithium ions is why an effect on the voltage called staging occurs. Staging is easiest to notice in the voltage profile of the negative electrode shown in Figure 8.

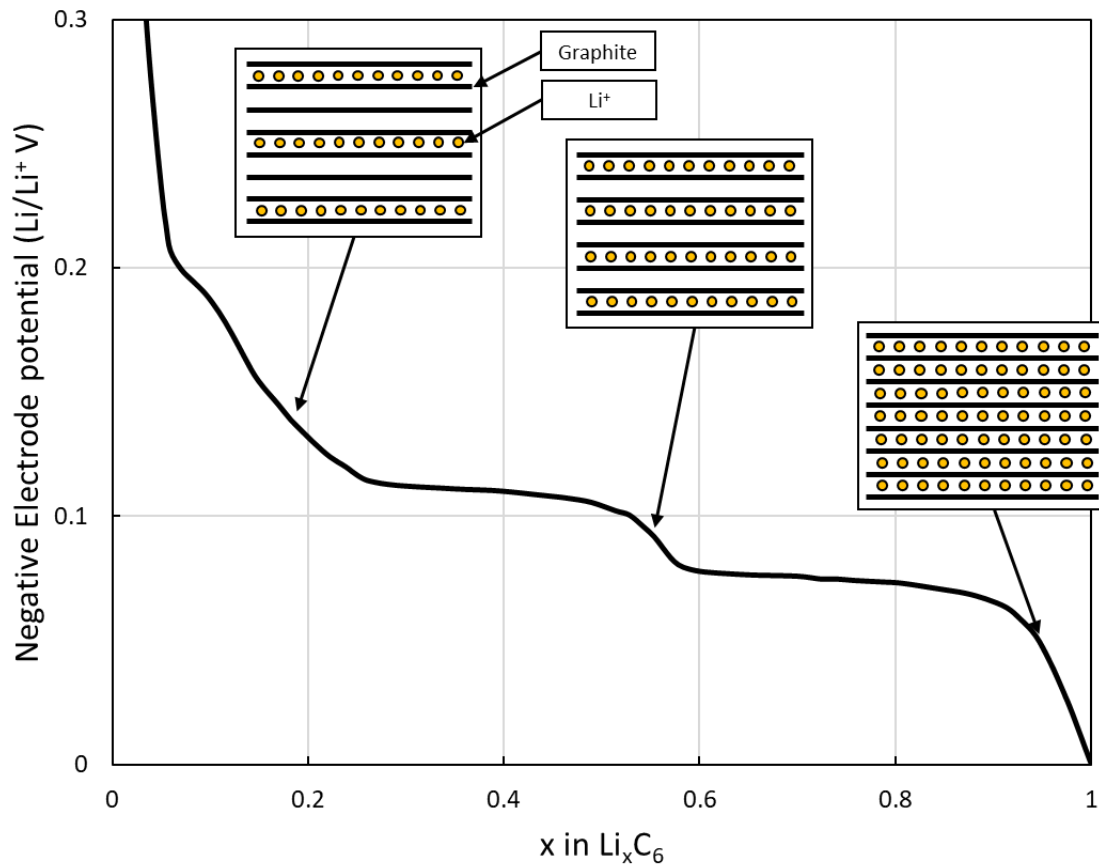


Figure 8: Voltage profile of a graphitic negative electrode with staging effect graphics adapted from [11]

Lithium is intercalated into the site where insertion energy is at a minimum. From the effects mentioned earlier this results in the stages that are shown on the upper right of the figure. It takes less energy to occupy a filled site compared to entering a new site, stretching the lattice, and being repelled by like charges of the neighboring occupied sites. Since the potential of the negative electrode is determined by the surface concentration of lithium the

voltage of the negative electrode and cell has this staircasing effect on the profile as the cell is charged or discharged.

When fully charged, SOC is 100%, there will be the maximum of lithium ions in the negative electrode and the potential of the cell will be at a maximum due to this. When fully discharged, SOC is 0%, the potential will be at a minimum. The potential of the negative electrode will increase as the SOC decreases due to the low potential of the reduction pair. This is represented graphically in Figure 9. This figure also shows that the positive electrode has the opposite effects of the negative electrode for charge and discharge.

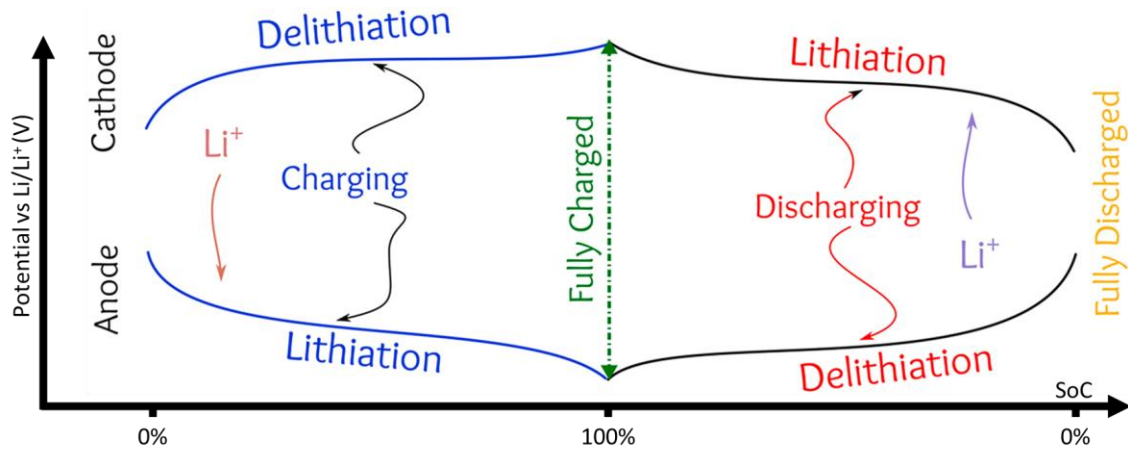


Figure 9: Schematic of charge and discharge of a lithium ion battery from the perspectives of the anode and cathode. (Not real curve shapes.) Reproduced from [12]

2.1.2 Solid electrolyte interphase

The SEI is a component of the battery which is not present during the construction of the cell. The SEI is created upon first lithiation cycle, of the negative electrode. The SEI is a passivating film layer between the negative electrode and the electrolyte. Assuming the salt in the electrolyte is LiPF_6 , the most common option, the SEI is constructed initially from LiF and Lithium Ethylene Dicarboxylate (LEDC). Over time the LEDC will decompose into other compounds the SEI will grow, and more Lithium will be absorbed. This is shown in Figure 10.

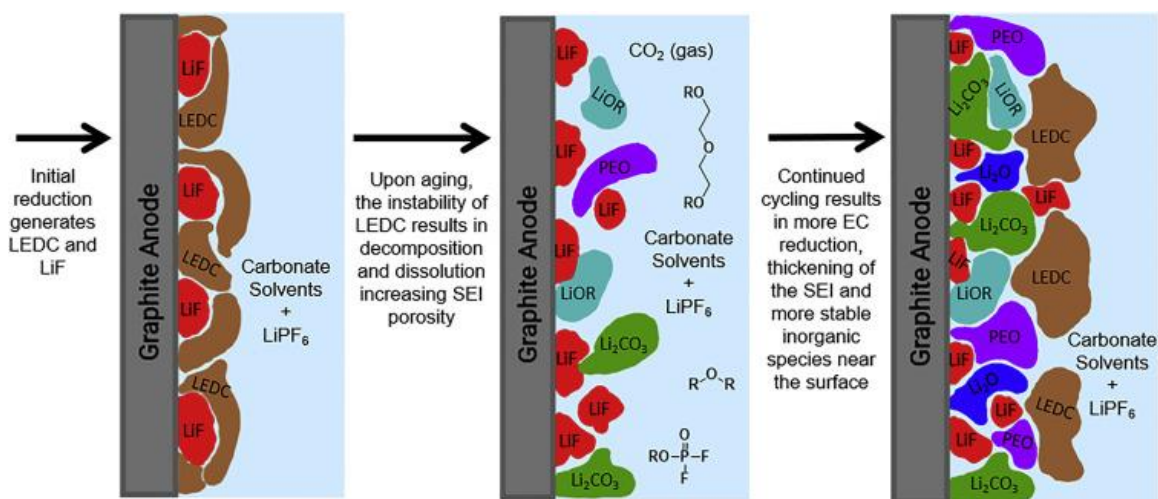


Figure 10: SEI formation reproduced from [13]

Should the electrolyte be chosen differently a similar process will occur. The compounds will be different, and the evolution will be different as well, but the effects on performance will be analogous.

The evolution of the SEI leads to increased resistance for a lithium ion being transported from one electrode to another, and a decrease in available lithium inventory, lowering the overall capacity since the growth is facilitated by compounds which require lithium to form. [13]

With these drawbacks it would seem logical to prevent the SEI from forming, however there are significant benefits to the SEI forming. First is that the SEI shields the highly reactive graphite anode from the electrolyte as it increases in lithium content. Next, the SEI decreases the voltage range that the electrolyte must be stable at by increasing the lowest voltage it will experience. Without these benefits the performance of the cell would decrease or be non-functional without an SEI. For these reasons the goal in cell creation is to have the best long term evolution of the SEI possible, minimal growth, but not to eliminate it.

2.2. Performance metrics

Once constructed, the lithium ion cell can not be taken apart for investigation and continue to operate. This is because it is not stable in a high energy state when exposed to air. The cell contents will react with air and can cause an explosion. Therefore, there are limited

methods of monitoring the battery. There exist three groups of performance metrics for LIBs which can be used to monitor a battery; these are primary performance, secondary performance, and battery defined metrics as can be seen in Figure 11.

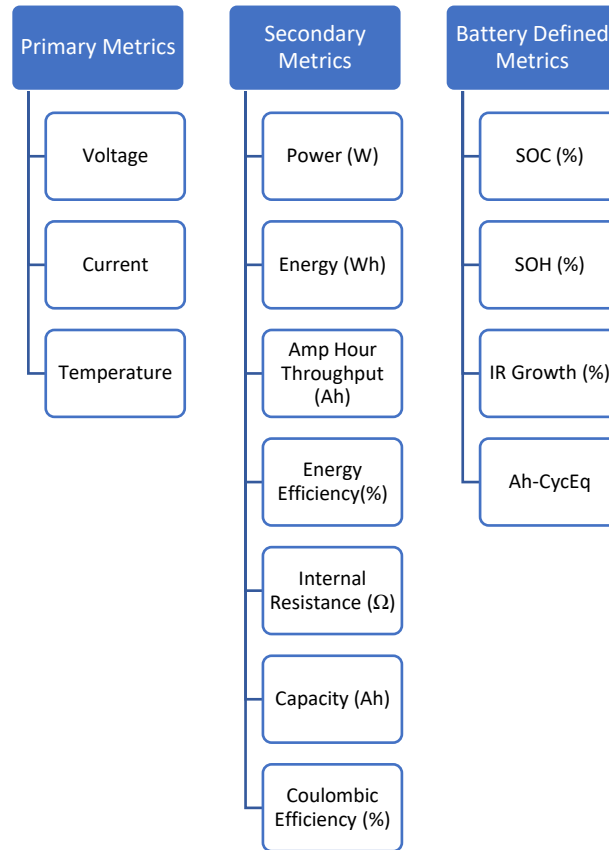


Figure 11: Performance metrics graphic

Primary metrics are the simplest group containing 3 measurements that can be made on the battery. These are the voltage, current, and temperature. These are primary because these are independently measured while operating the battery. The voltage and current are measured from the positive to the negative current taps, or from the positive cap to negative casing for cylindrical cells. Temperature is ideally measured as the surface temperature of the cell, however for many applications must be positioned further away for pack construction considerations. All primary metrics are used to then calculate the secondary metrics of the LIB, thus the naming convention.

Secondary metrics can not be directly measured as they are functions of the primary metrics, or compound functions of primary and other secondary metrics. Secondary metrics are often what is examined for absolute terms of performance. These are metrics such as:

- Power, calculated by current multiplied by voltage;
- Energy, integration of power with respect to time can be charge or discharge;
- Energy efficiency, ratio of discharge energy to charge energy;
- Capacity, the integration of current with respect to time can be charge or discharge;
- Ah Throughput, Total capacity cycled through battery can be charge or discharge;
- IR, calculated by quickly pulsing the current to watch the change in voltage;
- Coulombic efficiency, ratio of discharge capacity to charge capacity.

These metrics work well when examining a singular battery over its lifetime or can be useful for monitoring multiple batteries which should have the same performance.

Battery defined metrics are the final group of performance metrics and are often the most insightful. This is because they relate directly to the specific battery that is being tested and are defined by initial values or specifications from the specification sheet. They are:

- SOC, amount of usable capacity relative to maximum capacity;
- SOH, maximum capacity relative to initial capacity;
- IR Growth, IR of battery relative to initial IR;
- Ah-CycEq, total discharge Ah divided by rated capacity.

The reason these metrics are useful is best exemplified by Ah-CycEq. This metric gives a good measurement of how long a battery has been used and makes different chemistries comparable. If an LFP cell and an NMC cell have the same discharge Ah throughput (D-AhT) it appears they should have comparable results. The Ah-CycEq shows that the LFP cell has had more than twice the number of cycles as it has less rated capacity. The difference is only shown in the battery defined metric of Ah-CycEq. This is the ideology with all battery defined metrics, to show how primary and secondary metrics compared between batteries.

Lab testing equipment is made to monitor most or all of these metrics. They are calculated by the battery testing software used and arranged into timeseries data. For real world applications this is not always feasible. The monitoring hardware may not be able to perform these calculations or measurements. Data logging capabilities required for accurate coulomb counting, monitoring small currents for long periods, often are not included in BMS. Therefore, the BMS can not account for small parasitic loads that are applied over the time scale of weeks. This is a principle motivating factor for this thesis. If a non-intrusive, relatively simple algorithm can be implemented into a BMS or equivalent to determine some of these metrics, that has value to the producer and end user by accounting for these weaknesses.

2.3. State of charge estimation

State of charge refers to the remaining dischargeable coulombs in relation to the total capacity of a battery. This means that at 0% state of charge the battery will have no useable capacity left. Determination of SOC seems to be a simple case but in reality, there is no perfect method of SOC determination for an application. Thus, the engineering decision of acceptable drawbacks must be made.

2.3.1 Coulomb counting

The first method and often the ideal approach is coulomb counting. Coulomb counting is the process of monitoring the current and integrating with respect to time. Starting a battery at 100% SOC the discharge amp hours can counted relative to the total capacity of the cell to determine the SOC. This method works well even with charge and discharge occurring before a 100% is reached again as lithium ion cells are nearly 100% coulombically efficient. Equipment is required that can monitor the amperage of cells and store that data, which is commonplace for most applications. This is a common SOC estimation in many applications for its simplicity and low requirement of equipment.

As discussed previously accounting for small parasitic currents requires precise equipment which is not worth the investment for most applications. Another problem with coulomb counting comes with the question of what the capacity of the battery is. One solution would be to use the rated capacity from the manufacturer. As the cell ages the real capacity will

decrease while the SOC is still calculated from the original capacity. This means that the estimation of SOC will always be higher than reality and the low voltage limit will be hit while still being at mid-range SOC. This can be countered in one of two ways. First the D-AhT can be monitored over the life of the battery. The D-AhT can be related to a characteristic curve supplied from the manufacturer, which gives an estimate of where the capacity should be in relation to cycle count. This improves the results but doesn't work when the degradation that occurs is different than what was experienced on average from the manufacturer. As degradation is a complex process divergences from this curve are expected as the operating scheme or application needs are different than a lab environment. Second, a reference performance test can be run where a full discharge and charge cycle is obtained. By charging to full state of charge, discharge to 0% and charging back to 100% the true maximum capacity of the cell can be known. This maximum capacity can be used with coulomb counting for the best estimation of SOC. The issue is that this method is not feasible for many applications. For personal devices the time required to perform this test would be too long and impact the daily use. For commercial applications it could be performed but would reduce the operational time, which is not often acceptable as well. This means that performing a reference performance test is a niche solution to the problems of coulomb counting.

2.3.2 Open circuit voltage

As shown in Chapter 2.1 the SS-OCV is directly related to the energy remaining in a cell. The SS-OCV of a battery can then be related to the SOC through the relationship which is determined on a per cell basis with a cycle at the start of life. Relating SS-OCV to SOC requires performing a pseudo-OCV test as outlined by Barai et. al [14]. The pseudo-OCV test is a low rate cycle that produces a voltage profile representative of OCV vs SOC.

This method for evaluation of SOC is more accurate than coulomb counting as it is not highly dependent on the degradation of the cell. Ideally SS-OCV could be determined during regular operation. This is not feasible because it takes a long time to relax to SS-OCV from an operational voltage. Research into the settling time has stated times as long as 24 hours with most claiming roughly 5 hours. [15] [16] [17]. This long period of time often is what limits the use of SS-OCV for SOC determination.

2.4. Degradation of the lithium ion cell

One of the main drawbacks to LIBs is their degradation. Their performance degrades as they progress in calendar age and cycle count.

2.4.1 Effects on performance

As mentioned there are two main effects on performance from degradation. These are the loss of capacity, and the increase of IR. SOH is the battery defined metric that has been used to quantify degradation of the capacity, and IR growth can be monitored from DC or AC techniques in % resistance growth.

Capacity degradation has immediate and measurable effects on the operation of the cell for any use case. It is the primary degradation that is monitored over the lifetime of the battery. Capacity degradation should be how cells fail, as it is unavoidable, and it results in the longest life of the battery.

IR growth is a more insidious degradation effect than capacity degradation. It is harder to detect and therefore often viewed secondary to capacity degradation. IR will affect many different aspects of the battery performance. First the cell will lose energy efficiency, creating more waste heat as a by-product. This heat generation can cause the battery to degrade faster, and in extreme cases lowers the rate that can be safely run at. IR growth also increases the time to charge. This is because of Ohm's law from the current passing through the battery will increase the terminal voltage of the cell. This causes the constant current (CC) phase of a constant current / constant voltage charge to terminate earlier. This early termination causes the slower constant voltage (CV) phase to fill the remaining capacity.

Diagnosing IR in an application can also be difficult. If IR on a pack level is not being monitored there are many other components in the system which could cause similar effects but be reversible, such as high resistance contacts. This compounds with IR diagnostics requiring a specialized charge discharge control or increase in cost of the BMS. If IR could be monitored with minimal interference to the end user, this would be beneficial as a low cost and impact alternative.

2.4.2 Degradation causes, mechanisms, and modes

The mechanisms of LIB degradation are numerous and complex, they can promote other mechanisms, and only show in one of two effects. They can be categorized into four distinctions: cause, degradation mechanism, degradation mode, and effect seen in Figure 12.

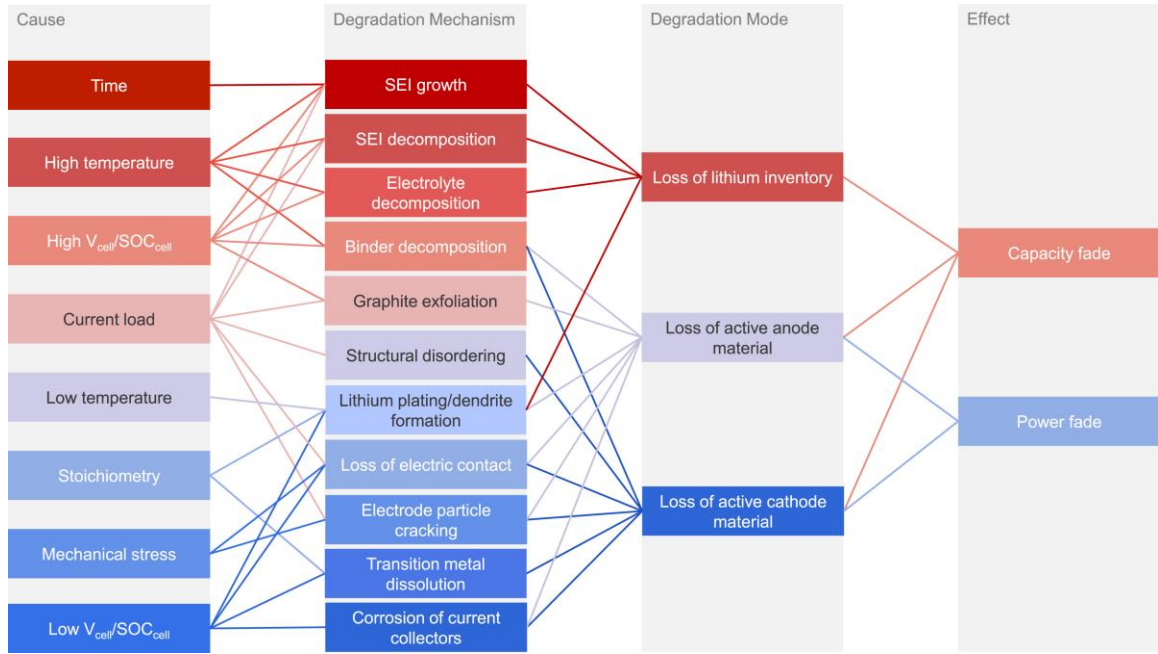


Figure 12: Degradation mechanism flow chart reproduced from [18]

Starting from the right, the two effects were previously mentioned as capacity degradation (Capacity Fade) and IR growth (Power Fade). These are directly caused by the degradation modes. If there is a loss of lithium inventory in the cell less can be intercalated and the capacity of the cell is decreased. This is the same reason that a loss of electrode material will cause capacity fade, less ions can be intercalated. When the active material becomes damaged more energy is required for a lithium ion to travel through cell. This extra energy can be represented as an electric resistance with a real and imaginary component, this is an increase in IR.

Often times these degradation causes are unavoidable for the application. For example, lithium intercalation causes mechanical stress on the lattices, which is one of the degradation causes. Furthermore, the best temperature for operation of the cell is at 40°C, what would be considered high temperature. As applications become more defined, they

can be the driving factor for how the cell has degraded. Take for example a battery used in an EV versus grid storage. The EV will experience more variability in temperature and power consumption, but the grid storage battery will be constantly cycling, meaning the mechanical stress on the electrode's lattice will be more of a factor over the same amount of time. These two batteries will degrade differently. Even if there is no usage of the battery degradation still occurs. Calendar ageing is a well studied effect [19] [20]. It is a minor factor compared to degradation from use, but important to recognize that the health of the battery is always lowering even when in rest.

2.4.3 Degradation considerations

SOH and IR growth are battery defined metrics to compare beginning of life (BOL) to present operations, making the understanding of the degradation process imperative to high quality operation of an LIB.

Degradation is a complex process of multiple causes and mechanisms with interplay between them influencing two observable effects, capacity degradation and IR growth. Degradation is unavoidable as regular usage or storage of a battery will progress it.

Similar to monitoring performance metrics there is a difference between monitoring in a lab environment versus an application. The lab environment can hold certain factors constant such as temperature and pressure. The monitoring of primary performance metrics is high quality from the battery testing systems. Once a battery has failed it can be destructively tested for the specific degradation that has occurred. These are luxuries not afforded to most real world applications. For these reasons determining the SOH and IR growth with simple tests that any monitoring system can perform would be a valuable contribution to the field.

2.5. Single cycle battery models

Battery modeling is an important task to improve the performance and prediction of metrics for all applications. The fact that there is no dominant model for all batteries shows that each application must make simplifications and assumptions guided towards their end goal. This is because of differences between individual cycles introduced from degradation. One cycle to another may have minor differences, but 100 cycles will have different model

coefficients and require alterations because of that. To complicate this further there are variables which effect SOH and IR growth that can only be known after destructive investigation. Therefore, no model can be made that has all pertinent information of the battery for a model. A concession must be made, and different models are optimized for different purposes.

This thesis requires monitoring the degradation and to use VR to examine how the battery's characteristics will change as a function of SOH or SOC. For this reason, lifecycle models are not used, which estimate the SOH based on usage and calendar life. Single cycle battery models are used. These can accurately predict the behaviour of the cell for a charge or discharge cycle. Single cycle models are useful as they can be adapted by altering their coefficients to account for degradation. Therefore, if the model's coefficients are fit, after some cycling, degradation can be determined and monitored from how these coefficients change. This is different as the degradation determination is a secondary effect of the model compared to lifecycle models for which require knowing the history of the battery.

Among single cycle battery models there are various forms. Ungurean et al. [21] summarized that there are three overarching types of battery models for individual cycle performance, these are:

- Electrical
- Electrochemical
- Mathematical

2.5.1 Electrical models

The electrical model of a battery is a simple but effective tool to show how a battery will interact in an electrical system. It uses basic circuit components, resistors, capacitors, and a capacity dependant ideal voltage source to show the dynamic voltage and current behaviour of a battery. The basic form of this model can be seen in Figure 13.

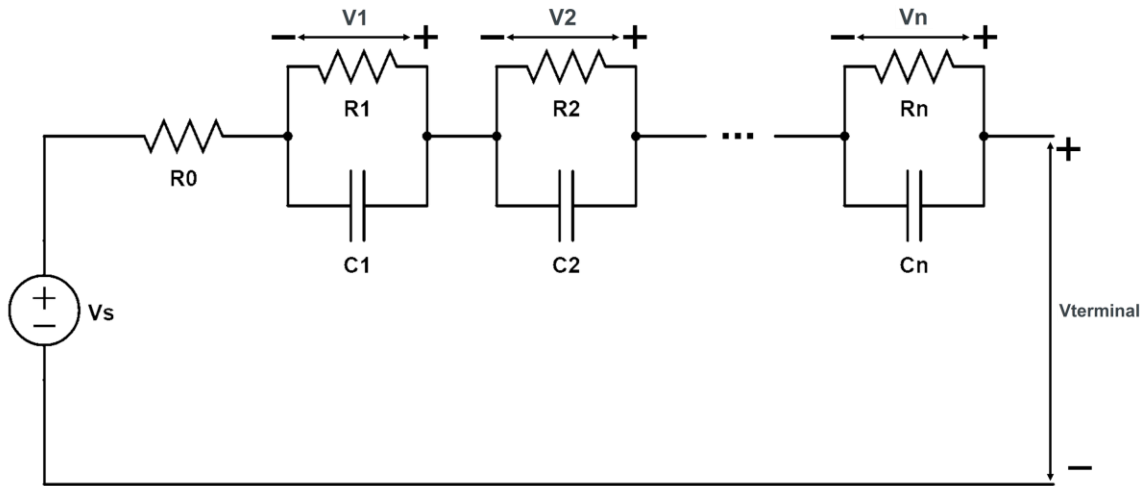


Figure 13: Equivalent circuit model of a lithium ion battery

The equivalent circuit model (ECM) is commonly used in industry for its adaptable simulation of a cycle. The main benefit of this model is the simplicity of it. An ECM only requires information that is readily available from cycling data. This is because the model coefficients are determined by curve fitting of data from a previous cycle. For simulations it is computationally simple relative to other battery models and integrates easily. There are no alterations based on the chemistry used, making it adaptable and easy to translate results from one chemistry to another. Since it can be curve fit to any cycle the previous history of the battery is not required to be known, and it can be adapted as the battery degrades.

The main drawback is that it does not represent the electrochemical effects on the battery, therefore interpretation of results is required for that to be achieved. Furthermore, the higher accuracy required causes more issues to consider. The model becomes more accurate by increasing the number of RC circuits. This increases the complexity, further obfuscates the electrochemical meaning of each component. With these considerations in mind the ECM should be optimized for the least number of RC circuits required.

2.5.2 Electrochemical models

Electrochemical models are powerful tools to examine the theoretical and practical function of LIBs. They are based on electrochemical principles to predict the function of a cell with a high degree of accuracy. Their main benefit over other models is that they

represent the electrochemical process. There is no single accepted form of an electrochemical model as there is with the equivalent circuit model being the most common for electrical models. This is because the purposes of electrochemical models are often varied.

They can be used to simulate the impedance of a cell for impedance spectroscopy [22] They can be used as single particle models to create an accurate SOC estimation throughout cycling [23]. They can even be used to determine SOH of a cell and can show trends with its lifecycle. This method is similar to how it is accomplished for the electrical model as well by monitoring how coefficients change as a function of Ah cycle equivalents.

With such powerful models there are drawbacks, and this comes in the complexity of the model. Since the models are based on the chemical processes in the cell these are often represented as a partial differential equation (PDE). Then these PDEs are only representative for one area of the cell or one period of time. For an example Figure 14 shows the process of estimating the impedance of the cell from theory to final results.

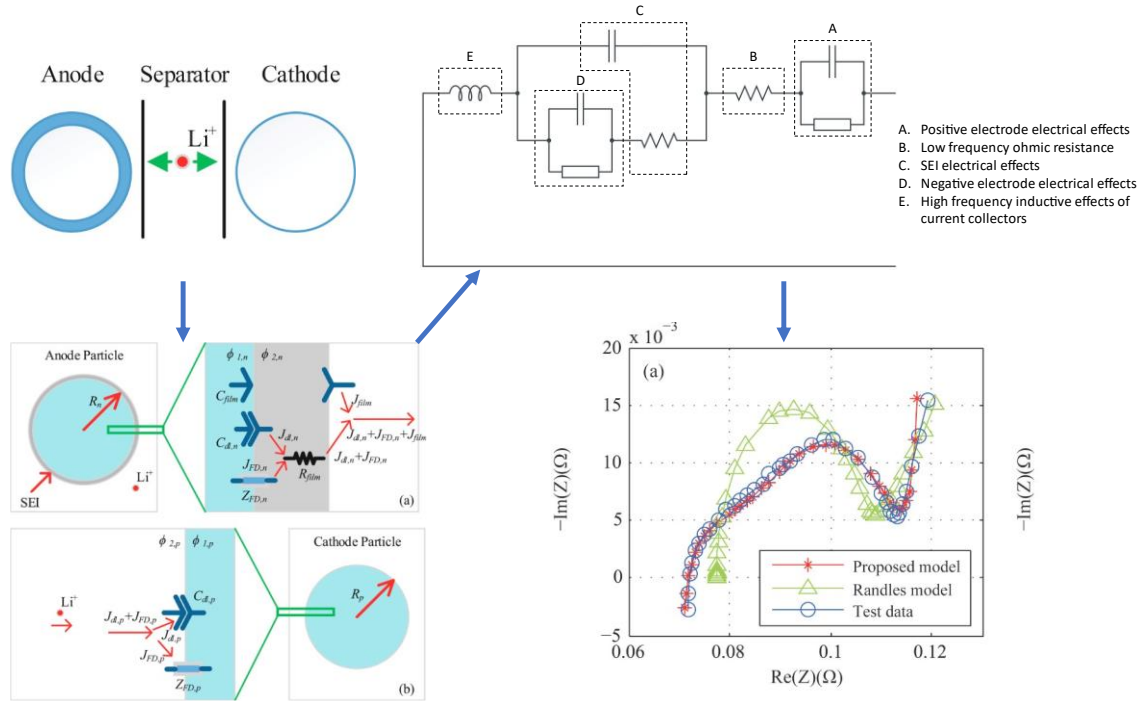


Figure 14: Example of electrochemical model from first principles to final simulation adapted from [24]

This process is for a 2 dimensional particle analysis. The path that an ion would travel is shown with each interface being examined for its impedance to this process. Then, these impedances are given electrical circuit allegories, which are then used to create an impedance of the cell that performs well at various frequencies. The drawback for electrochemical models like this is that they require a good understanding of the entire cell and significant processing power as they require use of multiple PDEs and then curve fitting.

These models quickly grow in scale and complexity as the requirements of the model increase in number. It is important to stress that Figure 14 only models the impedance of the cell and does not account for the concentration gradients of Li throughout the cell. This reduced scope is one method of making the electrochemical model feasible for real world applications. The alternative is to simplify the processes involved. The issue is that as the processes are simplified, they are then not completely representative of the electrochemical process. The benefit of using an electrochemical model is having the model coefficients be a direct representation of the battery. Without consideration these models can be overly complex without significant benefit to real world applications. When used correctly they

are powerful and precise models that give insights no other model can for the internal workings of a cell.

2.5.3 Mathematical models

Mathematical models can fall into two main distinctions, analytical and stochastic. First analytical mathematical models are constructed from the real workings of the cell. They do not necessarily represent the electrochemical function of the cell, but certain approaches use basic physical equations to start their models. A common analytical mathematical model is the Kinetic Battery Model (KiBaM), shown in Figure 15.

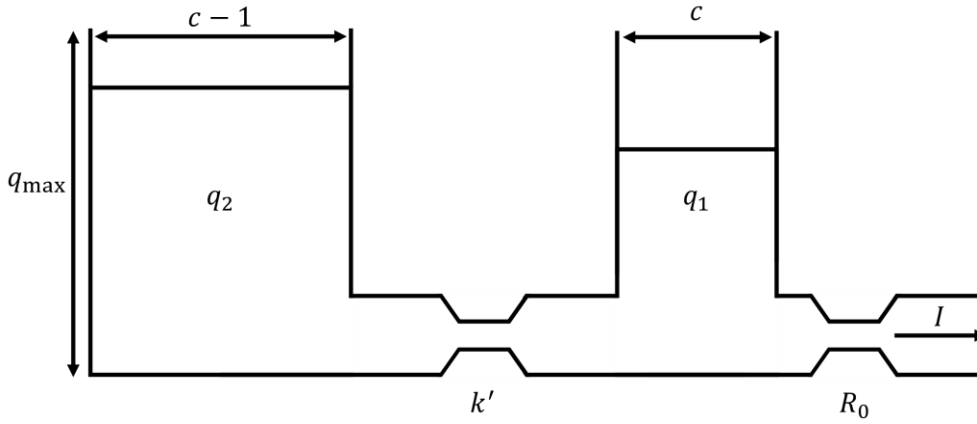


Figure 15: KiBaM graphic showing fluid equivalent battery system

Here the battery is conceptualized as a are two wells and an outlet. The load is supplied liquid, which is analogous to electrons, at a rate I from the first well with available charge q_1 . The first well is then supplied by the second well q_2 . There is the impedance to flow in the form of R_0 and k' . Each well has a capacity denoted by c and $c - 1$. From this interpretation of a battery a system of equations can be created that represents the function of the cell with acceptable accuracy. This model is extremely adaptable, it was originally created in 1993 by Manwell et al. [25] for lead acid cells and is still used today for LIBs.

Next, a stochastic model is a model where there is little relation to the real kinetics of lithium ions but are very quick at evaluating possible states in which the battery could be. An example of this type of battery model is to use a discrete Markov chain to model battery states. A discrete Markov chain is a stochastic process where there are a number of states which can be accessed from a previous state. There is a probability assigned to the

transition from one state to another, and this is only based on the current state. The previous behaviour of the battery has no effect on what the probabilities are. For batteries these states are values of SOC, and each time step the battery either recovers a small amount of SOC, remains constant, decreases a various amount of SOC. A discrete Markov chain was first proposed by Chiasserini et al. [26] and their proposed version can be seen in Figure 16

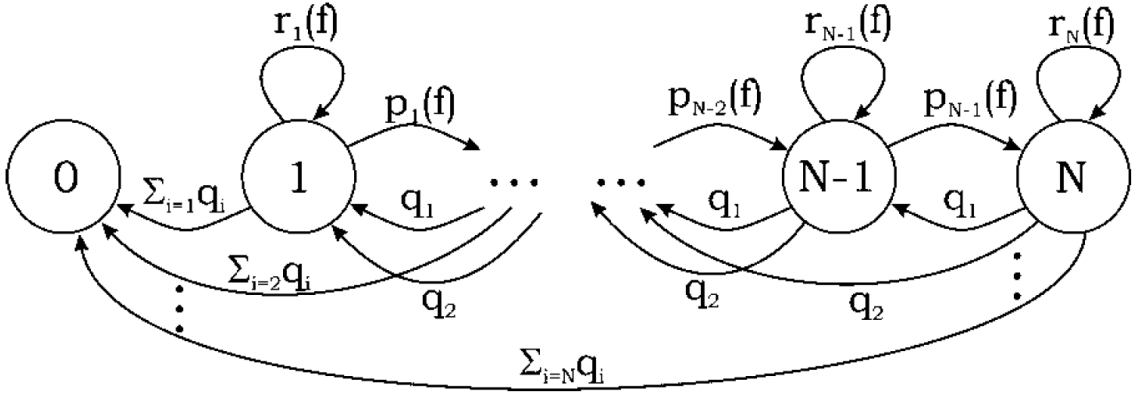


Figure 16: Discrete Time Markov Chain of an LIB reproduced from [26]

They claimed that roughly 4×10^6 states should be included for the numerical computation of the model. When parametrized correctly this model has a maximum deviation of 4% and average of 1%. This comes from a discharge cycle where the magnitude of current is changing over the discharge.

Mathematical models are strong tools that can reduce the prerequisite knowledge required to have a high quality battery model for a single cycle. They do not function well with battery ageing mechanics and require a reference test to parametrize them as the battery ages. These models are often optimized to run quickly and for their specifically designed applications are top of class. When comparing to other models they have their clear niche and use case.

2.6. Voltage relaxation

Open circuit VR is an electrochemical process that occurs after current passing through a battery is interrupted. The voltage relaxes back to SS-OCV from an operational voltage as

shown in Figure 17. SS-OCV was defined as the voltage settling within 1 mV. This was an achievable value for the monitoring equipment used. Figure 17 also shows the difference between VR magnitude and IR voltage drop. IR voltage drop is the instantaneous voltage drop that occurs from ohmic resistance of the cell, this is not included as part of the VR curve. This is made relevant as it must be distinct from VR magnitude. VR magnitude is the amount of voltage evolution between the IR drop and SS-OCV. Should IR voltage drop be included this will skew the relationship to match the IR vs SOC profile. Finally, the curve shape is shown in the figure as well.

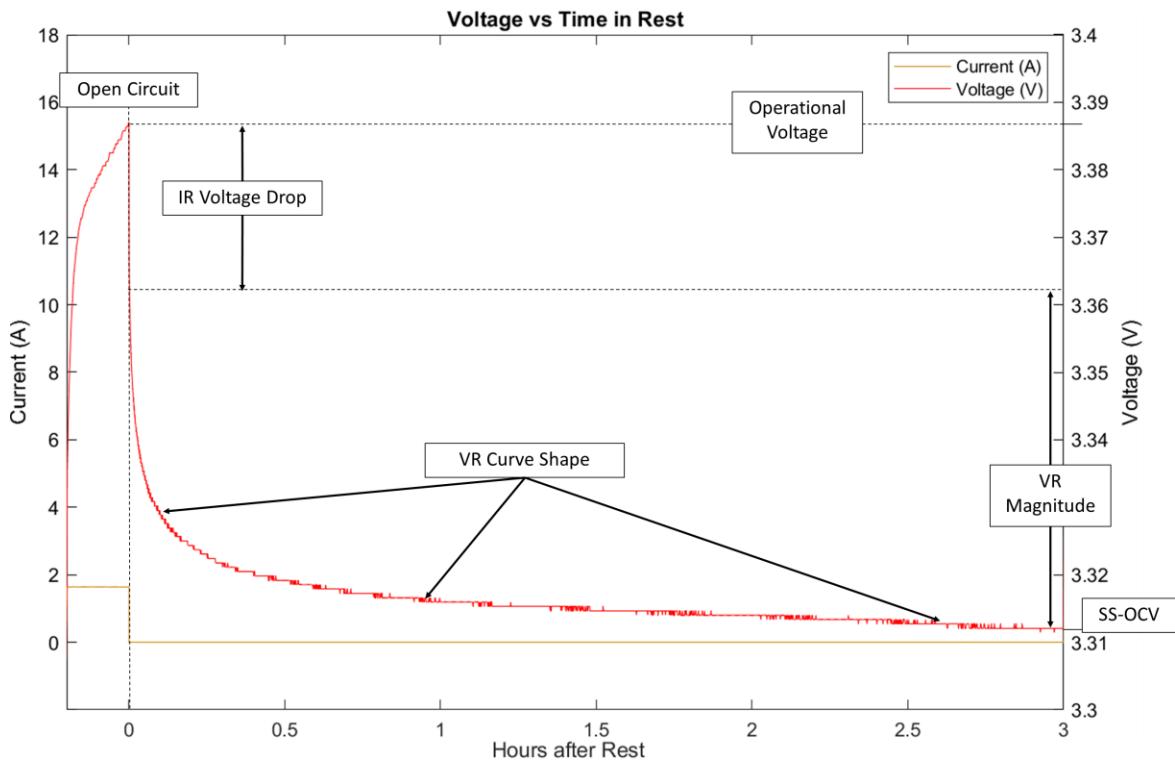


Figure 17: Voltage relaxation curve labeled with points of interest, data for this curve taken from tests performed in this thesis

Should this curve shape be predicted with high accuracy it could be used to determine the SS-OCV without having to perform the full process. From Chapter 2.3.2 we know that with SS-OCV the SOC can be estimated to a high degree of quality. This would be an in-situ monitoring technique that could alleviate the main issue with using SS-OCV to estimate SOC. VR has great potential to use as a high quality estimation for SOC. This is one of the motivating factors for this work, to determine the length of time required to have an

accurate SOC estimation. One issue with this technique is the VR curve shape is difficult to estimate.

VR curve shape is more complicated than a first viewing would suggest. From Figure 17, VR curve shape appears to be an exponential decay function progressing to SS-OCV after the IR drop. Figure 18 shows that by changing to a logarithmic time scale, the curve is more complicated than a single exponential. This is because of the electrochemical effects that are occurring in the battery which cause this curve shape.

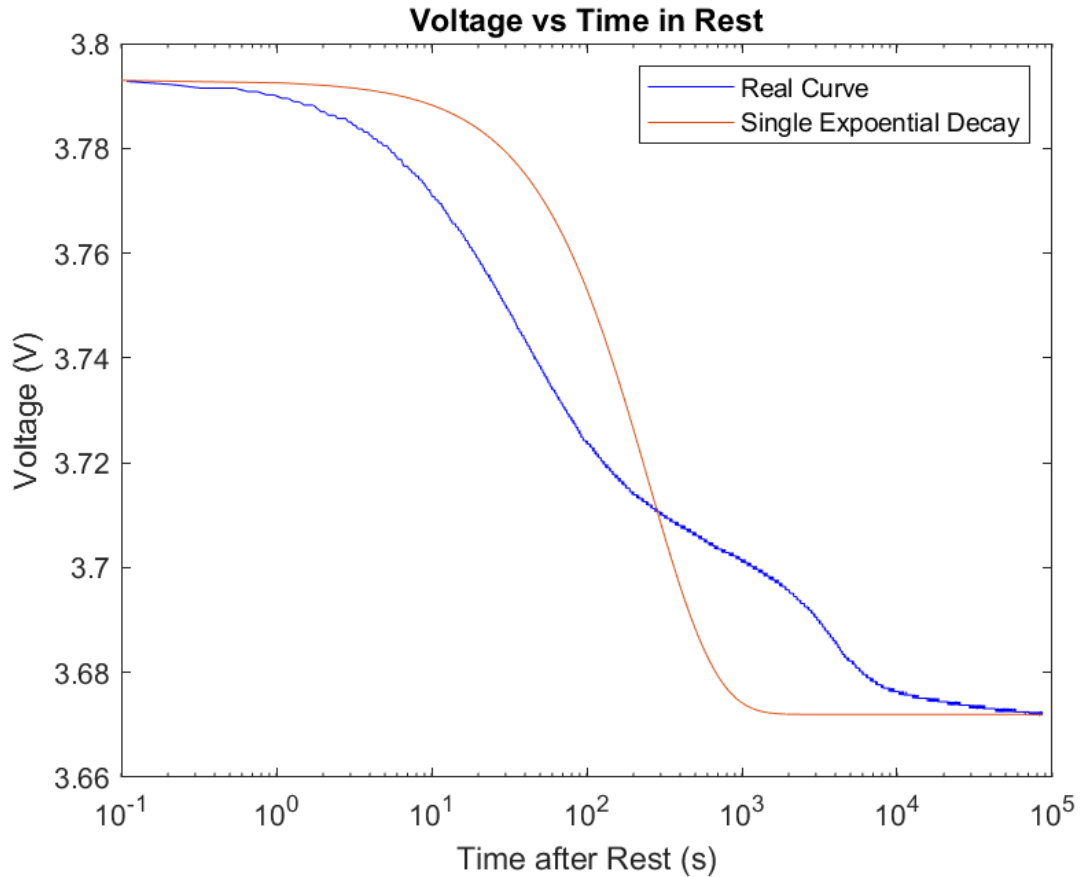


Figure 18: Curve Shape of VR shown to compare single exponential error

This relaxation process occurs since there is a gradient of lithium ions through both electrodes that will reduce to a minimum energy state after a partial charge or discharge. This is shown in Figure 19. As time progresses from open circuit to fully rested, shown in the figure as time scale a and b , the surface concentration will change. Note that both variables are arbitrary positive integers, where a is much less than b . Voltage is determined

by the surface concentration of lithium ions in an electrode, so when the gradient flattens out the voltage at the battery terminals will change as well.

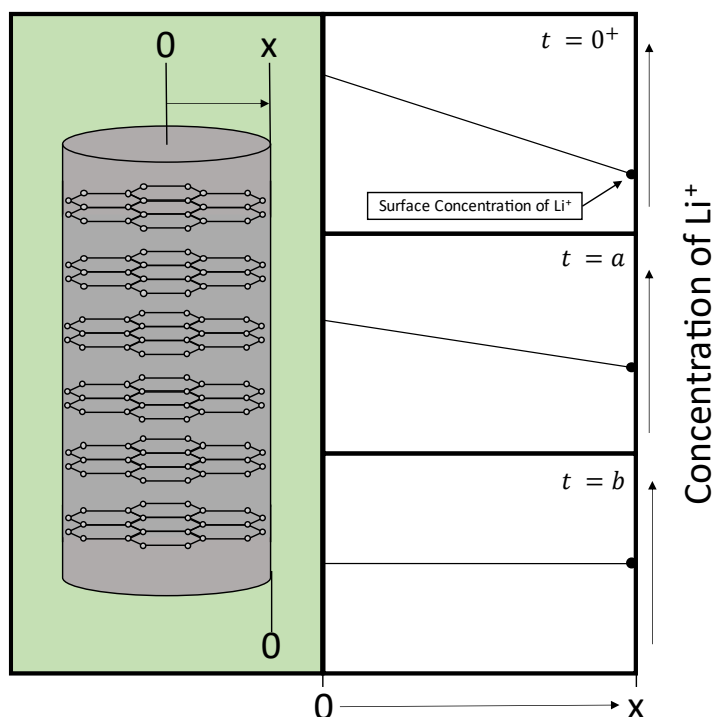


Figure 19: Voltage relaxation pictured in an electrode.

Using this framework, the real driving factor for VR magnitude and curve shape can be seen. The magnitude of change in the surface concentration is analogous to the VR magnitude. The leveling of the concentration gradient is how the VR curve shape results from the electrochemical process. Therefore, if a higher current is passed through the battery, a higher concentration gradient will be induced, there be higher VR magnitude and a different curve shape.

The magnitude and shape of VR have been used for electrochemical evaluation of the battery. Skrob et al. [27] observed there are two primary response domains in VR corresponding to fast (0-2 minutes), and slow (0.3-3.0+ hours). The fast domain is dependent on the preceding current magnitude, positive electrode thickness, and electrochemical active area. The slow domain is dependent on preceding current magnitude, a minimum coulombic transfer (Ah amount) and the positive electrode health. Consequently, short current pulses of less than 30 s are not typically useful for VR investigation.

As the battery becomes worn and aged the coulombic capacity will decrease and the electrode particle radius will increase. This will cause the lithium ion diffusion rate to decrease and change both the VR magnitude and curve shape [15]. From this research it can be reasoned that battery health determinants can be found from VR investigation. They should be first observed in the fast domain, and then later in the slow domain as the SOH decreases further. These changes should be measurable from the monitoring equipment that Li-ion batteries use. Making a strong case to characterize this growth and examine from an operational point of view how these metrics of VR magnitude and curve shape can be used to determine both the SOH.

Chapter 3 Literature review

The purpose of this literature review is two-fold. First is to determine what the state of the art is for techniques and approaches to evaluating VR. If the field has reached a consensus, how does it address the issues that come from investigating VR. The second purpose is to have a comprehensive understanding of the 4 research objectives of this thesis.

VR is a relatively new research topic, as most are in LIBs, where a majority of the work performed has been completed within the past 10 years. There is limited research into VR studies for the specific purpose of SOC estimation and SOH evaluation, meaning this is an area that could be contributed to from this thesis. There are more studies into methods of how to characterize VR and use it as an alternative to a pseudo-OCV test.

This review is organized by the model which was used to evaluate VR as this is an effective way to section off different fundamental approaches.

3.1. Equivalent circuit model for VR

The ECM is the most common model that is used in VR investigations. It uses basic circuit components, resistors, capacitors and an SOC dependant voltage source to model the behaviour of an LIB.

Not all studies use the same ECM, they can vary such as the fitting method, or the complexity of the model; i.e. how many RC circuits are used. Tran et al. [28] investigated the performance of different ECM complexities as a VR model on NMC, NCA, LFP, and LMO batteries. They use ECMs with 1 RC, 2 RCs, and 1 RC with a hysteresis term to compare error for a given chemistry. This hysteresis term is not given an equivalent circuit, simply a term which is summed to the equation. They run a reference performance test on the batteries followed by a pseudo-OCV test, then end with a pulse-rest test. They allow for a 30 minute rest after a charge pulse and a 60 minute rest after a discharge pulse. The ECM is then used to model a general driving profile for EV applications along with a constant current cycle. The root mean squared error (RMSE) is then calculated. These error values are as low as 6 mV to as high as 18 mV for a given chemistry and model. They

claim that for modeling LFP and NCA batteries the ECM should have 1 RC with a hysteresis term, where NMC and LMO should only use 1 RC.

Lin et al [15] show how temperature, age, and relaxation period change the OCV vs SOC relationship through VR investigation. Two tests were performed on NMC and LFP cells at various temperatures and SOHs, a pseudo-OCV test run at a 20 hour rate and another with VR periods of 2 hours. This data was then fit to a 1 RC model using an H_∞ and Kalman filter to predict coefficients. It was found that should the temperature be below 10°C that VR will take longer to reach SS-OCV and that VR methods outperform a pseudo-OCV test. It was also found that SOC could be predicted using this method in real time and operates at different SOH and ambient temperature. They claim that the VR method for characterizing a cells OCV vs SOC relationship was superior in terms of time required unless at low temperature ($< 10^\circ\text{C}$).

Petzl et al. [16] examine the difference between a pseudo-OCV test to a VR characterization for the purpose of finding the SOC vs OCV relationship similar to Lin et al [15]. They use a 2 RC model to extrapolate short rests to find an estimation of SS-OCV. After a 30 minute rest with a 5% SOC increment in charge until fully charged and then discharge. VR was shown to be a better representation for the SS-OCV vs SOC relationship than a 40 hour rate pseudo-OCV test. They show that using a 24 minute rest and 1% increase in SOC incremental voltage incremental capacity (dV/dQ) characteristics can be found to a higher quality than a 40 hour rate pseudo-OCV test. They claim that using a 6 minute rest VR can be extrapolated to within 4 mV of the SS-OCV of a 5 hour rest.

Li et al [29] investigated VR as a replacement of the pseudo-OCV test and for finding the SOC. The study was performed on LFP and NMC batteries. They use an ECM with 5 RC pairs to determine SS-OCV. They require multiple rests to characterize their model, first a 24 hour rest then 5 hour rests at 25%, 45%, and 85% SOC approaching from charge and discharge. This calibrates their model and results in a maximum error of 0.4% in SS-OCV estimation. They claim this set of tests can be used to find the OCV vs SOC curve while saving 52% of time from the original pseudo-OCV test which takes 72 hours.

Qian et al [8]. use a 2 RC ECM model to predict SOH of NMC batteries. They use VR over the lifetime of a cell to determine that there is a correlation between VR magnitude and

cycle count for two different voltage levels and directions of current. Then the cells are investigated with X-ray diffraction and half cell testing to confirm the cause of degradation. From this a VR algorithm is proposed for in-situ investigation of SOH.

Fang et al. [17] propose how to use an ECM model on VR to perform SOH investigations. They degraded NCA and NMC LIBs until 650 charge discharge cycles were reached via a 1 hour rate cycle. Every 100 cycles a calibration test was performed where the cell would charge or discharge 5% of SOC from bottom to top to bottom of charge. After each 5% increment in SOC a 2 hour VR period would occur where data was collected. An ECM with up to 3 RC circuits was used with one alteration. An α and β term were introduced into the definition of the time coefficient as can be seen in Eq [6].

Eq [6]

$$V_n e^{-\frac{t}{\tau_n}}; \tau_n = \alpha t + \beta$$

The definition of this time coefficient was a linear relation to time where α is the slope and β is the offset. This is different from convention as the time coefficient is normally a constant value known as the time constant. The α and β terms were curve fit for all the trials performed. They were monitored as a function of SOC and SOH. It was shown that as the batteries aged there was a general increase in α and β with a 3% error in SOH from a well trained model.

3.2. Electrochemical model for VR investigation

Secondly there is an electrochemical model which uses theoretical principles and equations to create specialized models of LIBs. Hu et. al [30] uses partial differential equations based on electrochemical principles. They modeled VR periods from 10 to 138 minutes at temperatures of 10°C and 40°C over a wide of range of SOC. They propose a schedule of short charge and discharge pulses to achieve SS-OCV faster than regular VR. They suggest it works by balancing the concentration of lithium in the positive electrode, electrolyte, and negative electrode via precise charge and discharge pulses. Because they are pulsing quickly the behavior can only be modeled by the more computationally complex models.

They claim the model can estimate SS-OCV within 2 mV while saving 33% to 78% of the procedure time depending on the cell temperature. They claim a 2 mV error would give an error of estimation of 4% SOC for a LFP cell.

Schindler et al. [22] investigated the possibility of using VR analysis with an ECM in conjunction with impedance spectroscopy for detecting lithium plating on the negative electrode. Equations based on Arrhenius' law were used to predict the impedance spectroscopy results. LFP cells from A123 were operated under conditions to promote lithium plating on the negative electrode to occur. A 5 hour VR period was analyzed via differential voltage analysis and compared to trials with a small current in the opposite direction of the current before relaxation. These tests were used in conjunction with impedance spectroscopy to show trends in the differential voltage profile during VR were shown to accurately determine lithium plating.

3.3. Mathematical model for VR investigation

Finally, there is a purely mathematical model which predicts the function of the battery by finding an equation that represents the voltage and current dynamics. A linear ordinary differential equation was used by Pei et al. [31] on LFP and lithium manganese oxide (LMO) cells. This equation was curve fit to four tests which approached various SOC values from charge and discharge. The VR period lasted for 24 hours, though only the first 60 minutes are shown. They show that for LMO batteries this model is valid for all SOC values, and that for LFP it is only valid for certain regions since there is more sensitivity required to make SOC estimations. They make an important distinction of current polarity, charge or discharge, being a factor to VR characteristics. As shown by Skrob et al. [27] there is a weak relationship between current polarity and the shape of the voltage vs time curve during relaxation. This relationship, while not as dominant as other factors, is shown to be significant for curve fitting, and so must consider the polarity of current before the relaxation period.

A mathematical analysis was done by Konz et al. [32] to identify lithium plating on the negative electrode through analysis of the VR curve shape. This was done by taking the derivative with respect to time of the VR profile. This would result in a peak, which

presents in the first 10 minutes of charge, that could be used with a basic mathematical model to quantify the plating severity. They showed that curve shape was dependent on the preceding current, SOC of rest, and lithium plating on the negative electrode. This is another indication of using VR for health analysis of an LIB.

3.4. Outcomes of literature review

3.4.1 Motivation for thesis objectives

The first objective is to determine a model which can accurately curve fit VR and account for changes between tests. There is no consensus on the specific model to use though the ECM has the most common. Even among this architecture there are significant variations. These variations make comparison of results in the field difficult as researchers have to base results on accuracy of the model and justify their model instead new findings and outcomes. For this reason, having a specific model that can be widely applied while retaining accuracy is valuable to the VR field.

The second objective is to estimate the SOC of the battery. Estimating the SOC is a difficult task for reasons outlined in Chapter 2. The time required is prohibitive as most of the literature agrees that 2-5 hours is required for an accurate estimation. This limits the applications where estimating SOC via VR is useful or feasible. EVs are an attractive area for this research to continue as a vehicle will often remain parked for hours. There exist some significant gaps in the literature here:

- The rest time used to determine SS-OCV can vary significantly from 2 mins to greater than 24 hours;
- No study mentions the separation of the IR voltage drop from the VR so it is unknown if this is being included in their curve fitting;
- The chemistries are often limited in studies with groups testing only one of the NCA, NMC, or LFP chemistries.

Because of this an investigation into how long a VR period is required could be impactful to consolidate future methods.

The third objective is to find a methodology to evaluate SOH and IR growth. There have been correlations found between evolution of VR characteristics (magnitude and curve shape), SOH, and IR growth [17] [8] [15] . There exist gaps in the literature here as there is no consistent methodology for SOH determination. Often tests are not performed at EOL conditions and therefore only capture a portion of the relationship. Having a study that can fully validate a methodology from BOL to EOL would be impactful.

The fourth and final thesis objective is to find and validate the findings of other research groups with the methodology created by the third objective. Should there be strong correlations between these VR metrics and degradation metrics validating them would serve as a contribution to the field.

3.4.2 Model architecture decision

From review of the literature, it is clear that the ECM is the most commonly used model. This is because of its adaptability, accuracy, computational simplicity, and familiarity. It can be easily altered to fit the required use case by adding more RCs or adding additional terms such as a hysteresis term. ECMs can be used with discrete time steps or can be functions of continuous time. The results from both models are similar and comparable for VR. The accuracy of the ECM is lower than an electrochemical or mathematical model but has been shown to produce reputable results from the studies reviewed. The VR field of study has reached a consensus on the ECM to be the primary model architecture used for good reasons:

- It does not require full history of the battery
- It is adaptable to different chemistries
- Curve fitting is well documented and uses common methods
- Computationally simple relative to other options

The ECM will be explored further and analyzed for the objectives of the thesis.

Chapter 4 Methods

Portions of this chapter have been published in the following article:

Theuerkauf, D.; Swan, L. Characteristics of Open Circuit Voltage Relaxation in Lithium-Ion Batteries for the Purpose of State of Charge and State of Health Analysis. *Batteries* 2022, 8, 77. <https://doi.org/10.3390/batteries8080077> [33]

And have been reproduced under MDPI licensing agreement (see Appendix A).

David Theuerkauf is the principal researcher and author of the article. He conducted the research as part of his MASc. He received supervision and guidance from his supervisor Dr. Lukas Swan, together they carried out the work, wrote the article, and communicated with the editor of the journal. Minor grammatical and content changes have been made to integrate the article within this thesis and incorporate the latest literature.

The Lithium-ion cells in this study were chosen from common high quality manufacturers. These cells were then tested on a battery testing system with procedures to achieve the thesis objectives. There were two studies performed to evaluate the research questions. Data from these procedures was captured and analyzed in MATLAB with a new voltage relaxation model based on an ECM.

4.1. Lithium ion cells

The lithium ion cells used in this experiment are high-quality commercially available cylindrical cells of the size format 18-65 (18 mm diameter, 65 mm length). The three cells chosen are pictured next to each other in Figure 20.

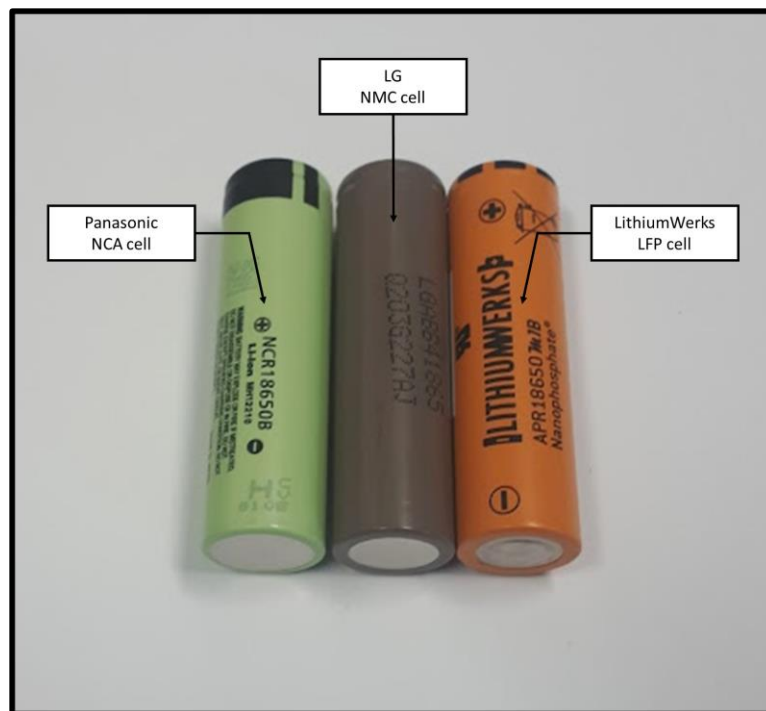


Figure 20: photograph of NCA, NMC, and LFP cells used in the studies.

All cells have graphitic negative electrodes, but different positive electrode materials which is how they are distinguished, they are:

- Panasonic NCR18650B (Nickel Cobalt Aluminum {NCA} positive electrode)
- LG Chem INR18650B4 (NMC positive electrode)
- Lithium Werks APR18650m1B {LFP} positive electrode; “nanophosphate”)

All cells have been designed for and deployed in a variety of applications including power tools, medical devices, EVs, E-bikes, and uninterruptable power supplies. Cells were purchased from reputable vendors and tested to verify they met capacity specifications. These cells are representative for their specific chemistry. A total of 12 cells were used, 4 from each chemistry. The first study used 1 cell from each chemistry where the second used 3. Their specifications of coulombic capacity, power capability, and cycle life are shown in Table 1. For their full specification sheet see Appendix C.

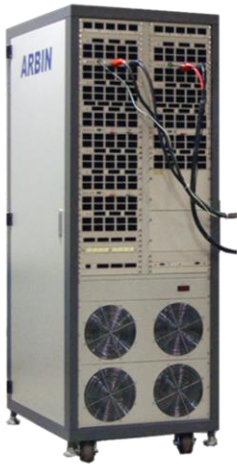
Table 1: Specifications of cells

Specification	NCA	NMC	LFP
Capacity (Ah)	3.2	2.6	1.1
Nominal voltage (V)	3.6	3.7	3.3
Voltage range (V)	2.50-4.20	2.75-4.20	2.00-3.60
Max Continuous Discharge Rate (C-rate; hour rate)	2; 0.5	2; 0.5	27; 0.037
Max Continuous Charge Rate (C-rate; hour rate)	0.5; 2	1; 1	3.6; 0.28
Cycles to 80% of original capacity	250	300	4000

4.2. Battery testing system

A Battery Testing System (BTS) is required for to cycle the batteries and measure the results. This BTS must measure the voltage, current, change in time, and temperature of the cells to a high degree of accuracy. The Arbin instruments BT2000 was chosen for its specifications and capabilities as can be seen in Table 2. Note that full scale range (FSR) is in both directions of charge and discharge for current.

Table 2: Arbin BT2000 specifications

Specification		Appearance	
Voltage			
	Range		0 – 20 V
	Accuracy		±0.01% of FSR*
	Stability		±0.01% of FSR*
	Interval		0.7 mV
Current			
	Range		0 – 100 A
	Accuracy		±0.01% of FSR*
	Stability		±0.01% of FSR*
	Impedance		~30 MOhm

The Arbin is a 3 Channel 2000W power cycler (20 V / ± 100 A). It is a high quality system that has all the capabilities required for this testing. There are 3 main channels for testing, one for each chemistry. It has 16 auxiliary voltage and temperatures which is more than enough to capture all the additional data required of cell voltage and temperature. The auxiliary channels can be assigned individually to one or multiple channels, meaning a consistent ambient temperature can be measured for all batteries. The software used to monitor the measurements for alarms and store the data on the local computer is MITS PRO 4.32.

There are some considerations that were kept in mind for testing on the Arbin. First is that the current requirement from a test is important. The Arbin has three measurement levels for the current. These are high (100 A/ -100 A), medium (2 A/ -2 A), and low (0.1 A/ -0.1

A) current settings. Each range has their own monitoring circuit with a different the specified accuracy due to the difference in FSR.

Calibration was performed on the Arbin to ensure that it would meet requirements of the test or specification of the machine. For calibration a professionally calibrated Fluke-289 digital multi-meter, was used as a true measurement device since it has superior accuracy for the voltage than the Arbin A full calibration report of the Fluke calibration is provided in Appendix D. The 289 was calibrated by the company Land and Sea on the 23rd of October 2021, with suggested recalibration on the 23rd of October 2024. The Fluke 289 was used to evaluate the calibration quality of the Arbin.

The process of calibration is such: Initial validation; Calibration; Secondary validation. Initial validation describes the previous state of the battery testing system, calibration alters the state, then secondary validation monitors how it changed. Error charts of before calibration and after calibration were created for voltage and current. Error in these charts is in percentage of FSR as defined by the specifications of the machine. There is also a line for what the manufacturer claimed as achievable by specification. Since voltage is important for this thesis it is shown in Figure 21.

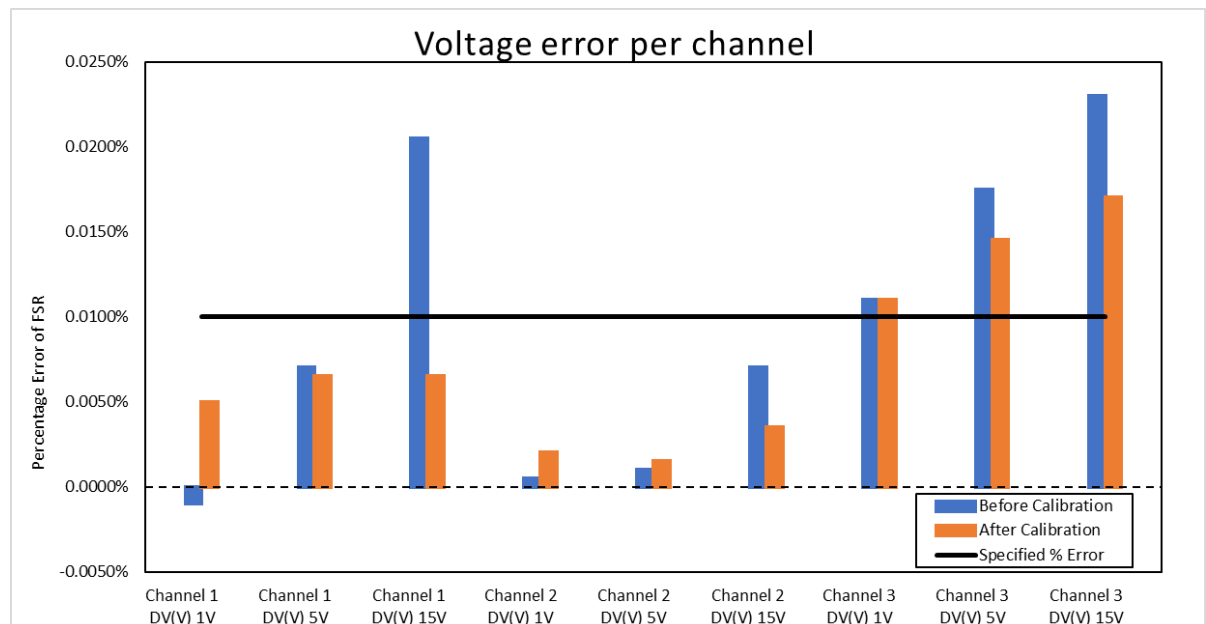


Figure 21: Calibration results of the Arbin II

From this figure we can see that calibration had the intended effect of reducing the percentage error of each channel or maintaining specification. Channels 1 and 2 had impeccable accuracy after calibration, while channel 3 improved but didn't achieve specification. Channel 3 was calibrated multiple times, and these were the best results received. Compared to the other battery testing systems in the lab it is still superior with this calibration. To determine the impact of this difference an analysis into the required sensitivity was performed.

VR magnitude is known from the literature review performed in Chapter 3 to be on the scale of 50 mV which is 0.25% of FSR. When this compared to the highest inaccuracy of 0.02% it shows that the calibration achieved should be sufficient. Having an order of magnitude lower inaccuracy relative to magnitude of measurement was deemed to acceptable for the required tests.

The current and temperature measurement also passed the calibration test of the machine. The full data for these can be seen in Appendix E.

4.3. Test set up

With the battery testing system chosen, calibrated, and validated a test set up was created to facilitate the 2 investigations. For the first investigation there were single cell tests with the set up seen in Figure 22

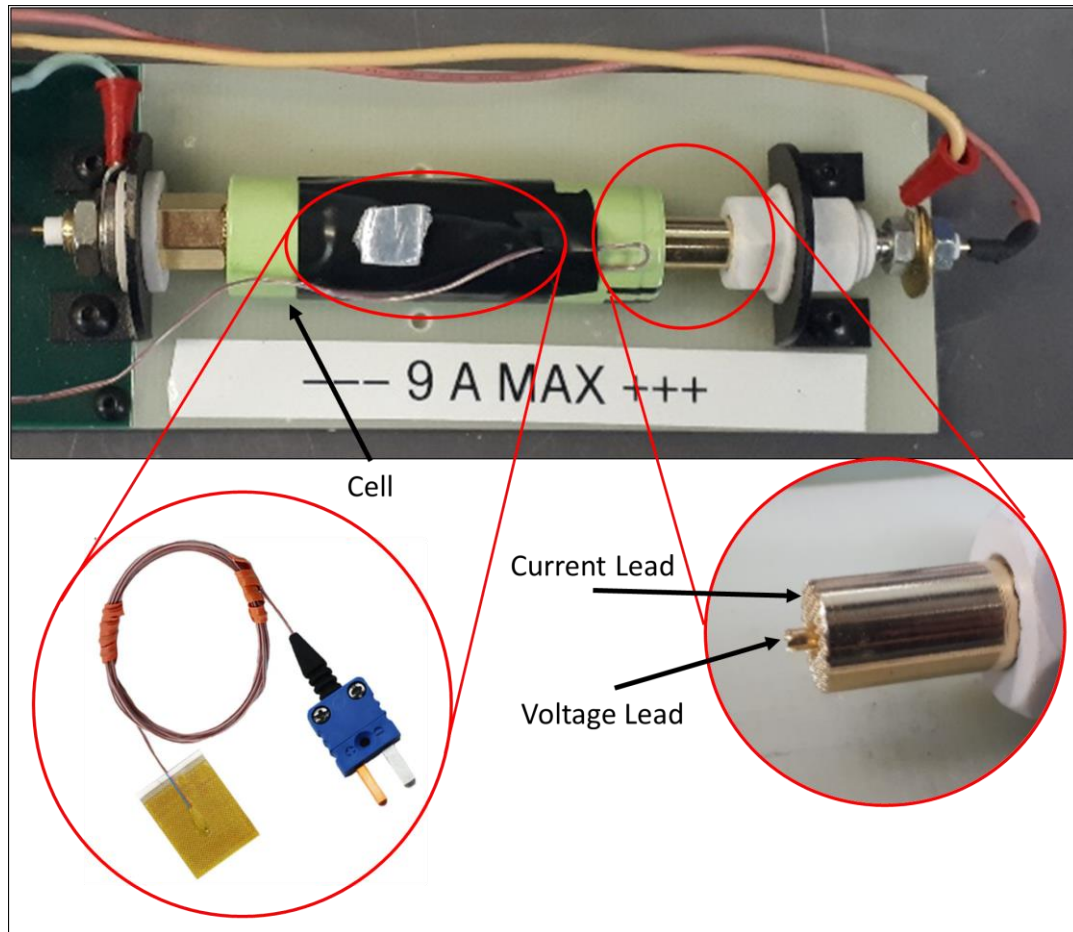


Figure 22: Test set up for a single cell

Here the cells were placed into a 4 wire cell holder with attached T-type thermocouple. The current leads are large and have good contact with positive and negative terminals. The voltage leads are in the center of the positive cell cap and negative casing's base. This allows for a consistent and repeatable voltage measurement. The temperature sensor is attached with electrical tape, and a small portion of thermal insulation tape over the sensor. This allows for better measurement of the cell temperature, while being small enough to not insulate the cell in any significant way.

For the second test set up all the cells were tested in 3P groups. For this investigation a new test set up was created and shown in Figure 23.

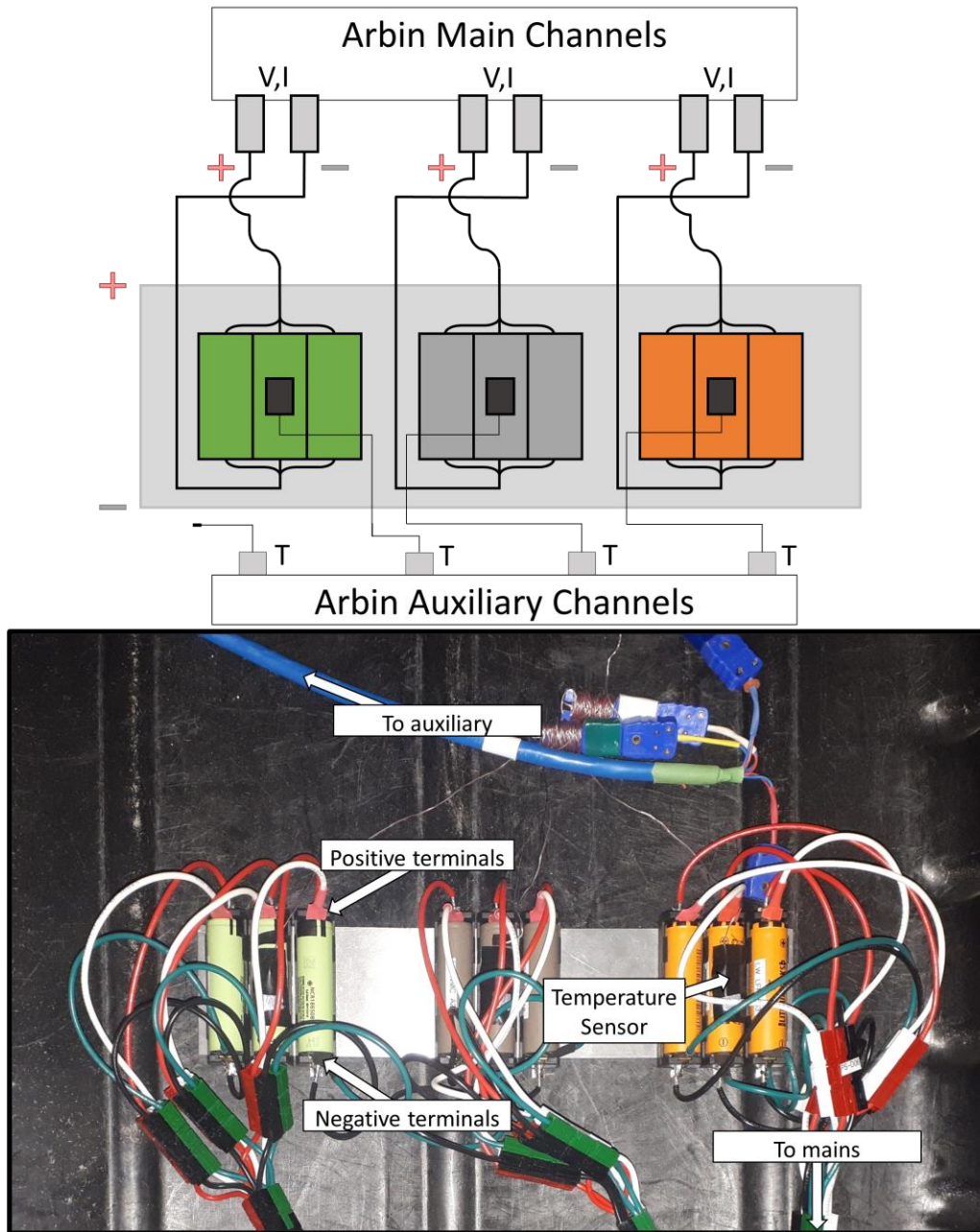


Figure 23: 3 parallel cells test set up as a diagram (top) and photograph (bottom)

The cells are parallelized from the wire harnesses and not a bus bar, or nickel strip. This is done for load balancing purposes. When a bus bar is introduced the placement of the BTS leads can load the cells unevenly. To alleviate this concern all the cells are placed into simple 4 wire cell holders, and connected via wires of consistent length, so that all

cells of the group have roughly similar measurement impedance. Next all the batteries are attached to metal back plate. This acts not only as structure but a conductive heatsink since there is increased heat generation. Finally, the temperature sensors are attached to the center cell only. This is because all cells are experiencing the same conditions and are conducting heat to each other. Therefore, in the case of a failure this temp sensor will read the value and end before catastrophic failure.

4.4. Test schedules for first study

4.4.1 Reference performance test

A Reference Performance Test (RPT) was created to evaluate the maximum discharge capacity of the cells. All the batteries in this study were run on an RPT twice to have confidence that they met specification. All specification sheets for the cells are available in Appendix C.

Table 3: Reference performance test schedule

The BTS monitors the temperature for safety control along with the voltage and current for data analysis and safety control. The 3 cycles in an RPT each have a purpose. The first is for capacity assurance as charging to 100% SOC removes any effects of starting the battery

Step	Type	Control parameters	Description
1	Rest	30 s and cell temperature < 30°C	Ensuring safe operations
2	CC Discharge	0.5 C to low voltage value	As defined by spec sheet
3	Rest	30 s and cell temperature < 30°C	
4	CC Charge	0.5 C to high voltage value	As defined by spec sheet
5	CV Charge	0.5 C / high voltage for 1 hour	1 hour results in lower currents than spec sheet requires
6	Rest	30 s and cell temperature < 30°C	
7	Loop	From Step 2 to 6 for 3 Loops	1 st charge cycle is for capacity assurance 2 nd charge cycle is for thermal acclimation 3 rd charge cycle is for results to be used

at partial SOC and not receiving the maximum discharge capacity. The second cycle is for thermal acclimation, batteries have improved performance at higher temperatures, therefore ensuring that the cells have reached a thermal equilibrium before results are measured is important. Finally, results are taken from the third cycle to have the highest

quality and confidence that they represent the consistent operation of the cell. By performing these 3 cycles every time the results are comparable and give a good comparison for the maximum discharge capacity of the battery. Once a battery has been run through the initial RPTs and meets specification it is then ready for the analysis testing.

4.4.2 Three hour voltage relaxation at 10% SOC increments

The 3 hour VR test was used to evaluate VR and SS-OCV at various SOC values. As seen in Table 4, the test begins by fully charging the battery. It then discharges in 10% SOC increments, each followed by a 3 hour relaxation. Once the low voltage limit is reached, the battery charges in 10% SOC increments, each followed by a 3 hour relaxation, until the high voltage limit is reached. This test takes more than 60 hours to complete and is not feasible for a vast majority of applications due to this time constraint. This allows the study to find where the best position in SOC would be for a real application. The end of constant current charge is dictated by a voltage limit. Should the rate or IR increase it will reach this voltage limit earlier in the SOC range limiting where can be evaluated as the cell degrades.

Table 4: Three hour voltage relaxation test schedule

Step	Type	Control parameters	Description
1	Rest	30 s and cell temperature $\leq 30^{\circ}\text{C}$	Initial data
2	CC Charge	2 hour rate to high voltage limit	As defined by specification sheet
3	CV Charge	hold voltage for 1 hour	1 hour results in lower currents than specification sheet requires
4	Rest	30 s and cell temperature $\leq 30^{\circ}\text{C}$	
5	CC Discharge	2 hour rate for 10% rated coulombic capacity	Discharge 10% SOC
6	Rest	3 hour rest	Collecting VR data
7	Jump	To Step 5 until low voltage value is reached	Discharging to low SOC for 9 data points
8	CC Charge	2 hour rate for 10% rated capacity	Charge 10% SOC
9	Rest	3 hour rest	Collecting VR data
10	Jump	To Step 8 until high voltage limit is reached	Charging to high SOC for 9 data points
11	Rest	30 s rest	End rest

One outcome for the first study was to show the relationship between VR magnitude and SOC. Another outcome was to confirm that 60% SOC had the highest VR magnitude, as suggested in literature [34]. This also determines what SOC value will be used in the 24 hour test should it be different from literature as the SOC with the highest VR magnitude is ideal for that test.

4.4.3 Twenty four hour voltage relaxation

The 24 hour VR test was created to evaluate VR at the SOC value with highest VR magnitude. The test schedule is shown in Table 5. Here the battery is fully discharged to hit a low baseline. Once this is reached it is charged to the optimal SOC for VR magnitude. Since there is a 24 hour rest this limits the number of rests that can occur to finish the study in a reasonable time frame. Therefore, only one rest can occur and picking an optimal SOC is important. This value was determined by the results of the 3 hour voltage relaxation test.

Table 5: Twenty-four hour VR test schedule

Step	Type	Control parameters	Description
1	Rest	30 s and cell temperature $\leq 30^{\circ}\text{C}$	Initial data
2	CC Discharge	2 hour rate to low voltage limit	As defined by spec sheet
3	Rest	30 s and cell temperature $\leq 30^{\circ}\text{C}$	
4	CC Charge	2 hour rate for optimal rated capacity	Charge to optimal SOC (LFP = 66%; NCA, NMC = 45%)
5	Rest	30 minute rest	Collecting VR data
6	Rest	23 hour 30 minute rest	Collecting VR data

The purpose of this test is to determine the period required to reach SS-OCV. It will also distinguish how long is required for high VR model accuracy, and the required complexity of the model for SOC and SOH investigations.

4.5. Test schedules for second study

4.5.1 Reference performance test

The purpose of the RPT is to have an accurate measurement of the capacity of the cell as it ages. For this reason, the RPT used to characterize the cells for the first study is used for this test schedule. Internal resistance test

IR was monitored as the cell aged for the purpose of finding any correlation between VR metrics and IR growth. To achieve this the following test schedule was created as can be seen in Table 6. i

Table 6: Internal resistance test schedule

Step	Type	Control parameters	Description
------	------	--------------------	-------------

1	CC Charge	High voltage limit	Charge to full SOC
2	CC/CV Charge	1 hour hold	Charge to full SOC
3	CC Discharge	2 hour rate rate for 12 minutes or until low voltage limit	Discharge 10% SOC
4	CC Discharge	1 hour rate pulse for 30 seconds or until low voltage limit	Discharge pulse to find IR
5	Rest	Rest 30 seconds at low voltage limit.	Rest before switching it charge
6	CC Charge	2 hour rate for 12 minutes or until high voltage limit	Charge 10% SOC
7	CC Charge	1 hour rate pulse for 30 seconds or until high voltage limit	Charge pulse to find IR
8	Rest	30 s rest	End rest

4.5.2 Voltage relaxation test

After the first study there was an interest in watching to see if the profile of VR vs SOC would change as a function of SOH or IR growth. To accomplish this the same 3 hour rest schedule was used at the various Ah-CycEq.

4.5.3 Degradation test

The goal and purpose of the degradation test was to cycle the cells as much as possible. Fifty cycles were set to be performed on the battery in approximately 3 days as can be seen in Table 7.

Table 7: Degradation test schedule

Step	Type	Control parameters	Description
1	Rest	30 s and cell temperature $\leq 30^{\circ}\text{C}$	Initial data
2	CC Discharge	1.5 hour rate until low voltage limit	Discharging to low SOC
3	Rest	30 s and cell temperature $\leq 30^{\circ}\text{C}$	Rest to switch from discharge to charge
4	CC Charge	1.5 hour rate until high voltage limit	Charging to high SOC
5	Jump	To Step 1 until 50 cycles	Repeating cycle 50 times
6	Rest	30 s rest	End rest

Fifty cycles was chosen as this would theoretically use 10% of the rated cycles of the NCA cells from the specification sheet. To achieve this in the smallest time frame possible, the fastest rate was chosen that would not endanger the batteries to fail catastrophically. A 1.5 hour rate was chosen for each battery chemistry. This rate was slightly above the suggested allowable rate for the NCA cells, but not to the level that promotes unrealistic degradation. The 1.5 hour rate is below the suggested rate for the NMC, and LFP cells. This means that the cells will degrade less per cycle and gives the ability to see small changes in SOH from VR.

4.6. Data capture

Experimental data is captured from the Arbin and put into a proprietary “.res” format. This is processed until it becomes a “.mat” format results output from MATLAB via the process found in Figure 24.

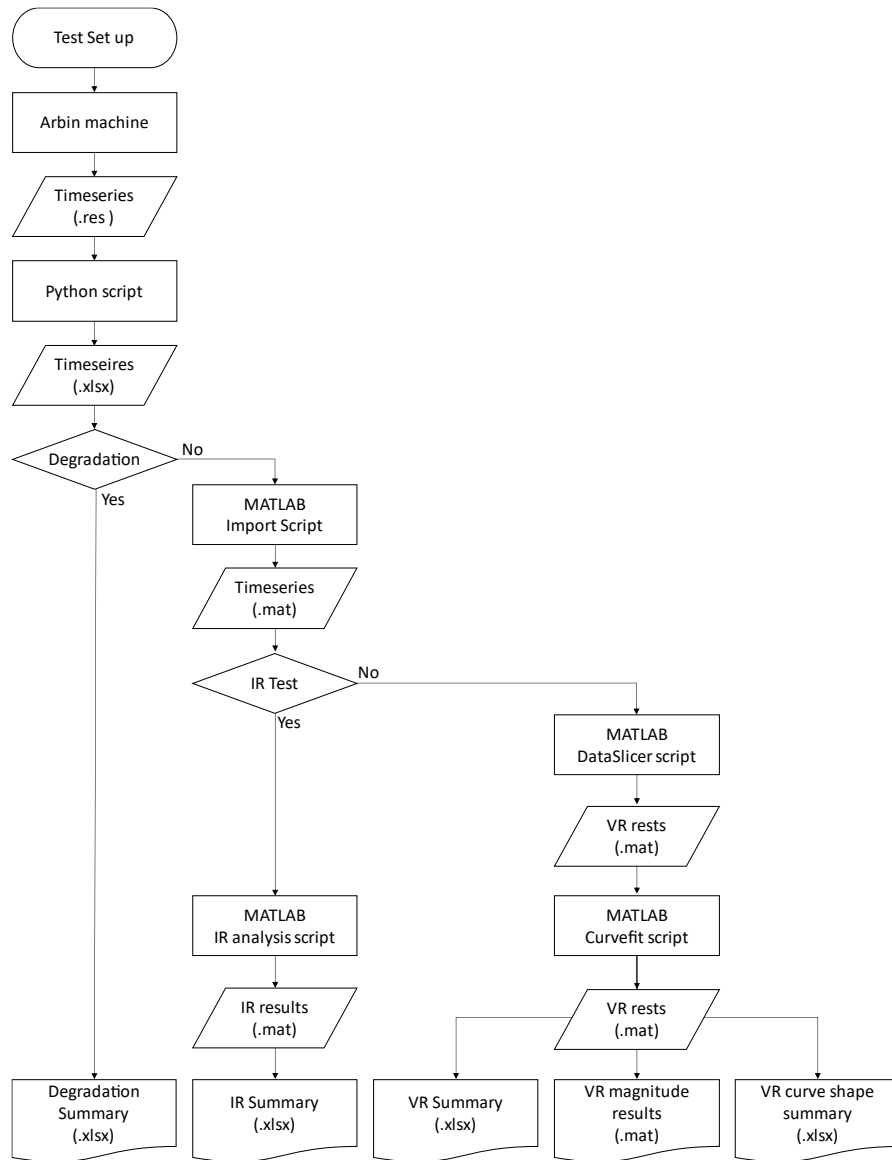


Figure 24: Data flow from BTS to MATLAB analysis and summary of results

Degradation tests require no alteration and are imported to MATLAB for cycle visualization purposes. IR tests require one analysis before they are compiled into an Excel spreadsheet for analysis of trends.

VR data requires more processing for curve fitting. The VR period is separated from the normal cycle to remove the initial instantaneous IR voltage drop. This is done by taking the first data point immediately following the open circuit condition as the start of the timeseries since the IR voltage drop is immediate at open circuit. Due to the limitations of

the battery cycler the first datapoint is 0.1 s after the IR drop. After this a curve fit is performed via a script. This script outputs a results file that has useful information for three different outputs of the data processing. All MATLAB analysis scripts are available in the Appendix F.

4.7. Mathematical analysis of voltage relaxation

4.7.1 Novel battery model architecture and coefficient determination

The model chosen was the ECM as expressed in Chapter 3. The standard ECM for a battery was altered for ease of fitting the VR curve shape and estimating SS-OCV since there is no need for modeling an entire cycle. These changes have not been made in any of the reviewed literature and are considered a research contribution to improve VR studies going forward. Since these alterations are novel, it is renamed to the Voltage Relaxation ECM (VR-ECM) as can be seen in Figure 25.

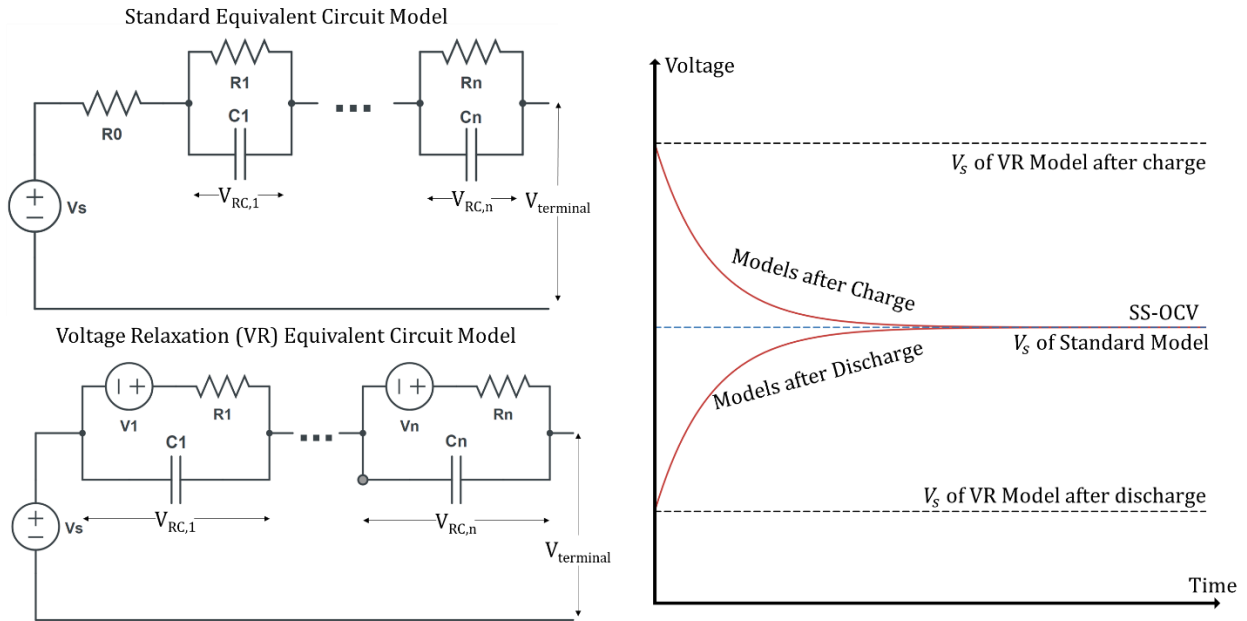


Figure 25: Standard equivalent circuit model and proposed VR-ECM of an LIB with its response to open circuit conditions

The alterations made were an additional ideal voltage source with each RC pair and a removal of the series resistance R_0 , which is responsible for the IR voltage drop in the original model. The ideal voltage sources are fit with the RC values for each VR period. In open circuit conditions the RC pairs in the VR-ECM will always be charging, whereas the

standard model will always have them discharging. These changes are primarily for SS-OCV determination which has impacts on curve fitting accuracy. For each model the definition of V_s is different. In the standard model it represents the SS-OCV, whereas in the VR model it represents the terminal voltage at open circuit. Both models have the same initial equation for V_{terminal} , the voltage that appears at the battery terminals, Eq [7]. Note that $t = 0$ is when the open circuit condition is applied and thus R_0 does not factor into the voltage equation for relaxation, which starts at $t = 0^+$. Therefore, it was removed in the VR model.

Eq [7]

$$V_{\text{terminal}} = V_s + \sum_{p=1}^n V_{\text{RC},p} \text{ @ } t = 0^+$$

In, Eq [7] $V_{\text{RC},p}$ is the voltage of each RC pair as a function of time. These terms are summed with V_s for the total voltage of the battery. As shown Figure 25 the initial value of voltage for each RC can be inverted to represent these curve shape approaching from discharge or charge. For the standard model the RC circuits are charged with a voltage that is negative relative to V_{terminal} at $t = 0^+$. For the VR model the ideal voltage source polarity is reversed. With the original model the RC pairs will operate via Eq [8] compared to the VR model where they operate via Eq [9].

Eq [8]: Voltage of an RC pair in the ECM

$$V_{\text{RC},m} = V_m e^{-\frac{t}{\tau_m}}; \tau_m = R_m C_m$$

Eq [9]: Voltage of an RC pair in the VR-ECM

$$V_{\text{RC},n} = V_n \left(1 - e^{-\frac{t}{\tau_n}} \right); \tau_n = R_n C_n$$

For both Eq [8] and Eq [9] τ is the time constant of the RC pair. Between Eq [8] and Eq [9] V has a different definition. For Eq [8] V_m represents the initial value of the RC pair as V_{RC} will decay to 0 as time approaches infinity. Eq [9] has V_n represent the final value of the RC pair since as time approaches infinity the value of the equation will be V_n . This

difference is what changes the meaning of the series voltage source V_s as well, which has significant consequence. First, if Eq [8] is substituted into Eq [7] V_s is the SS-OCV. This means that any curve fitting using this equation will take close to the final value of the data set as the SS-OCV. Using Eq [8], the standard model, is limited to long relaxations where the final value of the dataset is as close to SS-OCV as possible. An incorrect SS-OCV would misrepresent the long term effects on the battery. Next, Eq [9] is substituted into Eq [7] to produce Eq [10].

Eq [10]: Full definition of V_{terminal} in the VR-ECM

$$V_{\text{terminal}} = V_s + \sum_{p=1}^n V_p \left(1 - e^{-\frac{t}{\tau_p}} \right) \text{ for } t = 0^+$$

V_s is now the initial value of the battery at $t = 0^+$ instead of the SS-OCV. This makes the SS-OCV value the sum of all RC pairs voltage, $V_{RC,p}$, and the series voltage source, V_s . This was shown graphically in Figure 25. This way, when curve fitting SS-OCV can be larger or smaller than the final value of a dataset since it is not assumed to be V_s and dependent on multiple coefficients. This is the primary reason that the standard model was changed to the VR model for better curve fitting on VR datasets.

To curve fit Eq [10] the values of the coefficients $\{ V_s, V_1, \tau_1, V_2, \tau_2, \dots, V_n, \tau_n \}$ are iterated. The Levenberg Marquardt algorithm was chosen as it can perform fitting over the large time constant ranges while being quick to solution. This fitting technique for non-linear functions minimizes error based on the sum of the residuals squared. It is an interpolation between the Gauss-Newton algorithm and gradient descent method. The Levenberg-Marquardt algorithm is dependant on initial values and can be susceptible to ending in local minima should the initial value be poorly estimated. To alleviate this concern 5 initial values were used which were bound from 0 to half VR magnitude for the voltage terms and spanning 3 orders of magnitude for the time constants. Initial values were estimated by scaling previous estimations that produced a low error.

4.7.2 Assessing model inaccuracy impacts on SOC and SOH

To assess the model accuracy for SOC estimation and SOH evaluation 2 metrics are required. First, is the estimated settling time (EST) of a model. EST is the amount of time

that it will take for the RC circuit with the largest time constant to reach 98% of steady state. A value of 98% was chosen as it is equal to 5 time constants and after this point there is little evolution of the profile remaining. Second, Root mean squared deviation (RMSD) was evaluated and put in percentage of the VR magnitude, as shown in Eq [11] to evaluate goodness of fit.

Eq [11]

$$RMSD \% = \frac{\sqrt{\frac{\sum_{d=1}^D (\hat{V}_{\text{terminal},d} - V_{\text{terminal},d})^2}{D}}}{VR_{\text{magnitude}}}$$

In Eq [11] $\hat{V}_{\text{terminal},d}$ is the estimation of $V_{\text{terminal},d}$ at a given datapoint d , and D is equal to the total number of datapoints. This allows for an understanding of not only how good the fit is relative to the VR magnitude, but how it can change with different numbers of RC circuits.

For SOC estimation, SS-OCV will be found from the model and used to find SOC from the OCV vs SOC relationship found from previous lab studies performed on these cells. To determine the possible error the profile is examined for the smallest magnitude slope. This is important as it will produce a worst-case scenario of highest error in SOC estimation for an SS-OCV prediction. The RMSD is multiplied by the VR magnitude to find the possible voltage difference between modeled and measured SS-OCV. RMSD is used to calculate the SS-OCV error as it represents average deviation over the full data fit. This means that theoretically the SS-OCV prediction could be inaccurate by the RMSD percentage. In all cases of this study the RMSD calculated error is higher than or equal to the difference observed for all trials, so it is a conservative estimate. This voltage difference is then added and subtracted from the OCV value where the smallest slope occurs to produce an estimate of the SOC range each SS-OCV value could represent. Figure 26 shows this SOC error band visually along with the process. For practical applications, I propose that the error of SOC should be 0.5% or less. This level of measurement makes the limiting factor of accuracy the measurement equipment and not the process.

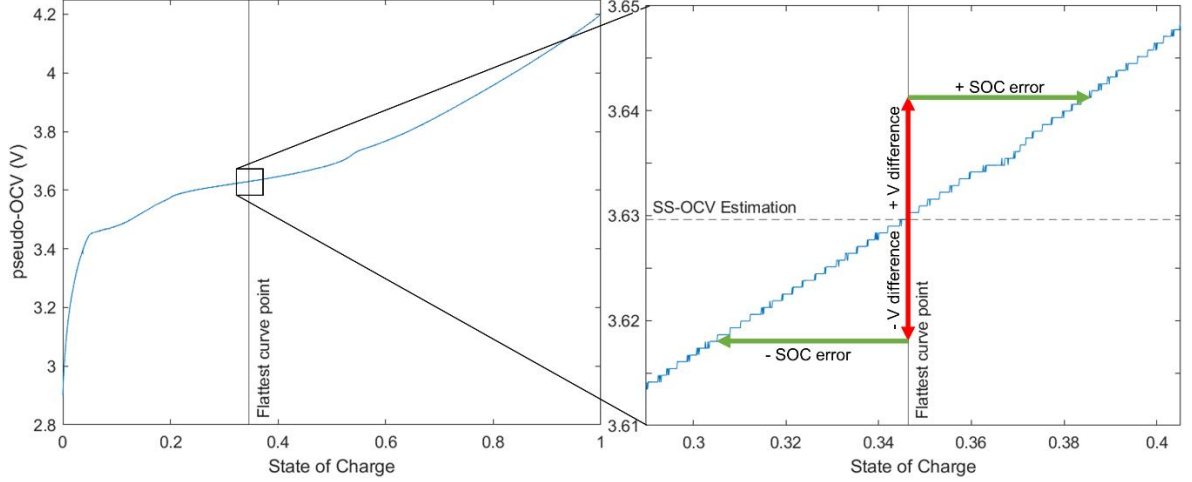


Figure 26: Pseudo OCV vs SOC with inset showing SOC error determination

For SOH evaluation it is important to have good VR curve representation in an appropriate projection period, so both EST and RMSD are used. EST is a pass-fail metric to show when the model predicts the profile will stop evolving and compare this to measured data obtained from the 24 hour test. If the modeled EST value is too high, the long term effects of VR are being misrepresented. RMSD shows how good the curve fit is for the captured data and minimizing this indicates the model is adequately capturing the VR trend.

4.7.3 Assessing correlation of variables

To determine the correlation between different metrics such as: IR; capacity; VR magnitude; and VR curve shape; visual inspection can give insight, but quantitative assessment is required. To find relationships between these variables Pearson correlation coefficients were used to determine if there was correlation between variables. A Pearson correlation coefficient is defined by the mathematical equation in Eq [12]

Eq [12]: Pearson correlation coefficient

$$r = \frac{\sum(x_i - \bar{x})(y_i - \bar{y})}{\sqrt{\sum(x_i - \bar{x})^2 \sum(y_i - \bar{y})^2}}$$

This value of r can range from 1 to -1 with higher magnitude values being more correlated and lower magnitude values being less correlated. If r is positive then there is positive correlation between the variables, as one increases the other increases as well. The same hold true for negative values and correlations.

After correlations are assessed, the variables are assessed by a goodness of fit to a linear interpolation of the data. This is done to show if there is a simple relationship that can be used between them. This R^2 value represents how good the fit to the linear relationship is. The reason both correlation and goodness of fit are required is to assess if there is a useful relationship between variables. Figure 27 shows that should there only be high R^2 or good correlation, cases a and b, there is no useful relationship that could be used to predict either variable. In case a any x value leads to the same y value. In case b there is no certainty that an x value is related to a y value. In case c however, knowing one variable leads to a reasonable estimation of the other.

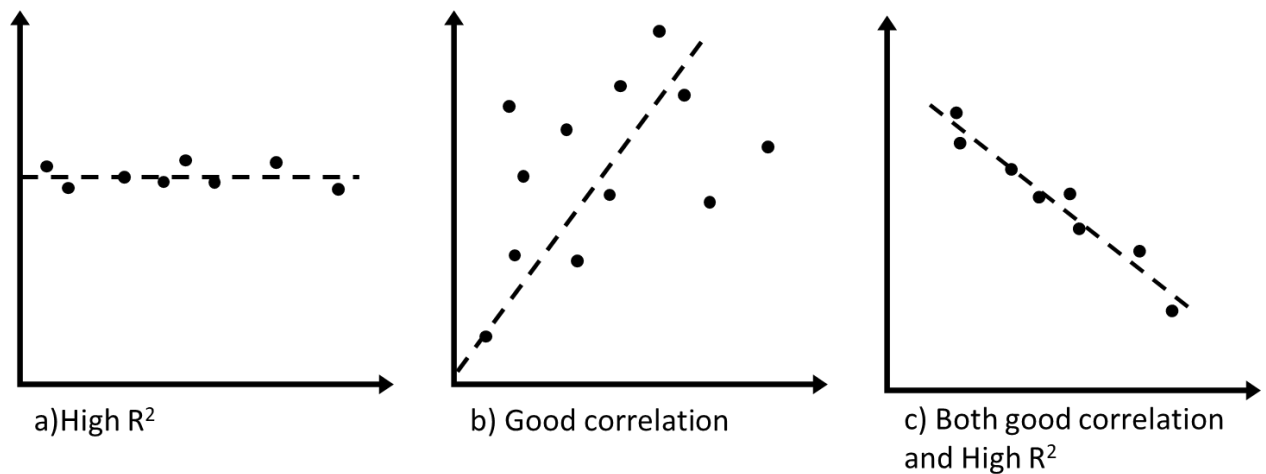


Figure 27: Importance of correlation and R^2 for useful relationship

Chapter 5 Investigation of Voltage Relaxation for Cell Parameterization

Portions of this chapter have been published in the following article:

Theuerkauf, D.; Swan, L. Characteristics of Open Circuit Voltage Relaxation in Lithium-Ion Batteries for the Purpose of State of Charge and State of Health Analysis. *Batteries* 2022, 8, 77. <https://doi.org/10.3390/batteries8080077> [33]

And have been reproduced under MDPI licensing agreement (see Appendix A)

David Theuerkauf is the principal researcher and author of the article. He conducted the research as part of his MASc. He received supervision and guidance from his supervisor Dr. Lukas Swan, together they carried out the work, wrote the article, and communicated with the editor of the journal. Minor grammatical and content changes have been made to integrate the article within this thesis and incorporate the latest literature.

5.1. Purpose

The purpose of this study is to determine methods for SOC estimation and SOH evaluation. Most commonly, the VR is used to estimate SS-OCV and correlate to SOC, via a lookup table. Some studies evaluate at singular SOC points which are not consistent, and do not account for the changing shape of VR curves at different SOC values. Other studies use a range of SOC values approaching from charge and discharge. The length of relaxation can be from 6 minutes to 24 hours, with claims of being fully rested at any of these values. The modeling techniques are different, and even similar models used different curve fitting methods. This makes it difficult to compare or contrast the findings of these studies or translate them into useful or practical applications for assessing SOC or SOH of a battery.

This leads to four research questions to improve the consistency of VR studies:

1. How does the VR magnitude and curve shape change as a function of SOC value?
2. What period of time is necessary for the battery to be considered fully rested at SS-OCV?
3. For estimating SOC, how complex must a model be, and how short can the VR period be, to accurately determine SS-OCV?
4. For estimating SOH, how complex must a model be, and how short can the VR period be, at a sensitive SOC position, to accurately capture VR magnitude and curve shape?

To be practical for use in applications some guidelines can be established:

1. The model should capture the dynamic behavior of the voltage curve while being computationally simple to curve fit.

2. VR for SOH evaluation will likely be implemented during charge as most applications have specific demands during discharge that prohibit long open circuit conditions. For example, EV and mobile devices are often left unattended while charging thus presenting a VR opportunity.
3. The model must function over the complete SOC operating range.
4. A consistent SOC for SOH estimation must be chosen to maximize VR magnitude sensitivity and curve shape changes for estimating SOH.

5.2. Results and discussion

5.2.1 VR magnitude vs SOC

Results of the 3 hour VR test for each battery chemistry are the left column of plots in Figure 28. Discharge values are shown in gray and charge values are shown in red. The left column of Figure 28 shows the terminal voltage profile vs SOC, throughout the discharge and charge cycle. The SS-OCV after a 3 hour VR period is also included as a circle point for each VR.

All discharge SS-OCV are lower than charge SS-OCV, illustrating voltage hysteresis in the battery. Substantial voltage profile changes occur at the beginning and end of discharge and beginning of charge, which is common in all LIBs. The SOC at which the charge control changes from constant current to constant voltage can be seen as the horizontal line portion of the terminal voltage plot. No SS-OCV points are given during the constant voltage charge phase since it would have a different current before relaxation making results non-comparable.

The right column of Figure 28 shows the calculated VR magnitude vs SOC for both discharge and charge. From the research questions and guidelines established, it is known that the VR magnitude should be maximized. Figure 28 clearly shows varying VR magnitude depending on both battery chemistry and SOC, suggesting an optimal SOC value for VR magnitude can be identified.

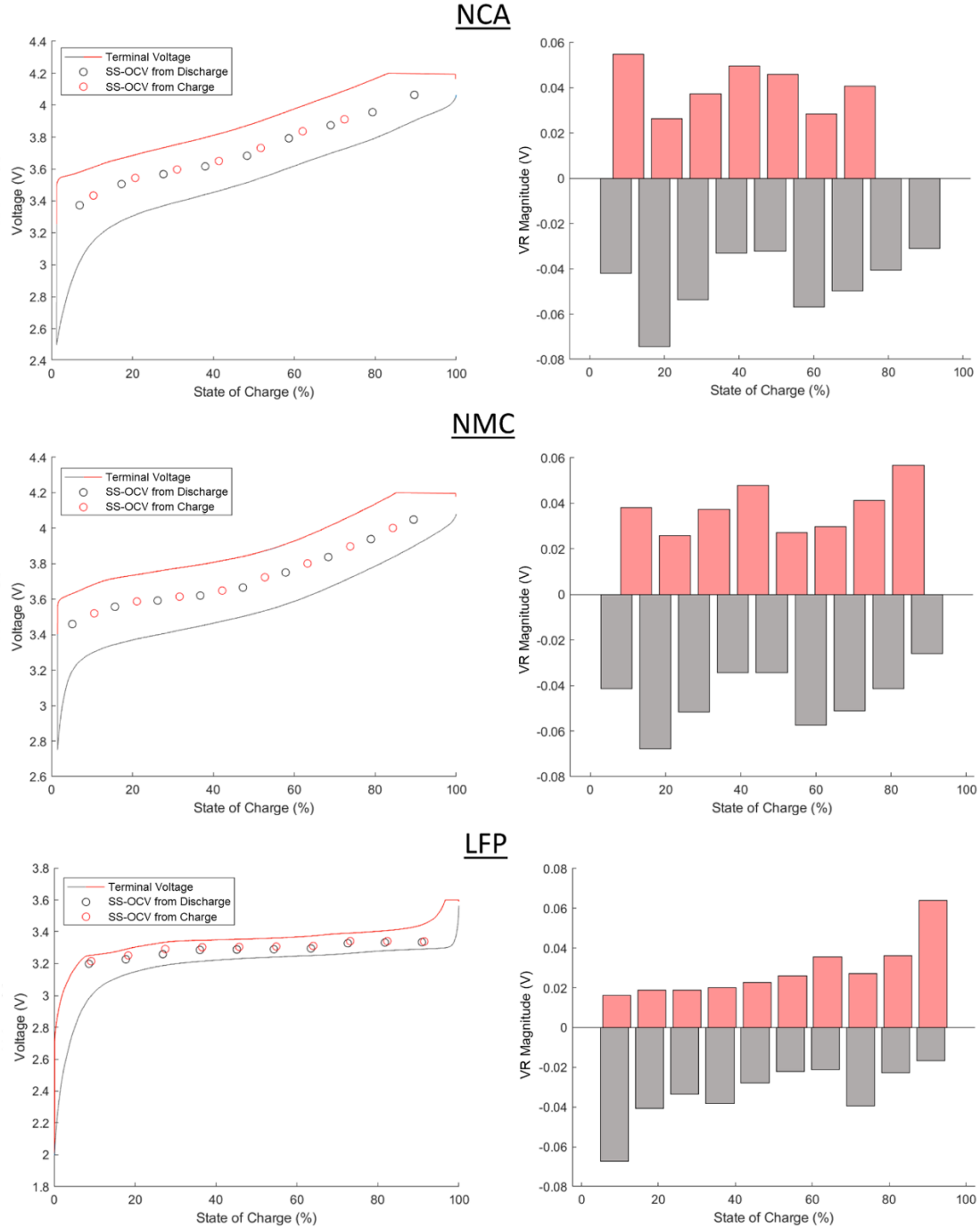


Figure 28: VR from operational profile as a function of SOC with values post discharge current shown in gray and values post charge current shown in red

NCA and NMC chemistries show similarities for terminal voltage profile, SS-OCV trends, and VR magnitude. A final charge VR magnitude datapoint is not obtained for the NCA chemistry at high SOC due to earlier exit of the constant current phase from reaching the high voltage limit. This shows why high SOC values on charge are not be selected due to

IR growth inhibiting a comparable VR as the battery wears. There is a local peak of VR magnitude while charging at low SOC for NCA. This should also not be selected as capacity loss from battery wear could inhibit it being captured appropriately. Both chemistries have local VR magnitude peaks at approximately 45% SOC on the charge, and at 15% and 55% on discharge. The VR magnitude at 45% SOC on charge is therefore suggested for use in assessing SOH and for the 24 hour VR of both NCA and NMC.

LFP shows different characteristics to NCA and NMC. First, it has a much smaller constant voltage phase than either the NMC or NCA. It is noteworthy that high SOC on charge and low SOC on discharge are the peaks of VR magnitude. This is correlated to the IR of the battery, however the test method ensured that these values were not biased by the IR voltage drop. High SOC values on charge may have high VR magnitude, but they should not be selected as IR growth may inhibit obtaining a comparable VR at this SOC as the battery wears since it will be in constant voltage instead of constant current. Instead, a local maximum of VR magnitude on charge can be identified at 65% SOC, and this value is suggested for use in assessing SOH and for 24 hour VR test of LFP.

5.2.2 VR shape and SS-OCV

Results of the 24 hour VR test are shown in Figure 29. Note that each battery approaches open circuit while charging to the SOC value with highest VR magnitude: 45% for NMC and NCA, and 65% for LFP. The batteries then enter open circuit and relax. The vast majority of VR magnitude occurs within minutes, so an inset plot of log time in seconds is given to provide better resolution. The profile of VR is more complicated than the linear time graph would suggest. For the time periods of $1\text{E}0\text{--}3\text{E}2$ s (up to 5 minutes) and $1\text{E}3\text{--}1\text{E}4$ s, (up to roughly 3 hours), these voltage profiles have the shape of exponential functions. They exhibit a clear lead in, linear region and fade to constant value that exponentials have when plotted in a semi-log plot. There is a cross over period in between them of $1\text{E}2\text{--}1\text{E}3$ s (approximately 2 minutes to 16 minutes). During this period, there is only a linear portion observed in log time with no lead in or fade to constant. Finally for the time period greater than $1\text{E}4$ s (roughly 3 hours), there is little change in the voltage profiles.

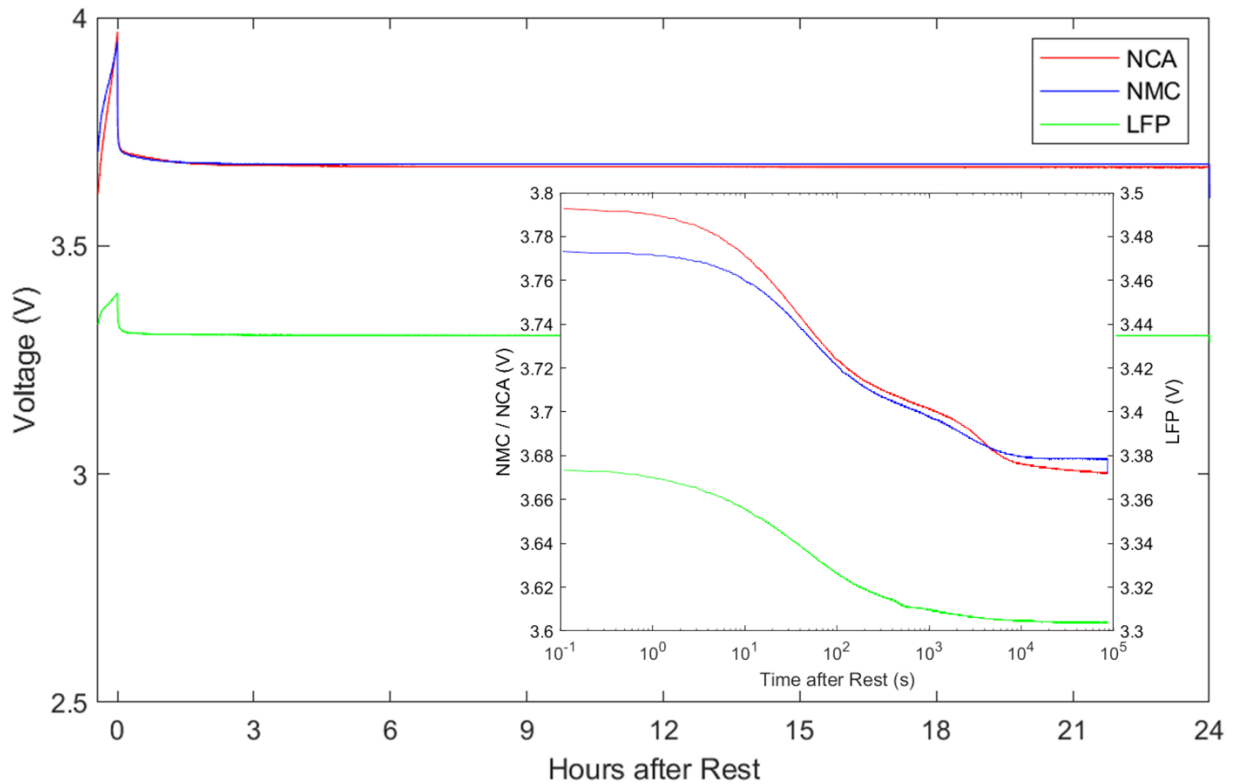


Figure 29: Twenty-four Hour Relaxation shown on a linear and logarithmic scale of NMC, NCA, and LFP chemistries

NCA and NMC have similar voltage values due to their nickel based positive electrode material. There are three notable comparisons between the batteries. First, the NCA battery starts at a substantially higher voltage, but by 3E1 s approaches the voltage value of NMC. Second, the NCA and NMC exhibit similar VR during time period 3E1 to 2E3 s. Third, the NCA voltage substantially declines at 4E3 s and crosses below the value of NMC.

The NMC battery achieves 98% of its SS-OCV value within 7E3 s (roughly 2 hours) and reach steady state at 2E4 s (roughly 5 hours). This is different from NCA which does not reach a SS-OCV value. There was concern that a parasitic current applied to the batteries by the voltage measurement (16 bit; 10 MΩ) could be slowly discharging the battery and influencing this. To investigate this the NCA cell was tested again but was normally physically disconnected from the voltage measurement circuit. Voltage leads were re-attached only temporarily to take a measurement at 1 s, 10 s, 100 s, 30 minutes, 3 hours, and 24 hours. This verification test produced identical results, indicating that this VR is an effect of the battery and not a function of the applied voltage measurement circuit.

The LFP battery achieves 98% of its SS-OCV value within 2 hours which is comparable to the NMC battery. It takes slightly longer at 4.6 hours to reach SS-OCV. LFP initially appears similar to the other chemistries in terms of its VR curve shape. There is a similar profile until 2E2 s with a clear lead in and linear region. However, after this time it lacks the visible inflections, points demonstrated by both NCA and NMC. This would suggest that simpler VR equivalent circuit model may be all that is required when modeling this chemistry.

From the guidelines the shortest VR period is preferable if the model can accurately capture the curve. A relaxation period of 3 hours is sufficient to achieve above 98% of the SS-OCV for SOC estimation from the captured data for NMC and LFP batteries. This means that there will be a small amount of voltage evolution that would occur after the rest period is finished. A relaxation period of 3 hours would also be reasonable to find the characteristics of the VR curve shape for fitting applications. This period represents all the significant VR curve shape data. For NCA batteries further investigation is required into their long-term effects as it continues to evolve and does not settle on a SS-OCV, even after 24 hours.

5.2.3 Model complexity

Curve fitting of the 24 hour relaxation data for the different chemistries was performed using the VR equivalent circuit model. Eq [10] was curve fit for RC circuit counts ranging from $n = 1$ to 6 . Example results are shown for $n = 1, 3, 5$ in Figure 30. They were then evaluated for their goodness of fit, also shown in Figure 30 as RMSD in the lower right plot.

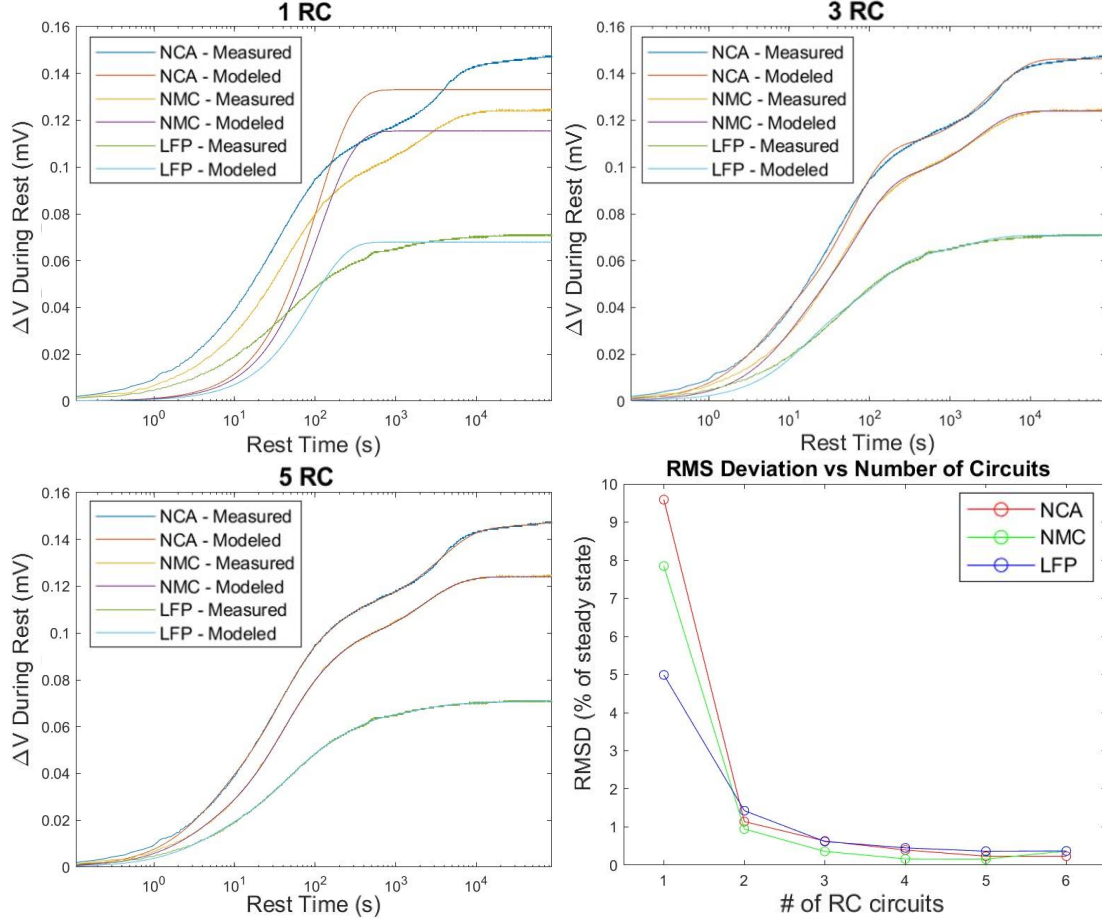


Figure 30: Equivalent circuit model curve fit for models employing 1, 3, or 5 RC circuits, along with the overall RMSD error for models ranging from 1-6 RC circuits

From these graphs it is clear that as n increases there is improvement to the RMSD of the model, albeit with diminishing returns. A difference in modeled and measured curves for the 1 and 3 RC models is noticeable, while the 5 RC model is almost indistinguishable from the measured results by visual inspection. Most of the VR curve shape can be captured with only 2 RC circuits as shown from the large drop in RMSD between the 1 and 2 RC models. This makes sense because the profile in the semi-log Figure 29 inset is predominantly two exponential decays. The improvements to fitting after this point are based on capturing the transition period between these RCs.

The fact that RMSD is still improving after 3 RC circuits prompted investigation into the effects of each individual RC circuit onto the total profile. This is shown in Figure 31 for the $n = 3, 4$, and 5 RC models for the NMC batteries. In these graphs the error shown on the secondary y-axis is calculated as the difference between the measured value and the

modeled value. This allows for visual inspection of the important differences in the modeled and measured curves. A vertical dashed line is included for each circuit representing the time it reaches 98% of its steady state value. This percentage was chosen for the same reasons as EST. When discussing this figure n RC means the model and circuit $V_{RC,p}$ refers to voltage magnitude attributable to a specific RC pair of the model.

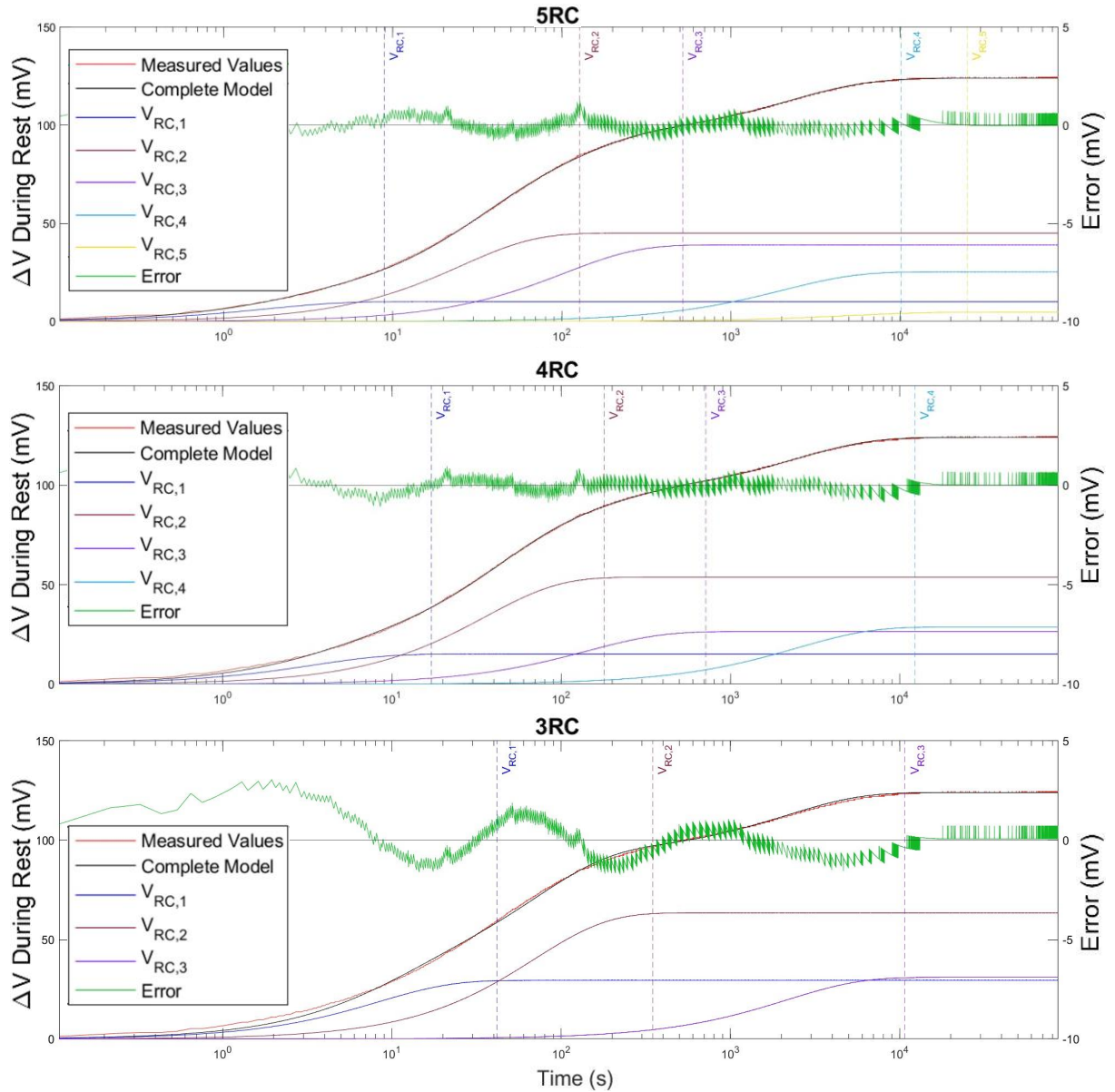


Figure 31: Impact of each RC circuit in a model on the VR profile for NMC batteries for 3, 4, and 5 RC circuit models

In the 3 RC model, $V_{RC,1}$, $V_{RC,2}$ and $V_{RC,3}$ line up with the 3 linear regions observed on the semi-log plot, explaining why there is such significant improvement to the accuracy from

the 1 to 2 to 3 RC models. It also explains the marginal improvements after this point as most of the behavior is captured with 3 RCs. These marginal improvements better represent the real electrochemical function which dictate the profile as it is not simply exponential decay functions.

It is important to recognize how the RC circuits resolve from the 5 RC to the 3 RC model. When changing from the 5 RC to 4 RC model, $V_{RC,5}$ and $V_{RC,4}$ appear to resolve into a single V_{RC} . This new V_{RC} has a time constant between the previous ones, and a higher V_n to account for the magnitude of both. When changing from the 4 RC to 3 RC model, the lower time constant circuits $V_{RC,3}$ and $V_{RC,2}$ appear to resolve. During these changes all RCs time constants migrate closer together to account for the simplification of the crossover period.

5.2.4 Quantifying inaccuracy impacts on SOC and SOH

Table 8 uses the RMSD technique given in Chapter 4 to determine the potential SOC error for each chemistry and n RC model. The n RC model at which minimum SOC error or 0.5% is reached is bordered. NCA and NMC can both use the 3 RC model as it reaches the suggested SOC accuracy of 0.5%. LFP should use the 4 RC model where it reaches minimum SOC error of 2.27% which is well above the suggested 0.5%. The flatter voltage profile of LFP drastically increases sensitivity to error when using OCV to SOC relationship. If SOC is required to be lower than this for an application then VR may not be applicable for LFP batteries.

Table 8: SOC error for various complexity of RC equivalent circuit model

n RC model	Chemistry		
	NCA	NMC	LFP
1	5.26%	6.67%	20.53%
2	0.57%	0.99%	6.80%
3	<0.5%	<0.5%	4.87%
4	<0.5%	<0.5%	2.27%
5	<0.5%	<0.5%	2.27%
6	<0.5%	<0.5%	2.27%

Table 9 shows RMSD and EST for each chemistry and n RC model. For NCA the RMSD reaches a minimum at the 5 RC model. However, the modeled EST is 85.35 hours, which is well beyond the testing information of 24 hours. As SS-OCV was not reached for NCA it is unknown what value of modeled EST signifies overfitting, but that it should be longer than 24 hours. Testing VR beyond 24 hours could be used to verify this finding.

For NMC and LFP Table 9 shows improvement in RMSD until the 6 RC model. However, the EST of this model is 6.95 and 5.36 hours, respectively, which are both substantially beyond the measured EST of 3 hours. This EST metric discredits both the 5 and 6 RC model and instead the 4 RC model with appropriate EST is selected (and bordered).

Table 9: EST and RMSD for each tested chemistry and number of RC circuits in the model

Chemistry:	NCA		NMC		LFP	
n RC model	RMSD	EST	RMSD	EST	RMSD	EST
1	9.59%	0.15 hours	7.84%	0.16 hours	4.99%	0.13 hours
2	1.14%	1.22 hours	0.94%	2.26 hours	1.43%	0.34 hours
3	0.62%	4.73 hours	0.36%	2.98 hours	0.62%	2.36 hours
4	0.40%	5.36 hours	0.16%	3.43 hours	0.45%	4.04 hours
5	0.23%	85.35 hours	0.15%	6.95 hours	0.36%	5.36 hours
6	0.23%	83.90 hours	0.37%	26.60 hours	0.37%	44.34 hours

5.3. Outcome

After examination of state of the art it was determined that there existed a gap for the improvement consistency between VR studies. This gap was defined with 4 research questions concerning: The SOC values relationship to VR magnitude and curve shape; The period of time required for resting; The complexity of model required for SOC estimation; The complexity of model required for SOH evaluation. With 4 guidelines to restrict scope for practical applications a VR methodology was trialed on multiple chemistries of LIB.

A 3 hour VR with 10% SOC increments in charge and discharge and a 24 hour VR at a specified SOC was created to evaluate the research questions. From these tests the data was curve fit using a VR specialized equivalent circuit model to best capture the VR curve

shape and minimize error in SS-OCV estimation. These curve fits were evaluated in terms of RMSD and SOC error. Differing amounts of RC circuits were modeled to determine the required complexity. Curve fitting was performed over the range of SOC values received to determine curve shape differences which could indicated SOC values for SOH evaluation.

From this group of tests there were good results found. First, the relationship between SOC and VR magnitude was found for each chemistry. There are trends that are present and from these and the guidelines, a highest point of VR magnitude can be found. For NCA and NMC this is 45% SOC. For LFP this is 65% SOC. Next it was determined that NCA does not relax completely over a 24 hour period. This was confirmed with secondary tests where confounding variables were taken away and the only influence was the internal workings of the battery. NMC and LFP both require 5 hours to be fully rested, but functionally can be claimed rested at 3 hours for curve fitting.

Using the VR equivalent circuit model 3 and 24 hour tests were curve fit. These were performed at various SOC and complexity. From these investigations it was found that error decreased significantly from 1 to 2 to 3 RC circuit models. For the purposes of SOC estimation within 0.5% accuracy, it was found that NCA required a 3 RC model, NMC required a 2 RC model, and LFP required a 4 RC model. For the purposes of SOH estimation, it was found that all batteries required a 4 RC model.

Chapter 6 Investigation of degradation via voltage relaxation

6.1. Purpose

The second study was performed to determine the relationship between VR characteristics and degradation metrics for the 3 chemistries in a 3P configuration. Capacity, IR, and VR were tested, then followed with an accelerated degradation test. During the study 7 sets of tests were performed on the NCA, NMC, and LFP batteries over 3 months. Relationships between VR metrics and degradation metrics were quantified by Pearson correlation coefficients and linear interpolations to determine if VR could accurately estimate SOH and IR. The following research questions guide this study:

1. Do time constants of VR curve shape change as a function of degradation metrics (SOH & IR growth) with a relationship that is useful to predict these degradation metrics.
2. Does VR magnitude change as a function of degradation metrics with a relationship that is useful to predict these degradation metrics.

With that in mind there were some practical guidelines to limit the scope to a realistic use case.

1. VR for SOH evaluation will likely be implemented during charge as most applications have specific demands during discharge that prohibit long open circuit conditions.
2. VR relaxation period should be as short as possible while maintaining good accuracy.
3. SOC should be calculated based on most recent maximum Ah capacity measurement as this gives most accurate SOC measurements while coulomb counting.
4. The SOC chosen for future investigations should be where the relationship is easiest to predict from having the largest changes in the VR metric.

6.2. Degradation results

After the set of tests performed, the batteries were found to have significant differences in their degradation. Their results however were consistent between degradation metrics. For example, the NCA battery had both the highest IR growth and capacity lost. The pertinent overall results are that the NCA battery failed completely, the NMC battery degraded a measurable amount and the LFP battery degraded minimally.

6.2.1 Capacity degradation

The batteries capacity degradation shows the large difference between the useful life of each battery chemistry. Each set of tests was labeled with the SOH value and Ah-CycEq from the RPT performed in that set. To make subsequent results presentation and discussion more clear test numbers will be given to explain these metrics. Table 10 shows the results which are then represented graphically in Figure 32. The top plot shows the maximum discharge capacity of the battery versus the AhCyc-Eq. Notice that each battery starts with a different amount of capacity, and the important observation is the reduction relative to the initial capacity, as shown in the bottom plot.

Table 10: SOH for each chemistry and test set

Test	NCA		NMC		LFP	
	SOH	Ah-CycEq	NMC	Ah-CycEq	LFP	Ah-CycEq
1	100.0%	5.0	100.0%	5.0	100.00%	5.2
2	92.6%	45.8	99.9%	48.2	99.99%	56.0
3	81.3%	79.7	99.0%	90.6	99.97%	108.3
4	73.7%	108.4	98.1%	131.4	99.59%	161.0
5	62.8%	133.9	96.2%	171.7	99.23%	213.4
6	58.4%	156.4	94.6%	210.9	99.07%	264.8
7	54.4%	179.3	90.8%	248.4	98.88%	317.0

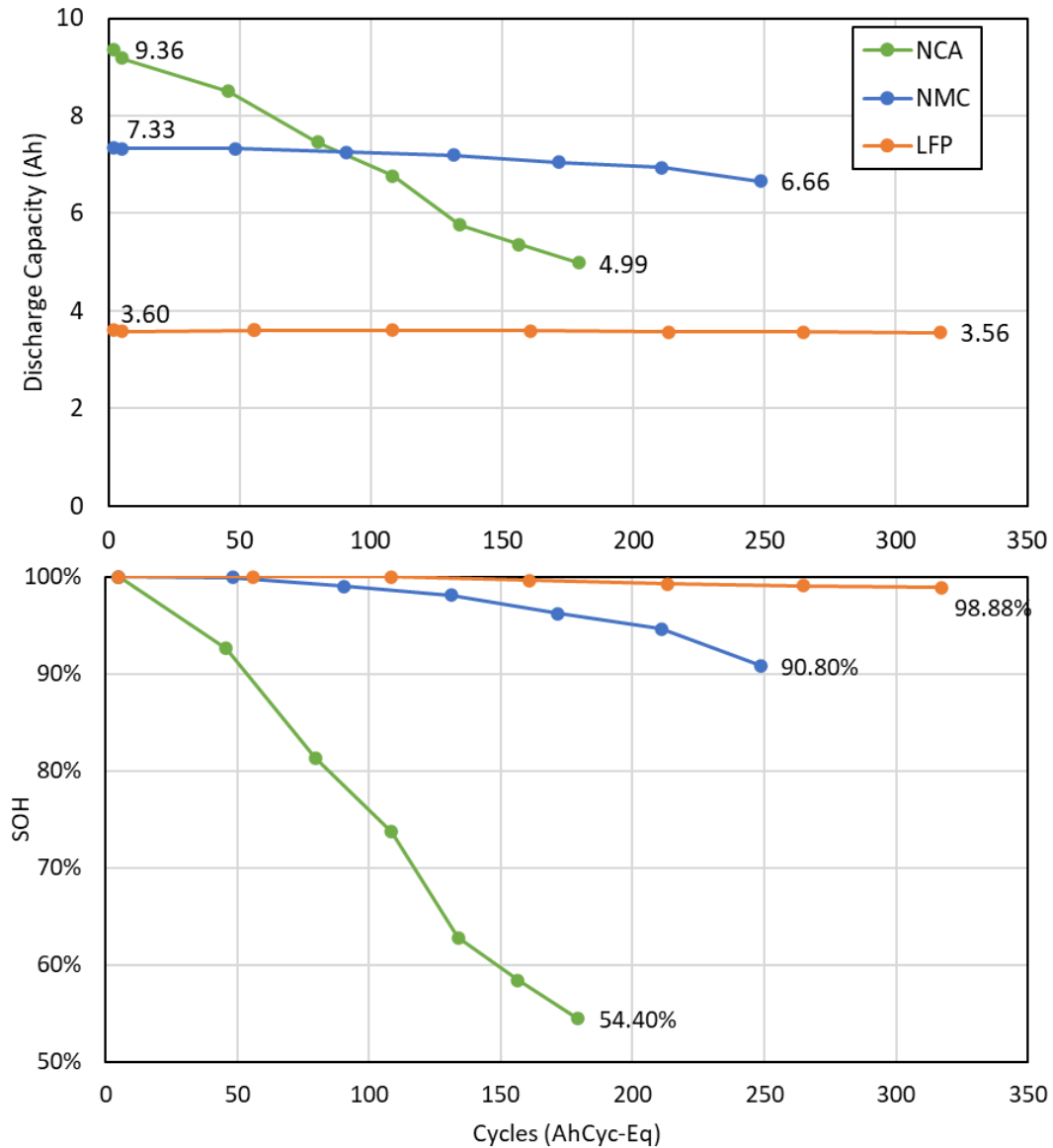


Figure 32: Degradation plot of Capacity vs cycles and SOH vs cycles

The NCA battery experiences the largest degradation of capacity in the least number of cycles. This was anticipated, the rated cycle life was 500 cycles however the battery reached less than 200 before it failed. The test on the NCA battery failed from a rapid increase in temperature which triggered a temperature alarm shown in Figure 33. This rise in temperature would have resulted in thermal runaway should the test have continued.

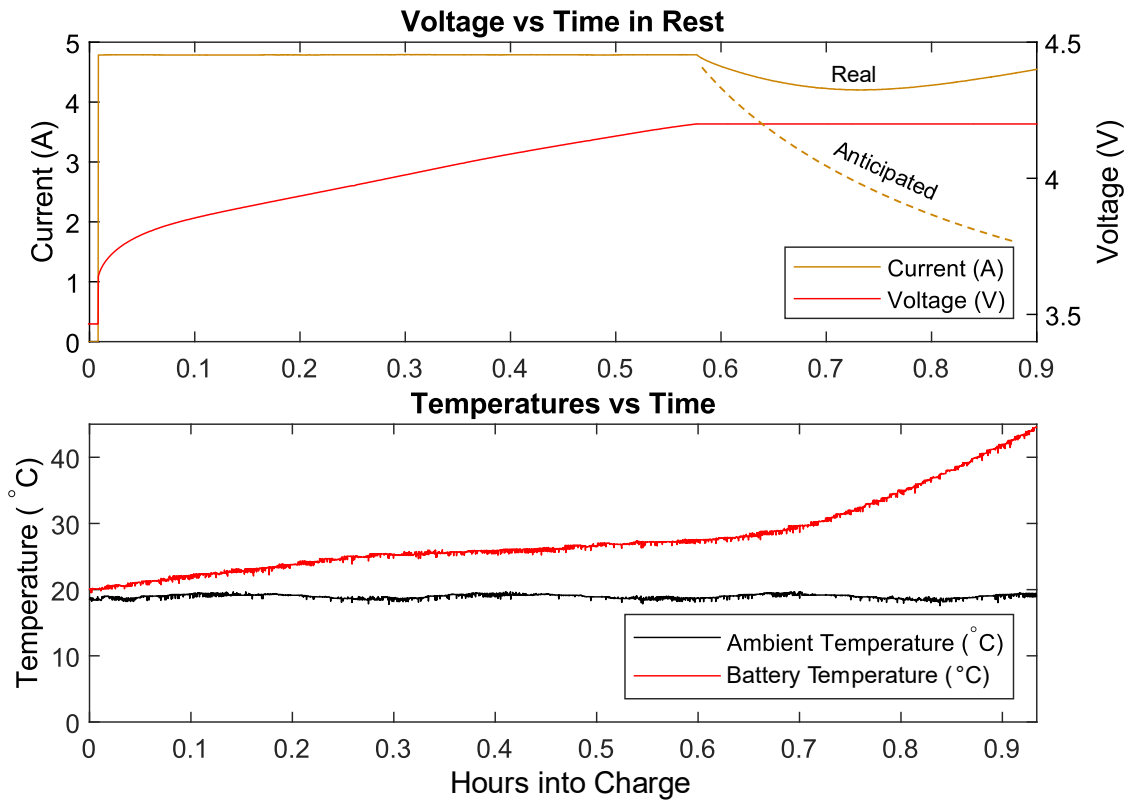


Figure 33: Final RPT of the NCA battery where failure due to thermal runaway occurred

Figure 33 shows the current increased during the CV phase, because of the heat generated during the charge cycle. This heating rate caused a large decline in the IR of the battery since at higher temperatures the cell less electrochemical resistance to the lithium ions moving. The lower IR increased the current, creating a feedback loop since heat generation is a square relationship with current compared to a linear relationship with resistance. This failure is significant as these batteries would be dangerous to operate again. The batteries were evaluated from BOL to EOL in the investigation, making the results more impactful since they represent the full spectrum of usable health.

The NMC and LFP batteries experienced significantly less SOH degradation over the study, with NMC losing 10%, and LFP losing 2%. Note that all batteries were run for the same period of time, and the difference in Ah-CycEq is from the higher SOH batteries experiencing more Ah throughput relative to their rated capacity.

6.2.2 IR degradation

Figure 34 shows that the NCA battery had significant growth of IR over the lifespan for both charge and discharge IR. Note that after test 4 the current pulse was changed to allow for more data points to be captured. This had no effect on the IR as it was accounted for in data analysis. On charge and discharge there is a growth by a factor of roughly 1.9 from test 1 to the test 7 for a given SOC.

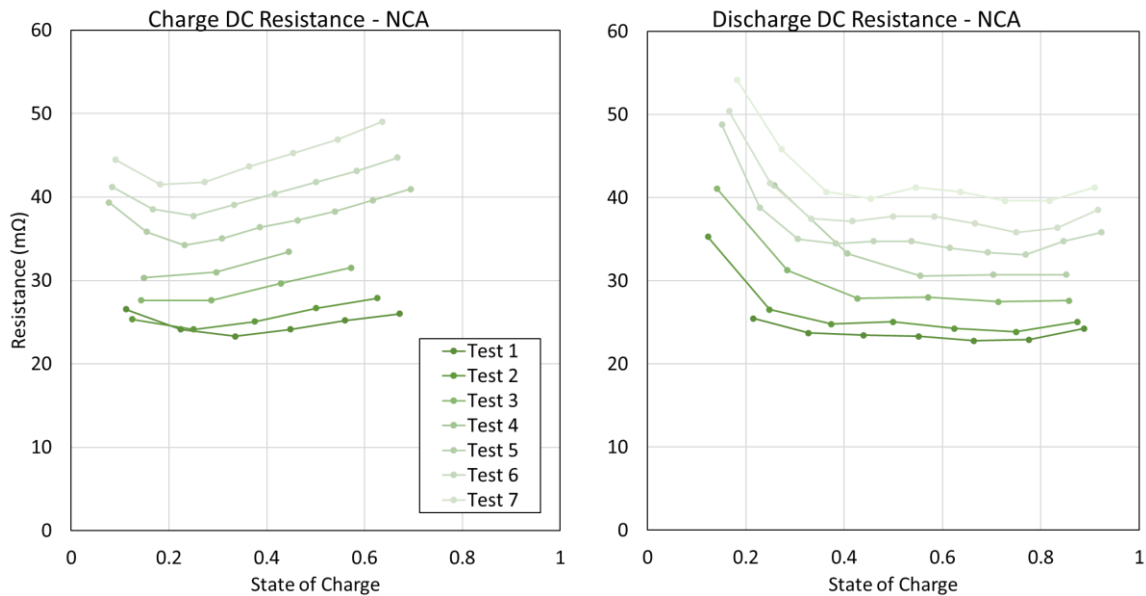


Figure 34: IR degradation results of NCA batteries for charge and discharge

Figure 35 shows that the NMC batteries showed measurable increase in IR as well. They started with an initial IR that was higher than NCA but grew at a slower rate. The IR has grown by a factor of roughly 1.4 on charge and discharge. It is important to observe that the growth was equivalent on charge and discharge as this shows that degradation was likely equal between the positive and negative electrode. If one had disproportionate degradation, there would be an increase in IR for either charge or discharge. The magnitude of IR growth was anticipated as the capacity degradation was also less severe than the NCA battery. As degradation progresses it is anticipated that both IR will grow, and capacity will decrease as explained in Chapter 2.

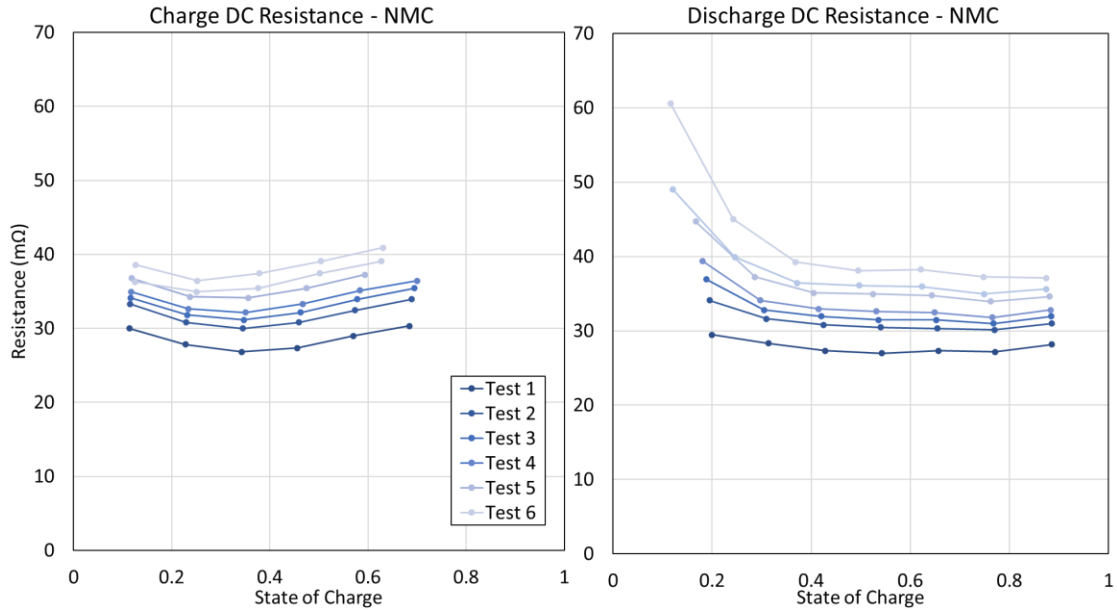


Figure 35: IR growth on charge and discharge for NMC battery

The LFP batteries showed minimal change in their IR as can be seen in Figure 36. They follow the same trend with some small variation between tests, but no significant change.

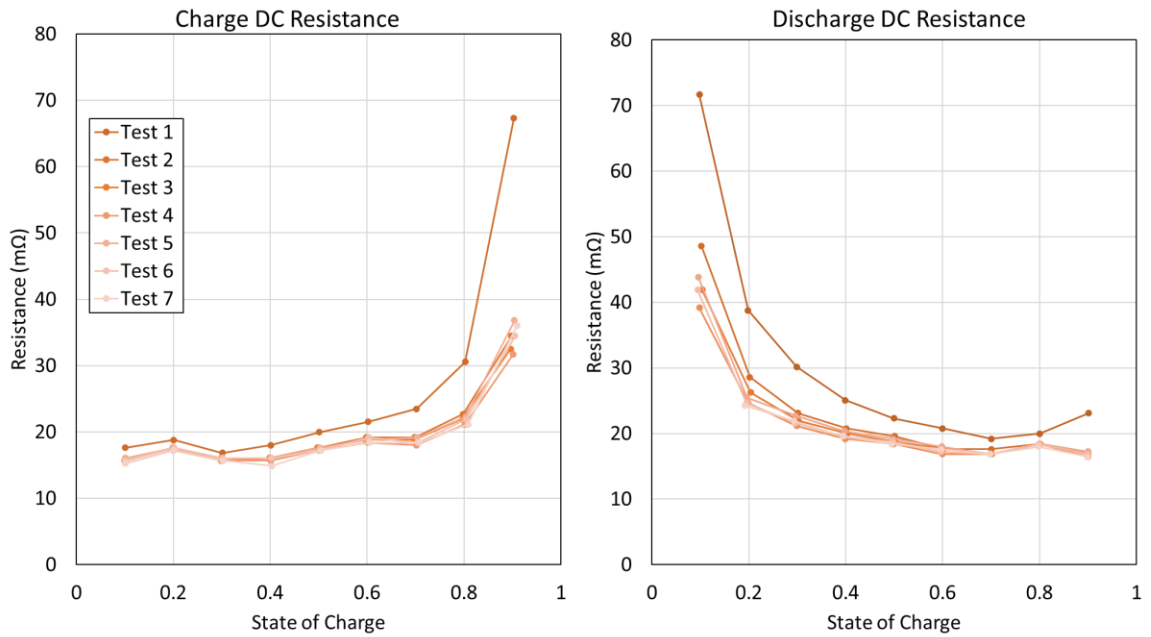


Figure 36: IR growth on charge and discharge for LFP battery

Note that LFP can capture more of the SOC range on charge and discharge since it does not end the CC until later in SOC. This shows the characteristic, that all LIBs have, of

highest IR at high and low SOC. The initial test has the largest values of IR which then decrease to the values observed for the rest of testing. As shown from Rangom et. al [35] the first set of cycles on an LIB has a measurable effect on the particle size. If the negative electrodes were run at a slow rate, they would have higher SEI particle size. The batteries in this study were purchased in 2019 and only been characterized when they first arrived, measured for IR, mass, and voltage. Therefore, the SEI would not have had any cycling to reduce the larger particles from mass transport of lithium, and the SEI would grow during this time as shown from Barré et al. [19] . This is thought to be captured in the LFP results since there is minimal change in IR over the lifespan of the battery, but high IR on the first test. Once the battery had been sufficiently cycled after the degradation schedule there was less resistance to the lithium ions being transported to either side since the larger particle size of the SEI would have broken down into smaller particles from the mass transport of lithium ions. I believe that this occurred for all of the batteries tested but is only visible on LFP since it had no large change in IR. This is the electrochemical reasoning for why this has occurred, but this claim cannot be confirmed without disassembly and dissection of the battery after the first IR test.

For the batteries of the nickel-based chemistry, as the capacity decreased the IR increased. If a relationship or correlation is found between VR metrics and either of these metrics it has high probability to also be true for the other metric. However, it does make distinguishing causes between SOH and IR growth harder, and potentially unfeasible. This is an area for future investigation.

6.3. VR results

After degradation metrics were examined from an RPT and IR test, the VR test was performed to evaluate the research questions. As the tests progressed and the SOH of the batteries decreased, this changed the positions in SOC that VR would occur at. This is because Ah was used as a control parameter and a set amount of Ah results in a different amount of SOC if the total capacity is lower. In the case of NCA this had a measurable impact as there was almost a 50% decrease in capacity as can be seen in Figure 37.

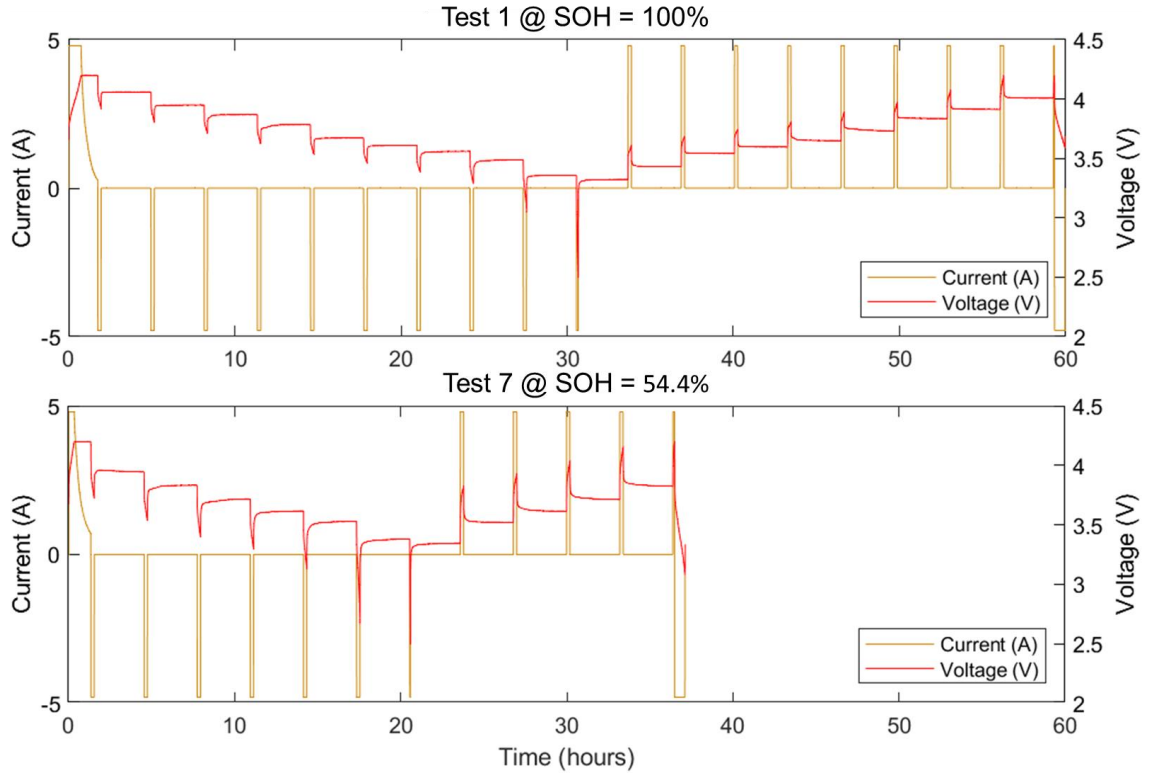


Figure 37: VR tests for NCA cells at 100% SOH and 54.4%

For NCA, the test takes 60 hours at BOL compared to the roughly 37 hours at EOL. The number of data points is lower as well, where BOL achieves 8 VR periods EOL only achieves 4. This has an important insight for a proposed schedule. It must consider the capacity of the battery to reach an SOC for VR investigation.

Using a 4 RC VR-ECM for each chemistry the VR period was curve fit for every test. This resulted in finding the VR magnitude and time constant for each RC circuit. From the curve fit RMSD and EST values were calculated used to determine that a fit was valid. This ensured that differences came from curve shape and not process. Each VR was assigned the SOC and test number at which it occurred, test number being analogous to SOH as shown in Table 10. These allow for useful sorting of the data. VR results can be sorted by test number to show how the VR vs SOC profile changes as a function of degradation metrics as can be seen in Figure 38 on the left plot. VR results can be sorted by SOC to show how VR metrics change at a specific SOC value as a function of degradation metrics, shown on the right.

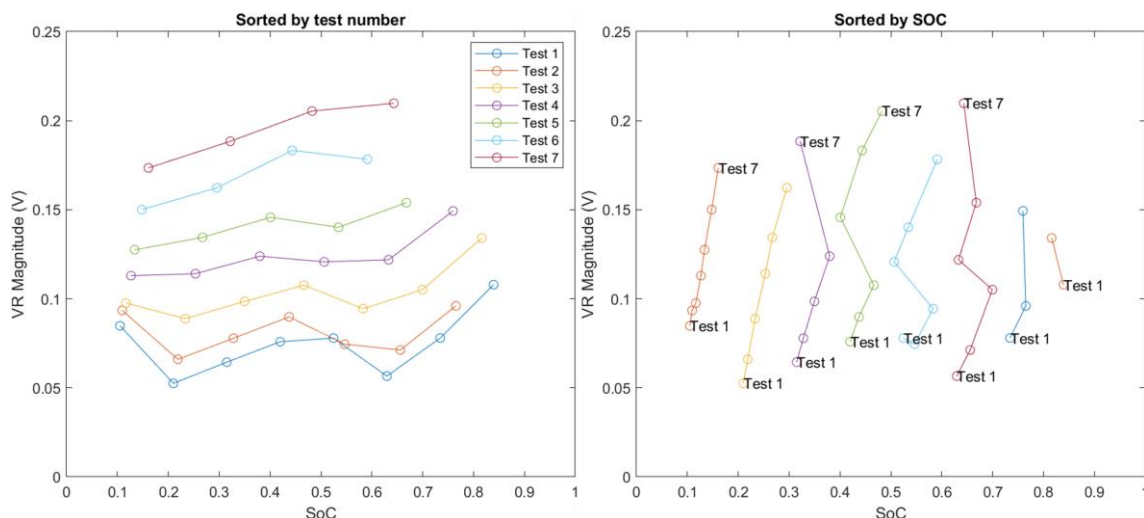


Figure 38: Different sorting of VR results to show features, exemplified from NCA results

6.3.1 NCA

In Figure 39 the time constants for NCA had no strong trends with SOH or IR. All of the time constants stayed within an order of magnitude. This was deemed acceptable as each time constant is an order of magnitude different from the others and these fits achieve low RMSD, and accurate EST. The only RC and SOC range that showed any consistent trend was RC 4 between 40-50% SOC. It increases in value but does not follow any consistent form of growth, so this is not a useful relationship. This lack of trends is in opposition to what was expected from the literature review. Time constants were said to be correlated to degradation metrics [8] [15] [17]. These studies claim that there should be a trend of the time constants increasing as the SOH decreases which has a consistent and predictable relationship. From the literature it is known that one of the features of the VR curve shape is from lithium plating on the negative electrode. Some of these studies were predicting this specific degradation mode and induced it in their methods. It could be that this specific degradation mode is what causes an increase in time constant, and these cells did not experience much lithium plating. This is a theoretical claim and must be confirmed through testing. To resolve this difference in results a new study is suggested into how inducing specific degradation modes in LIBs changes VR metrics and evaluating them after EOL to confirm degradation modes.

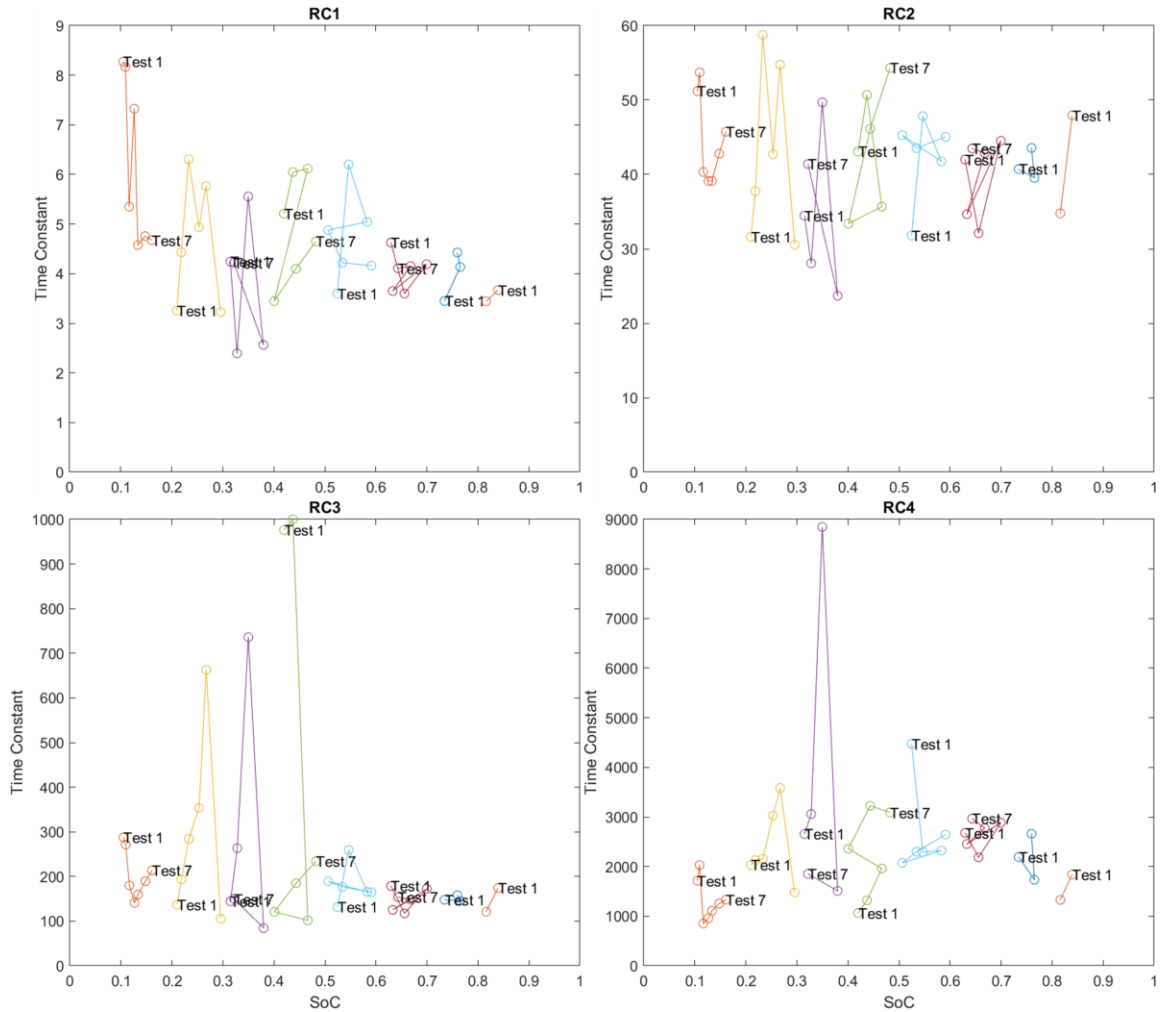


Figure 39: Modeled time constants for each RC circuit for NCA battery

The VR magnitude of each RC circuit was sorted into SOC ranges of 10% as shown in Figure 40. There is clear trend that as the battery ages there is an increase in the VR magnitude for almost every circuit at every SOC. Only one of the circuits does not show this behaviour at two ranges, RC 4 between 40% SOC and 60% SOC. RC 4 is the long term RC which for NCA is known to be not fully representative as expressed in Chapter 5.3 long term evolution is missed. For this reason, the VR magnitude of the entire model was plotted against the SOC and sorted via test number, shown in Figure 41

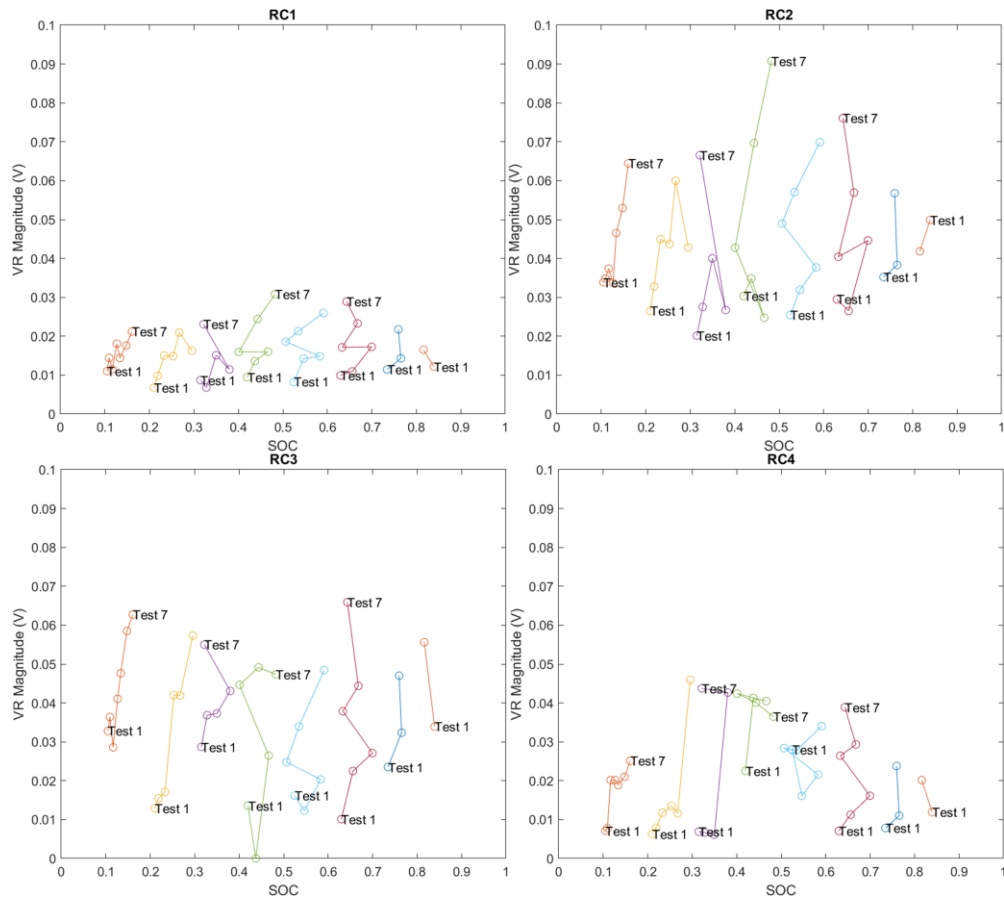


Figure 40: VR magnitude for each RC circuit of NCA battery

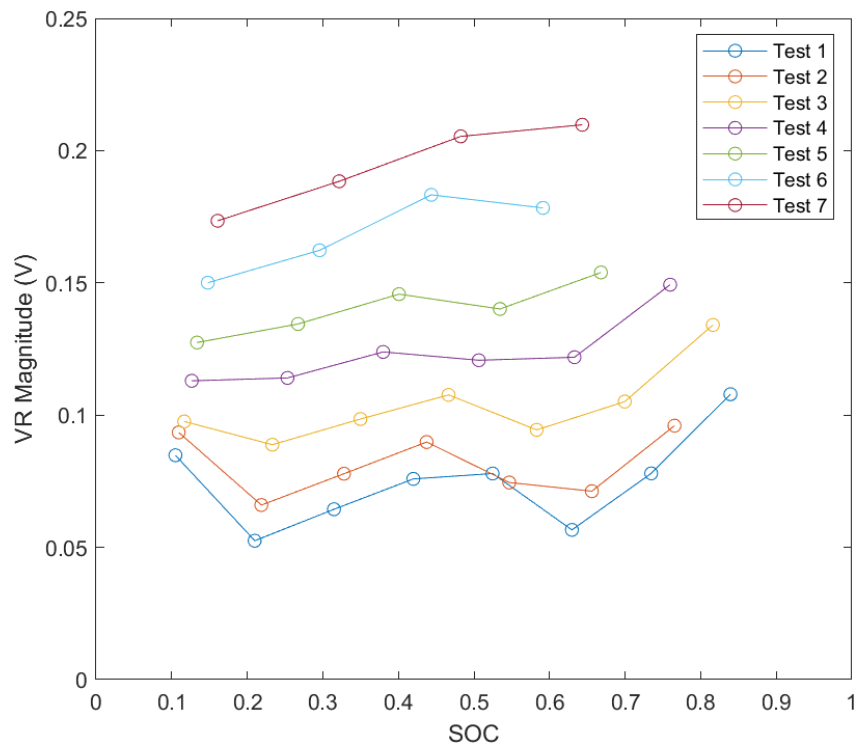


Figure 41: VR Magnitude of NCA cells vs SOC for all tests

From this Figure 41 the relationship is clear. As the cell increased in age the VR magnitude increased for every SOC range. It increased by a factor of 3.5 to 4.0 depending on the SOC. A small variation of growth means there is likely a consistent trend between the data. The magnitude of growth is a large and, more importantly, a measurable change in VR magnitude. The increase was consistent across the tests, further improving the viability of VR for SOH determination. This effect is also shown when the VR magnitude is plotted against the SOH and IR as in Figure 42.

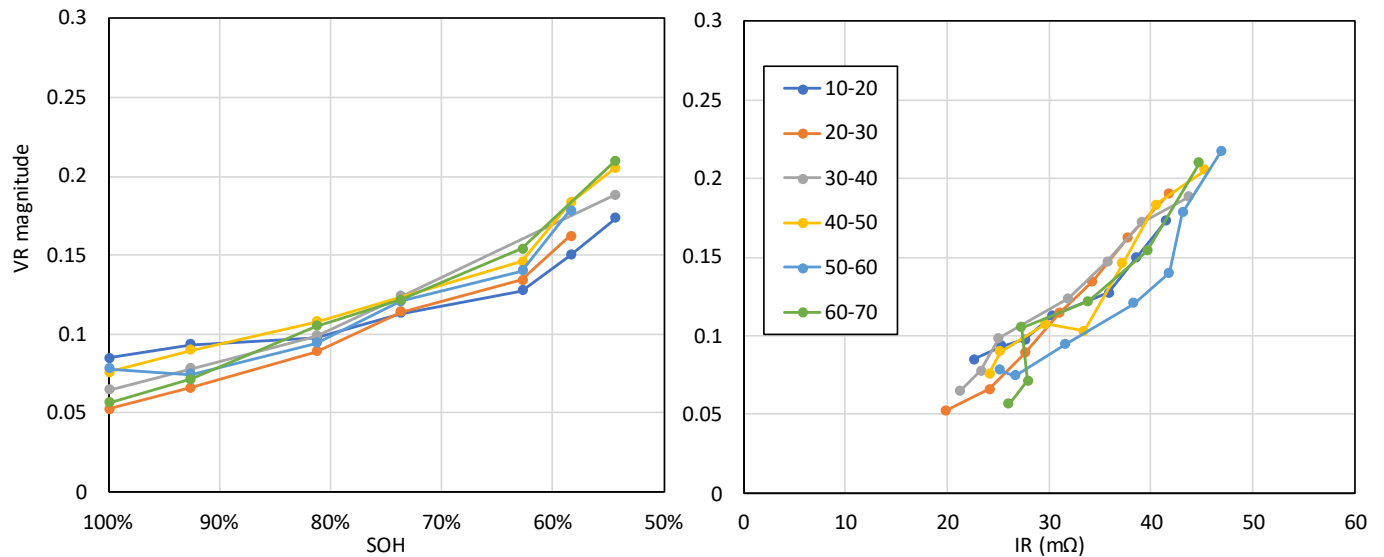


Figure 42: VR magnitude of NCA cells vs. SOH and IR

There is an apparent linear relationship between the VR magnitude and SOH, as well as the VR magnitude and IR for all SOC ranges. To confirm this a quantitative assessment was necessary. A Pearson correlation coefficient was used to confirm the negative and positive correlation between SOH and IR growth respectively. They were evaluated versus a linear interpolation of the data for a coefficient of determination. Table 11 shows that this was done for each SOC range.

Table 11: Results of Correlation and R^2 of VR magnitude and degradation characteristics for NCA batteries

SOC range	Pearson Correlation Factor		R^2	
	SOH & VR	IR & VR	SOH & VR	IR & VR
10-20	-0.934	0.977	0.956	0.956
20-30	-0.988	0.999	0.999	0.998
30-40	-0.989	0.996	0.999	0.990
40-50	-0.966	0.993	0.9179	0.988
50-60	-0.946	0.947	0.901	0.901
60-70	-0.963	0.996	0.888	0.992

The correlation factor between VR magnitude and both degradation metrics is close to 1 and -1 . This means there is a high correlation between these variables. Next the R^2 value is high for each SOC range as well. Meaning a linear approximation could estimate the relationship between both SOH and VR magnitude as well as IR growth and VR magnitude. This relationship is SOC dependant as well which is important to recognize in an application setting.

6.3.2 NMC

The time constants of NMC, shown in Figure 43, have some distinguishable trends compared to the NCA trials. Between 30% to 50% SOC there appears to be a general increase in the value for all for the RC pairs apart from RC4 between 40% to 50%. Apart from this all the other ranges for RCs show grouping within an order of magnitude with no distinguishable trend. It is interesting to note that RC3 and RC4 between 40% to 50% has a much higher values than any of the other SOC range and variability between tests. This could be impacted by the higher VR magnitude at this range as found from the first study.

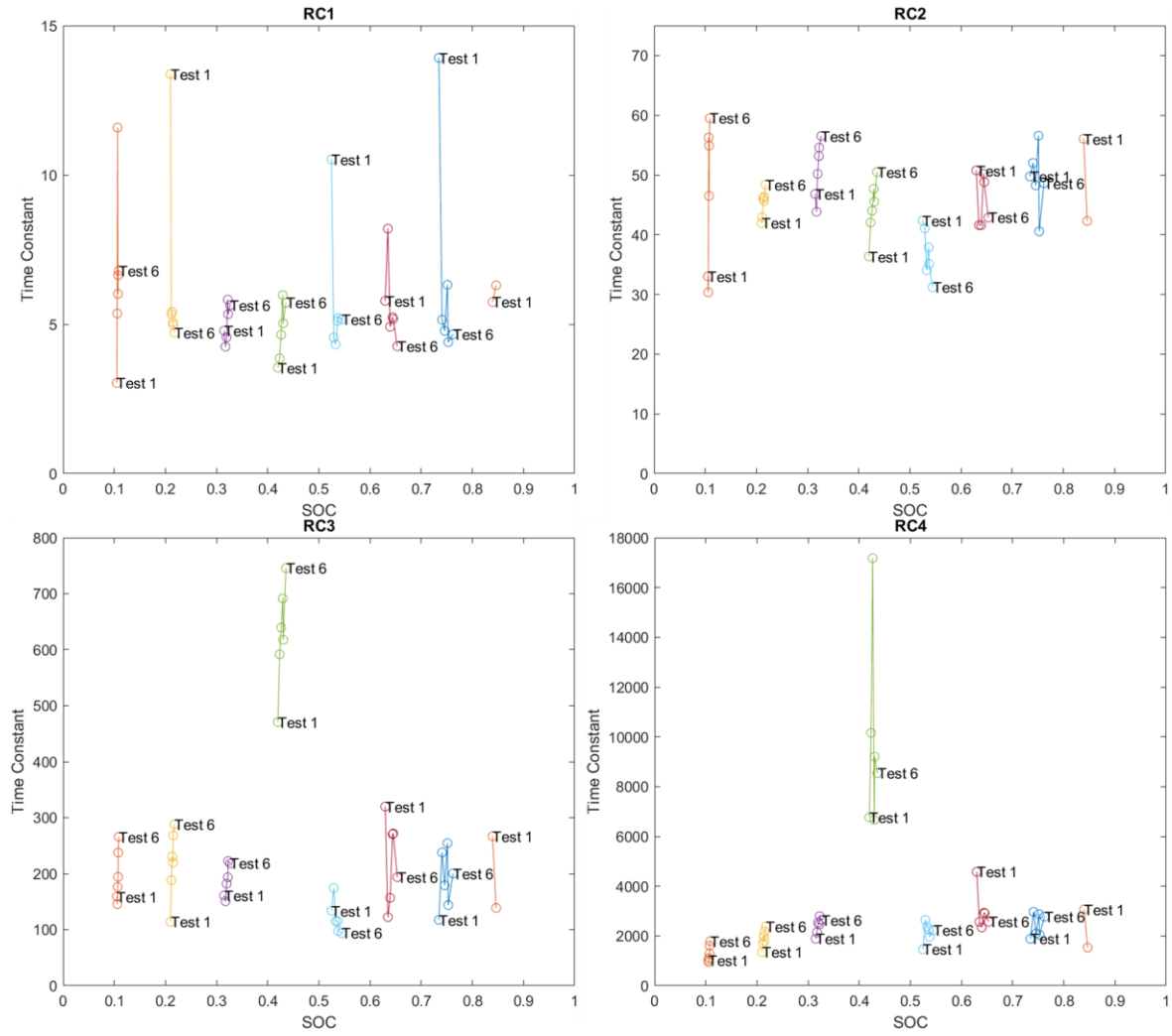


Figure 43: NMC time constants

Apart from these two observations there are no other consistent trends for the NMC battery. To quantify the trends the same analysis of correlation factor and R^2 was performed on the time constants. The results are shown in Table 12.

Table 12: Correlation and R^2 analysis of time constants for NMC

RC number	30-40 % SOC				40-50 % SOC			
	Pearson Correlation Factor		R^2		Pearson Correlation Factor		R^2	
	SOH	IR	SOH	IR	SOH	IR	SOH	IR
1	-73.25%	57.37%	0.99	0.99	-74.55%	79.65%	0.99	0.99
2	-91.26%	78.32%	0.18	0.19	-82.03%	90.22%	0.20	0.21
3	-93.07%	84.50%	0.05	0.05	-73.50%	83.35%	0.015	0.02
4	-80.28%	95.98%	<0.01	<0.01	16.71%	11.34%	0.01	<0.01

It is clear that there is some correlation between the time constants and the age of the battery between 30-50% for almost all the RCs, but none are as strongly correlated as the VR magnitude. If these are to be impactful for predicting SOH or IR, they should have both high correlation and R^2 values. Only RC circuit 1 has high R^2 , but the correlation is too low to be able to use this relationship. For these reasons it does not seem feasible to estimate SOH or IR from observing the time constants for the VR-ECM. This is also different from literature in the same way as the NCA battery.

The VR magnitude does show a similar trend to the NCA batteries. The total VR magnitude increases with cycle count as can be seen in Figure 44. There is less growth overall than with the NCA battery, which is expected as it experienced less degradation. The VR magnitude increased a factor of between 1.3 and 1.5 times the original value. This is slightly higher than the NCA batteries for the equivalent SOH degradation. The largest increase in VR magnitude occurs between 50 and 60 SOC. Should this band of SOC have a useful relationship it should be used for degradation evaluations in the future.

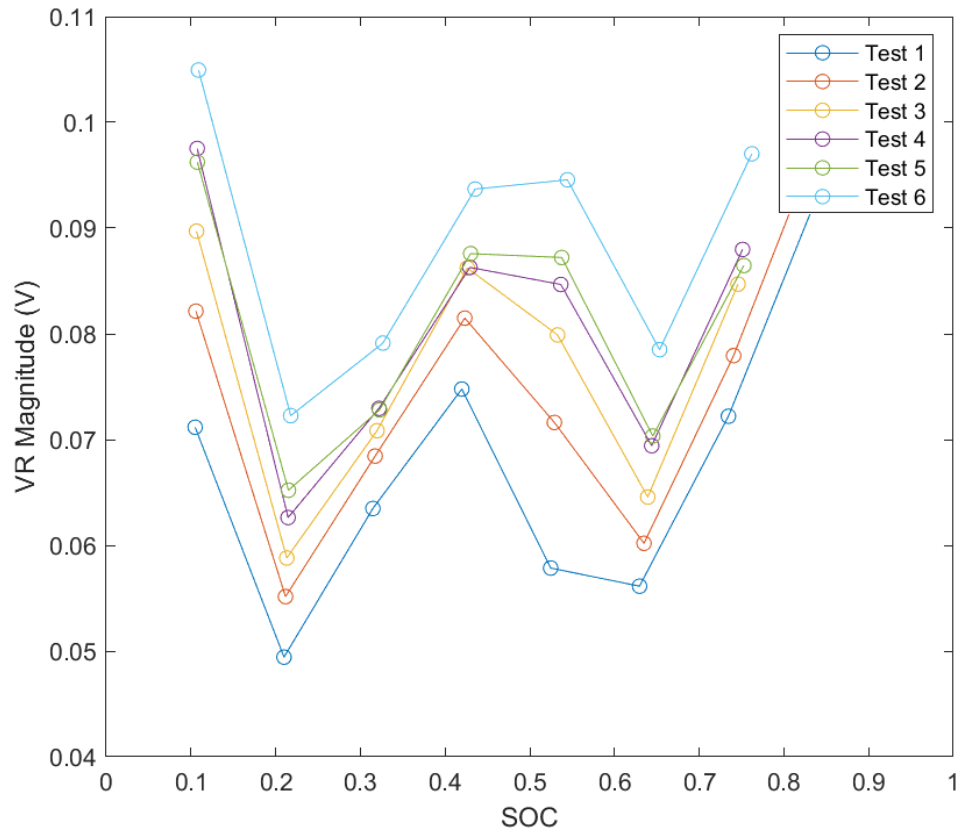


Figure 44: NMC VR Magnitude

As the relationship is similar to the NCA batteries the same analysis was performed on the NMC batteries to determine if there was linear growth between VR magnitude and degradation metrics. These results are shown in Table 13.

Table 13: Results of Correlation and R^2 of VR magnitude and degradation characteristics for NMC batteries

SOC range	Correlation Factor		R^2	
	SOH & VR	IR & VR	SOH & VR	IR & VR
10-20	-0.899	0.959	0.996	0.998
20-30	-0.947	0.977	0.998	0.999
30-40	-0.965	0.938	0.999	0.998
40-50	-0.945	0.953	0.999	0.999
50-60	-0.929	0.969	0.995	0.998
60-70	-0.975	0.965	0.998	0.998

As can be seen from the table there is again strong correlation both positive and negative between VR magnitude and degradation metrics. Furthermore, the relationship is highly

linear with R^2 values that are near 1. This means that knowing the VR magnitude should lead to accurate prediction of SOH and IR for NMC batteries.

6.3.3 LFP

The modeled time constants for LFP tests show a similar variability to that seen in the other two chemistries pictured in Figure 45. With LFP experiencing minimal degradation in capacity or IR growth, this means that the variability is from the differences from each test and the modeling method. This modeling method is based on a mathematical process so the exact same test will always produce the same results. There is some variability, but all within one order of magnitude and does not seriously alter curve shape, RMSD.

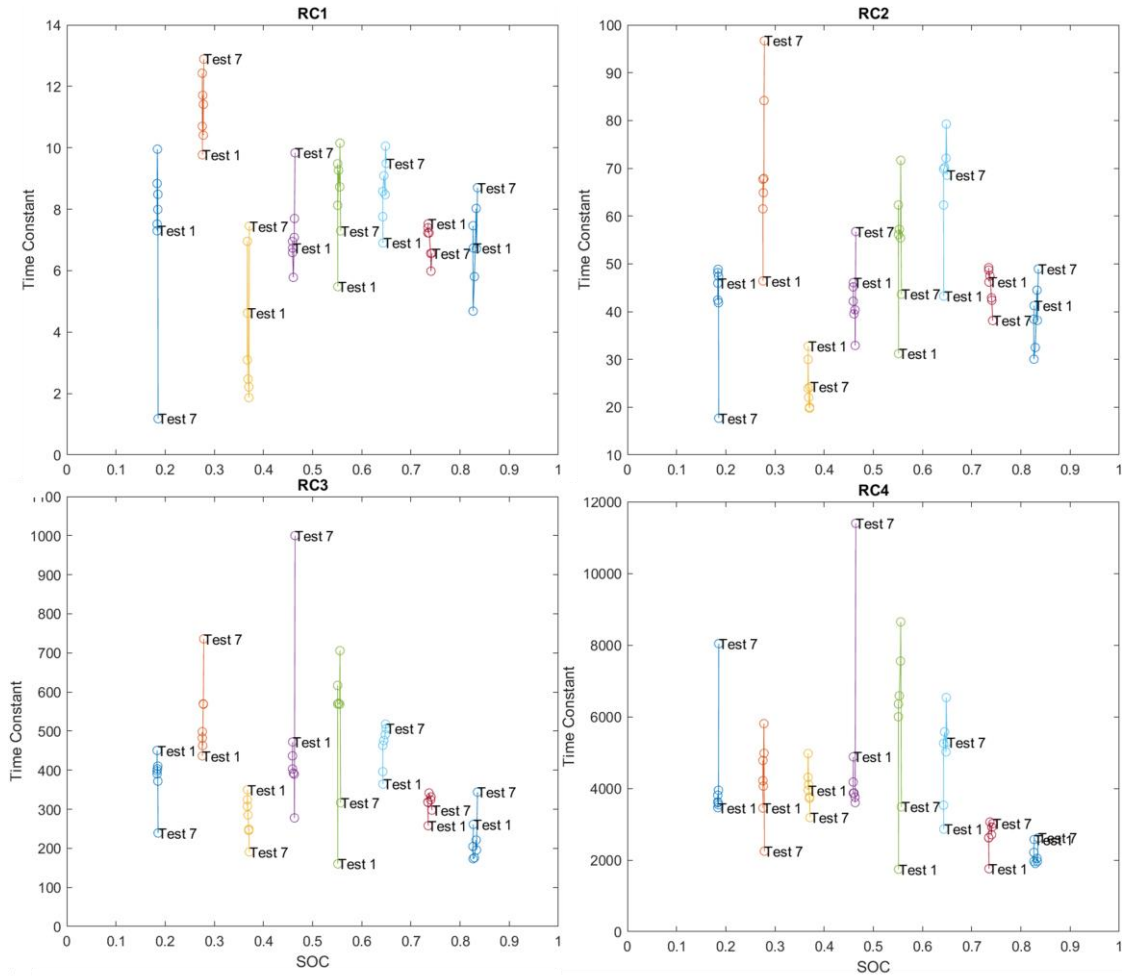


Figure 45: LFP modeled time constants

It is interesting to note that the variability in time constant is dependant on the SOC. This would make sense as the VR curve shape changes as a function of SOC and could be easier

to model. The spread of possible time constants seems to be highest at the middle SOC range. This is further in agreement with the trend seen in the NMC battery as well.

The VR magnitude of the LFP battery as the cycle count increases remains consistent. This is expected as again the LFP battery experienced minimal degradation. It should be noted that test 1 is higher for the VR magnitude as well as the IR. This correlated with higher IR on the first test as well. This does make sense if VR and IR were correlated as we have seen with the previous two chemistries.

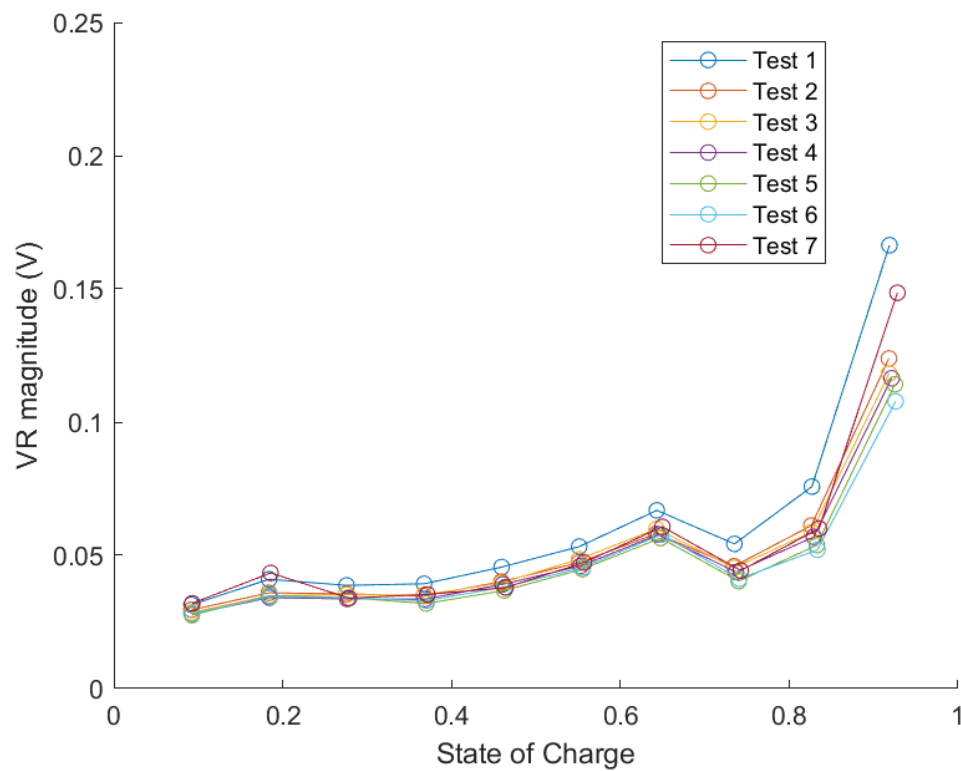


Figure 46: VR magnitude for LFP

As the results are tightly grouped a correlation or linear interpolation on the data would not have usable results as shown in Table 14 with the sensitivity of VR investigation.

Table 14: Correlation and R² of LFP VR results

SOC	Correlation Factor		R ²	
	IR & VR	SOH & VR	IR & VR	SOH & VR
10	0.35	0.01	0.99	0.99
20	0.28	-0.19	0.99	0.99
30	0.84	0.67	0.99	0.99
40	0.65	0.52	0.99	0.99
50	0.91	0.70	0.99	0.99
60	0.84	0.60	0.99	0.99

This data is not impactful since only BOL is being considered. The Pearson correlation factor shows that these are not correlated, which I anticipate to be from the minimal change being below the sensitivity threshold for this technique. The difference in VR magnitude is a maximum of approximately 10 mV over a change of 2% SOH. The first VR magnitude being higher than subsequent tests has a large affect on the results at this scale. This data is below the sensitivity threshold for VR analysis which could be an area for exploration in the future. LFP batteries have high cycle life count and a study that uses VR over the entire lifespan of an LFP battery would be insightful to confirm the results of this thesis and examine the sensitivity of VR analysis.

6.4. Outcomes

The goal of this study was to determine if VR metrics could be related to degradation metrics in a meaningful way to predict these degradation metrics from a VR analysis. The following outcomes were received from the study

- (1) It was found that VR magnitude changes as both a function of SOH and IR. These variables are highly correlated for NCA and NMC. The relationship between VR magnitude and these degradation metrics is linear for a given SOC band with a high degree of confidence. From this relationship VR magnitude can be used to estimate SOH and IR growth.
- (2) Modeled VR time constants do not change and / or cannot be used to estimate SOH or IR growth in contrast to other researchers' findings for NCA and NMC batteries.

As VR magnitude can be used to determine degradation metrics this means that VR is a valid methodology for performing in-situ SOH investigations.

This study showed potential improvements by:

- (1) Including LFP batteries examined over their lifetime to confirm results and investigate the sensitivity of VR would be useful.
- (2) Inducing particular degradation modes in the batteries to examine if they can be identified from VR metrics. This could bridge the differences between this study and the other studies in the field.

Chapter 7 Conclusions & Recommendations

LIBs are a cornerstone of the energy storage market which is only set to grow in the coming years. To get the best performance out of them monitoring must be performed to understand the SOC, SOH and IR. This is not an easy process and improvements are explored in the current research. VR is a method that could have benefits as an in-situ monitoring technique. Understanding VR and its various relationships can lead to prediction of SOC, SOH, and IR growth. A methodology was developed to perform these predictions.

Three chemistries of LIBs from reputable manufacturers were investigated in 2 studies. These batteries were tested and monitored for voltage, current and temperature at a polling rate of 0.1s for VR periods. This data was imported to MATLAB for model curve fitting via the Levenberg-Marquardt method with a specialized VR-ECM model for improved results. These results were compiled and analyzed to answer the research questions posed and achieve the thesis objectives. These major findings are shown in 7.1 and 7.2. From the investigation of these studies a list of recommendations was created for future work to improve on this thesis.

7.1. Outcomes from thesis objectives

- (1) A novel battery model was created based on the equivalent circuit model to evaluate VR. This is the VR-ECM which can accurately model VR magnitude and curve shape.
- (2) The study from Chapter 5 showed that using the VR-ECM with either 3 or 4 RCs depending on the chemistry, and a 3 hour rest, would result in the highest accuracy for SOC determination. For NCA and NMC batteries this could be estimated within 0.5% of SOC. For LFP batteries SOC could be estimated within 2.27% for a worse case scenario.
- (3) The study from Chapter 5 showed that using the VR-ECM with 4 RCs could represent curve shape and show differences as a function of degradation metrics. This was tested in the study from Chapter 6 where a methodology was trialed to examine SOH and IR growth in relation to VR characteristics. This trial had positive results showing the value in the methodology.

- (4) Relationships between VR magnitude and degradation metrics were found for NCA and NMC batteries with a high degree of correlation. The relationship between these variables is linear and can be used to estimate SOH or IR growth if the SOC and VR magnitude are known for a VR rest. LFP batteries were cycled but did not achieve the same degradation as they degrade slowly.

7.2. Findings from research questions

The following findings were gained from exploring the research questions:

- (1) It was found that the VR magnitude and curve shape changes as a function of SOC, but that VR magnitude has a distinguishable trend that the point of highest sensitivity can be found from.
- (2) It was found that NCA batteries require more than 24 hours to rest completely. For NMC and LFP batteries 5 hours will suffice to capture all the curve shape in the dataset, but shorter can be achieved if model curve fitting occurs.
- (3) It was found that to estimate SOC to the highest quality possible a 3 hour rest period is required with a 3 RC model for NCA and NMC batteries. For LFP a 4 RC model is required with the same rest period.
- (4) It was found that to estimate SOH a 3 hour rest with a 5 RC model would be sufficient for NCA. For NMC and LFP a 4 RC model would be sufficient.
- (5) Modeled VR time constants do not change and / or cannot be used to estimate SOH or IR growth in contrast to other researchers' findings for NCA and NMC batteries.
- (6) It was found that VR magnitude changes as both a function of SOH and IR. These variables are highly correlated for NCA and NMC. The relationship between VR magnitude and these degradation metrics is linear for a given SOC band with a high degree of confidence. From this relationship VR magnitude can be used to estimate SOH and IR growth.

7.3. Recommendations

From performing these studies and learning about VR certain recommendations were found to improve the quality of future studies and investigations.

1. A study should be performed into the long term relaxation of NCA batteries to find how long they take to fully relax. It is proposed that relaxation should occur at 45% SOC for upwards of 85 hours to begin and increase should the battery not be fully relaxed by then.
2. Extend the 2nd study to capture the full life cycle of LFP. This will confirm the results and allow for an analysis of required sensitivity for VR magnitude to be used to estimate SOH and IR growth.
3. Examine how different configurations of parallel and series cells effect the VR. There is concern that characteristics of a poor performance cell could be masked by other cells. Does a 1P battery have the same VR characteristics as a 36P battery? This could have useful applications for EVs and balancing circuits.

References

- [1] IRENA, "World Energy Transitions Outlook 2022," IRENA, Abu Dhabi, 2022.
- [2] IEA, "Energy Storage," IEA, Paris, 2021.
- [3] D. Deng, "Li-ion batteries: basics, progress and challenges," *Energy Science and Engineering*, vol. 3, no. 5, pp. 385-418, 2015.
- [4] C. Curry, "Lithium-ion Battery Costs and Market," Bloomberg New Energy Finance, London, 2017.
- [5] X. Li, Y. Liu, A. Pan and X. Yang, "A fast classification method of retired electric vehicle battery modules and their energy storage application in photovoltaic generation," *International Journal of Energy Research* , vol. 44, no. 3, pp. 2337-2344, 2020.
- [6] R. Spotnitz, "Simulation of capacity fade in lithium-ion batteries," *Journal of Power Sciences*, vol. 113, no. 1, pp. 72-80, 2003.
- [7] T. B. Reddy and D. Linden, *Linden's Handbook of Batteries* 4th ed., New York: McGraw-Hill, 2011.
- [8] K. Qian, B. Huang, A. Ran, Y.-B. He, B. Li and F. Kang, "State-of-health (SOH) evaluation on lithium-ion battery by simulating the voltage relaxation curves," *Electrochimica Acta*, vol. 303, pp. 183-191, 2019.
- [9] C. Liu, Z. G. Neale and G. Cao, "Understanding electrochemical potentials of cathode materials in rechargeable batteries," *materials today*, vol. 19, no. 2, pp. 109-123, 2016.

- [10] G. Hautier, A. Jain, S. P. Ong, B. Kang, C. Moore, R. Doe and G. Ceder, "Phosphates as Lithium-Ion Battery Cathodes: An Evaluation Based on High-Throughput ab Initio Calculations," *Chemistry of Materials*, vol. 23, no. 15, pp. 3495-3508, 2011.
- [11] P. J. Osswald, S. V. Erhard, J. Wilhelm, H. E. Hoster and A. Jossen, "Simulation and Measurement of Local Potentials of Modified Commercial Cylindrical Cells: I. Cell Preparation and Measurements," *Journal of The Electrochemical Society*, vol. 162, p. A2099, 2015.
- [12] A. Eftekhari, "Low voltage anode materials for lithium-ion batteries," *Energy Storage Materials*, vol. 7, pp. 157-180, 2017.
- [13] S. K. Heiskanen, J. Kim and B. L. Lucht, "Generation and Evolution of the Solid Electrolyte Interphase of Lithium-Ion Batteries," *Joule*, vol. 3, no. 10, pp. 2322-2333, 2019.
- [14] A. Barai, K. Uddin, M. Dubarry, L. Somerville, A. McGordon, P. Jennings and I. Bloom, "A comparison of methodologies for the non-invasive characterisation of commercial Li-ion cells," *Progress in Energy and Combustion Science*, vol. 72, pp. 1-31, 2019.
- [15] C. Lin, Q. Yu, R. Xiong and L. Y. Wang, "A study on the impact of open circuit voltage tests on state of charge estimation for lithium-ion batteries," *Applied Energy*, vol. 205, pp. 892-902, 2017.
- [16] M. Petzl and M. A. Danzer, "Advancements in OCV Measurement and Analysis for Lithium-Ion Batteries," *IEEE Transactions on Energy Conversion*, vol. 28, no. 3, pp. 675 - 681, 2013.

- [17] Q. Fang, X. Wei, T. Lu, D. Haifeng and J. Zhu, "A State of Health Estimation Method for Lithium-Ion Batteries Based on Voltage Relaxation Model," *Energies*, vol. 12, no. 7, pp. 1349-1367, 2019.
- [18] C. R. Birkl, M. R. Roberts, E. McTurk and P. G. Bruce, "Degradation diagnostics for lithium ion cells," *Journal of power sciences*, vol. 341, pp. 373-386, 2017.
- [19] A. Barré, B. Deguilhem, S. Grolleau, M. Gerard, F. Suard and D. Riu, "A review on lithium-ion battery ageing mechanisms and estimations for automotive applications," *Journal of Power Sciences*, vol. 241, pp. 680-689, 2013.
- [20] K. Liu, T. R. Ashwin, X. Hu, M. Lucu and W. Dhammika Widanage, "An evaluation study of different modelling techniques for calendar ageing prediction of lithium-ion batteries," *Renewable and Sustainable Energy Reviews*, vol. 131, p. 110017, 2020.
- [21] L. Ungurean, G. Cârsoiu, M. V. Micea and V. Groza, "Battery state of health estimation: a structured review of models, methods and commercial devices," *International journal of Energy Research*, vol. 41, no. 2, pp. 151-181, 2016.
- [22] S. Schindler, M. Bauer, M. Petzl and M. A. Danzer, "Voltage relaxation and impedance spectroscopy as in-operando methods for the detection of lithium plating on graphitic anodes in commercial lithium-ion cells," *Journal of Power sources*, vol. 304, pp. 170-180, 2016.
- [23] T. R. Tanim, C. D. Rahn and W. Chao-Yang, "State of charge estimation of a lithium ion cell based on a temperature dependent and electrolyte enhanced single particle model," *Energy*, vol. 80, pp. 731-739, 2015.
- [24] S. E. Li, B. Wang, H. Peng and X. Hu, "An electrochemistry-based impedance model for lithium-ion batteries," *Journal of power sciences*, vol. 258, pp. 9-18, 2014.

- [25] J. F. Manwell and J. G. McGowan, "Lead acid battery storage model for hybrid energy systems," *Solar energy*, vol. 50, no. 5, pp. 399-405, 1993.
- [26] C.-F. Chiasserini and R. R. Rao, "Energy Efficient Battery Management," *IEEE Journal on Selected Areas in Communications*, vol. 19, no. 7, pp. 1235-1245, 2001.
- [27] I. A. Shkrob, M.-T. F. Rodrigues and D. P. Abraham, "Fast Charging of Li-Ion Cells: Part III. Relaxation Dynamics and Trap-Controlled Lithium Ion Transport," *Journal of The Electrochemical Society*, vol. 166, no. 16, pp. A4168-A4174, 2019.
- [28] M.-K. Tran, A. DaCosta, A. Mevawalla, S. Panchal and M. Fowler, "Comparative Study of Equivalent Circuit Models Performance in Four Common Lithium-Ion Batteries: LFP, NMC, LMO, NCA," *Batteries*, vol. 7, no. 3, 2021.
- [29] A. Li, S. Pelissier, P. Venet and P. Gyan, "Fast Characterization Method for Modeling Battery Relaxation Voltage," *Batteries*, vol. 2, no. 2, 2016.
- [30] Y. Hu, Y. Yin and S.-Y. Choe, "Accelerated equilibration for lithium-ion battery using optimal time control," *Journal of Power Sciences*, vol. 480, 2020.
- [31] L. Pei, R. Lu and C. Zhu, "Relaxation model of the open-circuit voltage for state-of-charge estimation in lithium-ion batteries," *IET Electrical Systems in Transportation*, vol. 3, no. 4, pp. 112-117, 2013.
- [32] Z. M. Konz, E. J. McShane and B. D. McCloskey, "Detecting the Onset of Lithium Plating and Monitoring Fast Charging Performance with Voltage Relaxation," *ACS Energy Letters*, vol. 5, pp. 1750-17557, 2020.
- [33] D. B. Theuerkauf and L. Swan, "Characteristics of Open Circuit Voltage Relaxation in Lithium-Ion Batteries for the Purpose of State of Charge and State of Health Analysis," *Batteries*, vol. 8, no. 8, p. 77, 2022.

- [34] M. Petzl and M. A. Danzer, "Advancements in OCV Measurement and Analysis for Lithium-Ion Batteries," *IEEE TRANSACTIONS ON ENERGY CONVERSION*, vol. 28, no. 3, pp. 675 -681, 2013.
- [35] Y. Rangom, T. T. Duigan and X. S. Zhao, "Lithium-Ion Transport Behavior in Thin-Film Graphite Electrodes with SEI Layers Formed at Different Current Densities," *ACS Applied Material Interfaces*, vol. 13, no. 36, p. 42662–42669, 2021.
- [36] O. Capron, R. Gopalakrishnan, J. Jaguemont, P. Van Den Bossche, N. Omar and J. Van Mierlo, "On the Ageing of High Energy Lithium-Ion," *Materials*, vol. 11, no. 2, p. 176, 2018.

Appendix A Batteries journal copyright agreement

Copyright and Licensing

For all articles published in MDPI journals, copyright is retained by the authors. Articles are licensed under an open access Creative Commons CC BY 4.0 license, meaning that anyone may download and read the paper for free. In addition, the article may be reused and quoted provided that the original published version is cited. These conditions allow for maximum use and exposure of the work, while ensuring that the authors receive proper credit.

In exceptional circumstances articles may be licensed differently. If you have specific condition (such as one linked to funding) that does not allow this license, please mention this to the editorial office of the journal at submission. Exceptions will be granted at the discretion of the publisher.

Reproducing Published Material from other Publishers

It is absolutely essential that authors obtain permission to reproduce any published material (figures, schemes, tables or any extract of a text) which does not fall into the public domain, or for which they do not hold the copyright. Permission should be requested by the authors from the copyright holder (usually the Publisher, please refer to the imprint of the individual publications to identify the copyright holder).

Permission **is required** for:


1. Your own works published by other Publishers and for which you did not retain copyright.
2. Substantial extracts from anyone's works or a series of works.
3. Use of Tables, Graphs, Charts, Schemes and Artworks if they are unaltered or slightly modified.
4. Photographs for which you do not hold copyright.

Permission **is not required** for:

1. Reconstruction of your *own* table with data already published elsewhere. Please notice that in this case you must cite the source of the data in the form of either "Data from..." or "Adapted from..."
2. Reasonably short quotes are considered *fair use* and therefore do not require permission.
3. Graphs, Charts, Schemes and Artworks that are completely redrawn by the authors and significantly changed beyond recognition do not require permission

Appendix B Copyright Permission

[9]



Understanding electrochemical potentials of cathode materials in rechargeable batteries
Author: Chaofeng Liu, Zachary G. Neale, Guozhong Cao
Publication: Materials Today
Publisher: Elsevier
Date: March 2016
Copyright © 2015 The Authors. Published by Elsevier Ltd.

Creative Commons Attribution-NonCommercial-No Derivatives License (CC BY NC ND)

This article is published under the terms of the [Creative Commons Attribution-NonCommercial-No Derivatives License \(CC BY NC ND\)](#). For non-commercial purposes you may copy and distribute the article, use portions or extracts from the article in other works, and text or data mine the article, provided you do not alter or modify the article without permission from Elsevier. You may also create adaptations of the article for your own personal use only, but not distribute these to others. You must give appropriate credit to the original work, together with a link to the formal publication through the relevant DOI, and a link to the Creative Commons user license above. If changes are permitted, you must indicate if any changes are made but not in any way that suggests the licensor endorses you or your use of the work.

Permission is not required for this non-commercial use. For commercial use please continue to request permission via [RightsLink](#).

[BACK](#)[CLOSE WINDOW](#)

[10]

TERMS AND CONDITIONS

Aug 04, 2022

This Agreement between Dalhousie University -- David Theuerkauf ("You") and Elsevier("Elsevier") consists of your license details and the terms and conditions provided by Elsevier and Copyright Clearance Center.

License Number	5361950488929
License date	Aug 04, 2022
Licensed Content Publisher	Elsevier
Licensed Content Publication	Energy Storage Materials
Licensed Content Title	Low voltage anode materials for lithium-ion batteries
Licensed Content Author	Ali Eftekhari
Licensed Content Date	Apr 1, 2017
Licensed Content Volume	7
Licensed Content Issue	n/a
Licensed Content Pages	24
Start Page	157
End Page	180
Type of Use	reuse in a thesis/dissertation
Portion	figures/tables/illustrations
Number of figures/tables/illustrations	1
Format	electronic
Are you the author of this Elsevier article?	No
Will you be translating?	No
Title	Voltage Relaxation Methods for Voltage, State of Charge, and State of Health Estimation in Lithium-Ion Batteries
Institution name	Dalhousie University
Expected presentation date	Aug 2022

Portions
Requestor Location

Figure 2b
Dalhousie University 5273 DaCosta Row,
Halifax, NS B3J 0H6 Canada Attn:
Dalhousie University

Publisher Tax ID GB 494 6272 12

Total 0.00 USD

Agreement in accordance with Terms and Conditions provided from journal.

[11]

Phosphates as Lithium-Ion Battery Cathodes: An Evaluation Based on High-Throughput ab Initio Calculations

Author: Geoffroy Hautier, Anubhav Jain, Shyue Ping Ong, et al

Publication: Chemistry of Materials

Publisher: American Chemical Society

Date: Aug 1, 2011

Copyright © 2011, American Chemical Society

PERMISSION/LICENSE IS GRANTED FOR YOUR ORDER AT NO CHARGE

This type of permission/license, instead of the standard Terms and Conditions, is sent to you because no fee is being charged for your order. Please note the following:

- Permission is granted for your request in both print and electronic formats, and translations.
- If figures and/or tables were requested, they may be adapted or used in part.
- Please print this page for your records and send a copy of it to your publisher/graduate school.
- Appropriate credit for the requested material should be given as follows: "Reprinted (adapted) with permission from (COMPLETE REFERENCE CITATION). Copyright (YEAR) American Chemical Society." Insert appropriate information in place of the capitalized words.
- One-time permission is granted only for the use specified in your RightsLink request. No additional uses are granted (such as derivative works or other editions). For any uses, please submit a new request.

If credit is given to another source for the material you requested from RightsLink, permission must be obtained from that source.

BACK CLOSE WINDOW

[12]

ELSEVIER LICENSE TERMS AND CONDITIONS

Aug 04, 2022

This Agreement between Dalhousie University -- David Theuerkauf ("You") and Elsevier("Elsevier") consists of your license details and the terms and conditions provided by Elsevier and Copyright Clearance Center.

License Number	5361951184431
License date	Aug 04, 2022
Licensed Content Publisher	Elsevier
Licensed Content Publication	Joule
Licensed Content Title	Generation and Evolution of the Solid Electrolyte Interphase of Lithium-Ion Batteries
Licensed Content Author	Satu Kristiina Heiskanen, Jongjung Kim, Brett L. Lucht
Licensed Content Date	Oct 16, 2019
Licensed Content Volume	3
Licensed Content Issue	10
Licensed Content Pages	12
Start Page	2322
End Page	2333
Type of Use	reuse in a thesis/dissertation
Portion	figures/tables/illustrations
Number of figures/tables/illustrations	1

Format	electronic
Are you the author of this Elsevier article?	No
Will you be translating?	No
Title	Voltage Relaxation Methods for Voltage, State of Charge, and State of Health Estimation in Lithium-Ion Batteries
Institution name	Dalhousie University
Expected presentation date	Aug 2022
Portions	Figure 3
Requestor Location	Dalhousie University 5273 DaCosta Row Halifax, NS B3J 0H6 Canada Attn: Dalhousie University
Publisher Tax ID	GB 494 6272 12
Total	0.00 USD

Agreement in accordance with Terms and Conditions provided from journal.

[17]

Publisher: Elsevier

Copyright © 1969, Elsevier

Creative Commons


This is an open access article distributed under the terms of the [Creative Commons CC-BY](#) license, which permits unrestricted use, distribution, and reproduction in any medium, provided the original work is properly cited.

You are not required to obtain permission to reuse this article.

To request permission for a type of use not listed, please contact [Elsevier Global Rights Department](#).

Are you the [author](#) of this Elsevier journal article?

[24] C.-F. Chiasserini and R. R. Rao, "Energy Efficient Battery Management," *IEEE Journal on Selected Areas in Communications*, vol. 19, no. 7, pp. 1235-1245, 2001.



Energy efficient battery management

Author: C.-F. Chiasserini

Publication: IEEE Journal on Selected Areas in Communications

Publisher: IEEE

Date: July 2001

Copyright © 2001, IEEE

Thesis / Dissertation Reuse

The IEEE does not require individuals working on a thesis to obtain a formal reuse license, however, you may print out this statement to be used as a permission grant:

Requirements to be followed when using any portion (e.g., figure, graph, table, or textual material) of an IEEE copyrighted paper in a thesis:

- 1) In the case of textual material (e.g., using short quotes or referring to the work within these papers) users must give full credit to the original source (author, paper, publication) followed by the IEEE copyright line © 2011 IEEE.
- 2) In the case of illustrations or tabular material, we require that the copyright line © [year of original publication] IEEE appear prominently with each reprinted figure and/or table.
- 3) If a substantial portion of the original paper is to be used, and if you are not the senior author, also obtain the senior author's approval.

Requirements to be followed when using an entire IEEE copyrighted paper in a thesis:

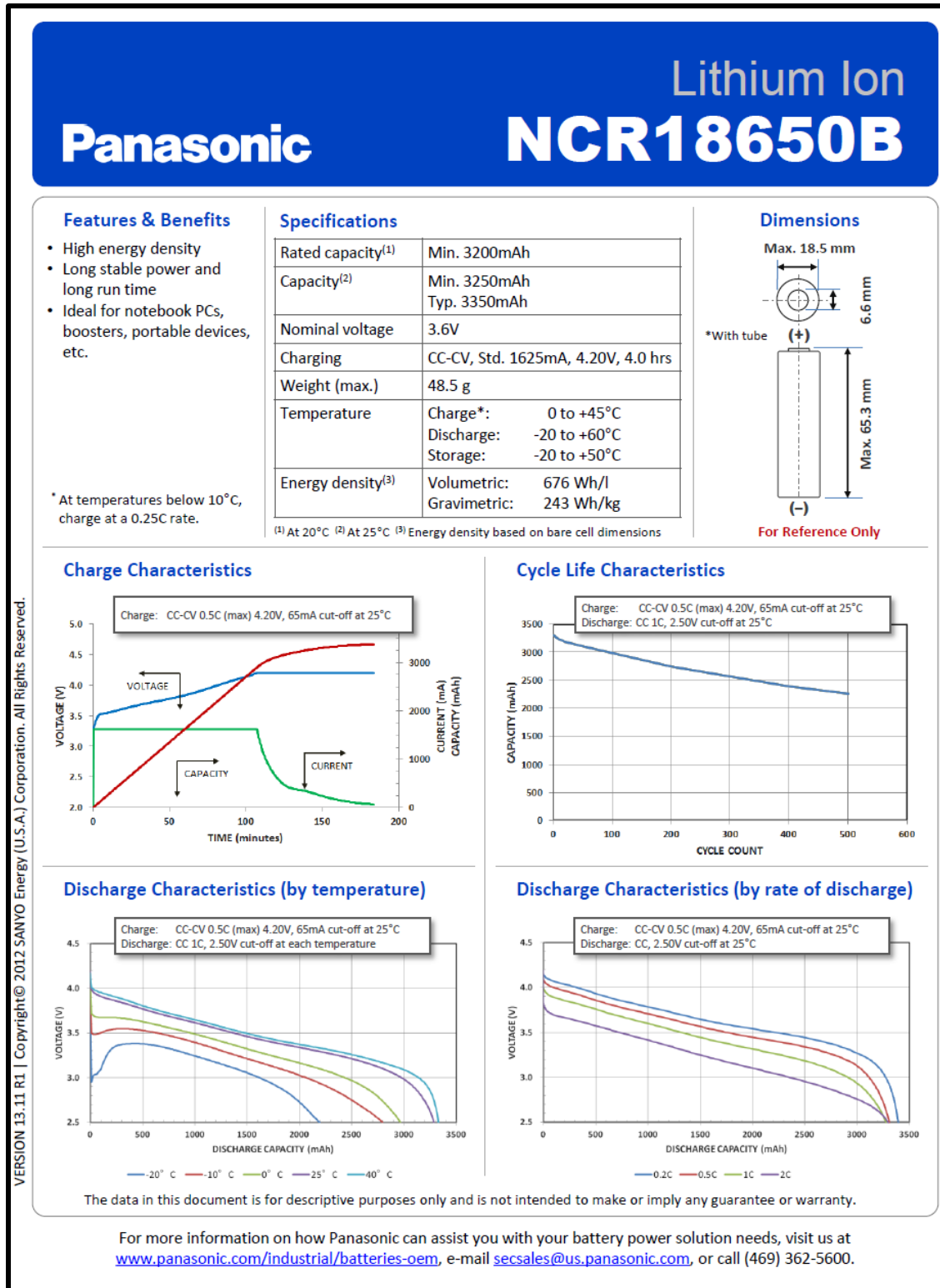
- 1) The following IEEE copyright/ credit notice should be placed prominently in the references: © [year of original publication] IEEE. Reprinted, with permission, from [author names, paper title, IEEE publication title, and month/year of publication]
- 2) Only the accepted version of an IEEE copyrighted paper can be used when posting the paper or your thesis on-line.
- 3) In placing the thesis on the author's university website, please display the following message in a prominent place on the website: in reference to IEEE copyrighted material which is used with permission in this thesis, the IEEE does not endorse any of [university/educational entity's name goes here]'s products or services. Internal or personal use of this material is permitted. If interested in reprinting/republishing IEEE copyrighted material for advertising or promotional purposes or for creating new collective works for resale or redistribution, please go to http://www.ieee.org/publications_standards/publications/rights/rights_link.html to learn how to obtain a License from RightsLink.

If applicable, University Microfilms and/or ProQuest Library, or the Archives of Canada may supply single copies of the dissertation.

BACK
CLOSE WINDOW

Appendix C Cell specification sheets

NCA





Description

Lithium Ion ICR18650 B4 2600mAh

PRODUCT SPECIFICATION

Date

2010-04-20

Rev

0

1. General Information

1.1 Scope

This product specification defines the requirements of the rechargeable lithium ion battery to be supplied to the Customer by LG Chem.

1.2 Application: Note PC

1.3 Product classification: Cylindrical rechargeable lithium ion battery

1.4 Model name: ICR18650B4

2. Nominal Specification

Item	Condition / Note	Specification
2.1 Capacity	Std. charge / discharge	Nominal 2,600mAh (C_{nom}) Minimum 2,500mAh (C_{min})
2.2 Nominal Voltage	Average	3.6V
2.3 Standard Charge (Refer to 4.1.1)	Constant current Constant voltage End current(Cut off)	0.5C(1250mA) 4.2V 50mA
2.4 Max. Charge Voltage		4.2V
2.5 Max. Charge Current		1.0C(2500mA)
2.6 Standard Discharge (Refer to 4.1.2)	Constant current End voltage(Cut off)	0.2C(500mA) 2.75V
2.7 Max. Discharge Current	-20 ~ 5 °C	0.5C(1250mA)
	5 ~ 45 °C	2.0C(5000mA)
	45 ~ 60 °C	1.5C(3750mA)
2.8 Weight	Approx.	Max. 48.0g
2.9 Operating Temperature	Charge	0 ~ 45 °C
	Discharge	-20 ~ 60 °C
2.10 Storage Temperature (for shipping state)	1 month	-20 ~ 60 °C
	3 month	-20 ~ 45 °C
	1 year	-20 ~ 20 °C

LFP

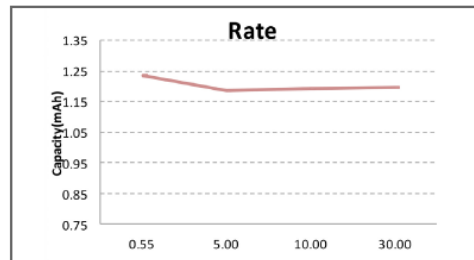
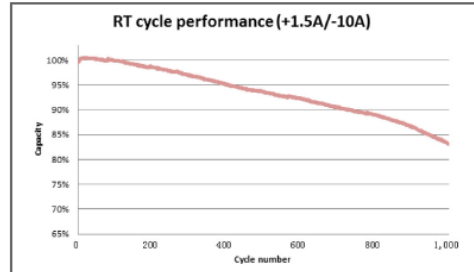
18650 Lithium Ion Power Cell

NanoPhosphate® Technology

Specs for APR18650m1B

Nominal Ratings	
Voltage	3.3 V
Capacity	1.1 Ah
Energy	3.63 Wh
Impedance (1KHz AC Typical)	12 mΩ
Cycle Life at 1C/1C, 100% DOD	> 4000 cycles
Discharging	
Max Continuous Discharge	30 A
Max Pulse Discharge Current <50% SOC (10s)	50 A
Minimum Voltage	2 V
Temperature	-30°C to 55°C
Charging	
Recommended Standard Charge	1.1 A
Max Charge Rate	4 A
Max Pulse Charge Current >50% SOC (10s)	10 A
Float Voltage	3.45 V
Recommended charge V & Cut-off Current	3.6 V, taper to 50mA
Temperature (reduce charging current to <40mA when under 0°C)	0°C to 55°C
Mechanical	
Diameter	Ø18.2 +/- 0.2 mm
Length	64.95 +/- 0.2 mm
Mass	39 g
Certifications	
Transportation	UN 3480 (UN38.3), CIQ
Safety	UL 1642, IEC 62133
Part Number 300749-006	

Cell Data



Abuse

Nail penetration	Pass - EUCAR4
Over-Discharge	Pass - EUCAR3
Thermal Stability	Pass - EUCAR4
External Short	Pass - EUCAR3
Crush	Pass - EUCAR3
Overcharge	Pass - EUCAR2

18650 Data Sheet
Aug 2018

LithiumWerks™

www.lithiumwerks.com/contact

North America Sales
1807 W. Braker Ln.
Suite 500
Austin, Texas 78758 USA

Tel +1 (512) 527-2900
Fax +1 (512) 527-2910

Europe / Middle East / Africa Sales
Unit 63 Mallusk Enterprise Park
Mallusk Co. Antrim
Northern Ireland BT36 4GN

Tel +44(0) 28 9084 5400
Fax +44(0) 28 9083 8912

Performance may vary depending on, but not limited to cell usage and application. If cell is used outside specifications, performance will diminish. All specifications are subject to change without notice. All information provided herein is believed, but not guaranteed, to be current and accurate.
Copyright © 2018 Lithium Werks Inc.



Land & Sea



Certificate of Calibration



ISO 9001:2015

Instrument Information

Certificate Number: 2017121-1

Customer Name: Dalhousie University

Customer Address: Engineering
1236 Henry Street
Halifax, NS

Manufacturer Name:	Fluke
Model Number:	289
Serial Number:	36750150
Asset Number:	N/A
Description:	Multimeter

Calibration Information

Date of Calibration:	<u>Sep-22-2021</u>	
Next Calibration Due:	<u>Sep-22-2022</u>	
Calibration Interval:	<u>12 months</u>	
Calibration Procedure:	Procedure	Revision Date
	OEM Manual	Mar 2009
	33K1-4-2522-1	Nov 30, 2019

Calibration Location:	Electrical Lab
Ambient Temperature:	23.0°C
Ambient Humidity:	35.1%
Received Condition:	Pass
Returned Condition:	Pass

Traceability Information

Land & Sea Instrumentation Ltd. hereby certifies that the above described instrument met the manufacturers published specifications at the time of calibration unless otherwise noted. It has been calibrated using standards which are traceable to the National Research Council of Canada and/or the U.S. National Institute of Standards and Technology, or other recognized national standards laboratories. A minimum of 4:1 accuracy ratio has been used for all measurements unless otherwise noted in the Calibration Data Report. This Calibration Certificate and the associated Calibration Data Results apply only to the instrument identified herein.

Standards Used

Asset	Mfg	Model	Serial	Description	Cal. Date	Due Date
STD 093	Omega	TRC III	5109901	Ice Point Cell	Feb-23-2021	Feb-23-2022
STD 094	Omega	TRP-K		Transition Probe	N/A	N/A
STD 008	HP	3458A	2823A16708	Digital Multimeter	Jul-29-2021	Jul-29-2024
MST 668	Fluke	5502A/SC600	5128802	Calibrator	Oct-23-2020	Oct-23-2022

Notes

Calibrated.

Approvals

Quality Inspector: David Bingley

Calibration Technician: Trevor Harvey

Copyright of this report is owned by Land & Sea Instrumentation Ltd., and shall not be reproduced other than in full without prior written permission of both stated customer, and Land & Sea Instrumentation Ltd. 25 Estates Road, Woodside Industrial Park, Dartmouth, Nova Scotia, Canada, B2Y 4K3
Phone 902-461-2009 Fax 902-461-0848 www.landseainstruments.com



Land & Sea



Calibration Data Results

Instrument Information

Certificate # 2017121-1
Work Order : 2017121
Manufacturer : Fluke
Model: 289

Description: Multimeter
Serial: 36750150
Asset: N/A

Power LED Test:		Reading:	
Verify the power LED lights for about 4 sec on power-up.		As found	As left
		pass	pass
Backlight Test:		Reading:	
Verify backlight has two different intensity levels.		As found	As left
		pass	pass
Current Sensing Test:		Reading:	
Verify the meter chirps with leads in the current terminals and the rotary switch set to non-current settings.		As found	As left
		pass	pass
Verify the meter does not chirp with leads in the current terminals and the rotary switch set to current settings.		pass	pass
Keypad Test:		Reading:	
Verify all pushbuttons respond with a beep for each button.		As found	As left
		pass	pass
Display Test:		Reading:	
Verify all segments of the display are displayed.		As found	As left
		pass	pass
IR Port Verification:		Reading:	
Verify proper operation of the IR Port.		As found	As left
		pass	pass
Temperature Accuracy Test:		Tolerance:	
Type:	Applied:	Minimum	Maximum
K	(°C) (mV)	(°C)	(°C)
	0.0 0.000	-1.0	1.0
	100.0 4.096	98.0	102.0
	1000.0 41.276	989.0	1011.0
		Reading:	
		As found	As left
		(°C)	(°C)
		0.5	0.5
		100.4	100.4
		1000.4	1000.4
			pass
			pass
			pass



Land & Sea



Calibration Data Results

Instrument Information

Certificate # 2017121-1
 Work Order : 2017121
 Manufacturer : Fluke
 Model: 289

Description: Multimeter
 Serial: 36750150
 Asset: N/A

DC Voltage:		Tolerance:		Reading:		
Range:	Applied:	Minimum	Maximum	As found	As left	
(mV)	(mV)	(mV)	(mV)	(mV)	(mV)	
50	0.000	-0.020	0.020	0.009	0.009	pass
	0.025	0.005	0.045	0.033	0.033	pass
	-0.025	-0.045	-0.005	-0.017	-0.017	pass
	50.000	49.955	50.045	50.005	50.005	pass
500	500.00	499.85	500.15	499.98	499.98	pass
	-250.00	-250.08	-249.92	-249.99	-249.99	pass
mV DC/AC:		Tolerance:		Reading:		
Range:	Applied:	Minimum	Maximum	As found	As left	
(mV)	(mV)	(mV)	(mV)	(mV)	(mV)	
500	50.00 (@ 0 Hz)	49.97	50.03	50.00	50.00	pass
mV AC/DC:		Tolerance:		Reading:		
Range:	Applied:	Minimum	Maximum	As found	As left	
(mV)	(mV)	(mV)	(mV)	(mV)	(mV)	
500	250.00 (@ 35 kHz)	237.10	262.90	248.62	248.62	pass
Resistance:		Tolerance:		Reading:		
Range:	Applied:	Minimum	Maximum	As found	As left	
(Ω)	(Ω)	(Ω)	(Ω)	(Ω)	(Ω)	
50 (Lo ohms)	0.200	0.180	0.220	0.213	0.213	pass
	50.000	49.905	50.095	50.015	50.015	pass
500 (Lo ohms)	0.00	-0.10	0.10	0.02	0.02	pass
	0.20	0.10	0.30	0.22	0.22	pass
	500.00	499.65	500.35	499.98	499.98	pass
(kΩ)	(kΩ)	(kΩ)	(kΩ)	(kΩ)	(kΩ)	
5	5.0000	4.9973	5.0027	5.0003	5.0003	pass
50	50.000	49.973	50.027	49.998	49.998	pass
500	500.00	499.73	500.27	500.07	500.07	pass
(MΩ)	(MΩ)	(MΩ)	(MΩ)	(MΩ)	(MΩ)	
5	5.0000	4.9921	5.0079	5.0013	5.0013	pass
30	30.000	29.546	30.454	30.044	30.044	pass
500	300.0	275.8	324.2	303.6	303.6	pass



Land & Sea

Calibration Data Results



Instrument Information

Certificate # 2017121-1
Work Order : 2017121
Manufacturer : Fluke
Model: 289

Description: Multimeter
Serial: 36750150
Asset: N/A

AC Voltage:			Tolerance:		Reading:		
Range:	Applied:		Minimum	Maximum	As found	As left	
(mV)	(mV)		(mV)	(mV)	(mV)	(mV)	
50	5.000 (@ 20 Hz)		4.865	5.135	4.987	4.987	pass
	50.000 (@ 65 KHz)		48.210	51.790	48.969	48.969	pass
500	50.00 (@ 100 KHz)		47.85	52.15	49.41	49.41	pass
	250.00 (@ 65 kHz)		240.85	259.15	248.55	248.55	pass
	500.00 (@ 45 Hz)		498.25	501.75	499.93	499.93	pass
(V)	(V)		(V)	(V)	(V)	(V)	
5	0.1000 (@ 60 Hz)		0.0952	0.1048	0.0988	0.0988	pass
	0.5000 (@ 10 kHz)		0.4945	0.5055	0.4966	0.4966	pass
	3.0000 (@ 100 kHz)		2.8160	3.1840	3.0059	3.0059	pass
50	15.000 (@ 100 kHz)		14.435	15.565	14.944	14.944	pass
500	500.00 (@ 10 kHz)		497.75	502.25	499.33	499.33	pass
	(Lo Pass) 50.00 (@ 60 Hz)		48.60	51.40	49.92	49.92	pass
	(Lo Pass) 50.00 (@ 1600 Hz)		0.00	8.00	6.79	6.79	pass
1000	1000.0 (@ 10 kHz)		993.5	1006.5	998.6	998.6	pass
Frequency:			Tolerance:		Reading:		
Range:	Applied:		Minimum	Maximum	As found	As left	
(mV)	(Hz)		(Hz)	(Hz)	(Hz)	(Hz)	
500	45 (@ 500 mV)		44.986	45.014	45.000	45.000	pass
	(KHz)		(KHz)	(KHz)	(KHz)	(KHz)	
	950 (@ 600 mV)		949.90	950.10	950.00	950.00	pass
Duty Cycle:			Tolerance:		Reading:		
Range:	Applied:		Minimum	Maximum	As found	As left	
(V)	(V p-p)		(%)	(%)	(%)	(%)	
5	5.0 (@ 50 kHz,)		1.40	28.60	23.38	23.38	pass
	(15% duty cycle, square wave)						
ACV Peak:			Tolerance:		Reading:		
Range:	Applied:		Minimum	Maximum	As found	As left	
(V)	(V p-p)		(V)	(V)	(V)	(V)	
5	4.0 (@ 2 kHz,)		1.863	2.137	1.996	1.996	pass
	(Square wave, +1V offset)						
DC Voltage:			Tolerance:		Reading:		
Range:	Applied:		Minimum	Maximum	As found	As left	
(V)	(V)		(V)	(V)	(V)	(V)	
5	4.0000		3.9988	4.0012	3.9999	3.9999	pass
50	-40.000		-40.012	-39.988	-39.997	-39.997	pass
500	400.00		399.86	400.14	399.99	399.99	pass
1000	600.0		599.6	600.4	600.0	600.0	pass



Land & Sea



Calibration Data Results

Instrument Information

Certificate # 2017121-1
Work Order : 2017121
Manufacturer : Fluke
Model: 289

Description: Multimeter
Serial: 36750150
Asset: N/A

DCV DC/AC:		Tolerance:		Reading:		
Range:	Applied:	Minimum	Maximum	As found	As left	
(V)	(V)	(V)	(V)	(V)	(V)	
5	0.2000 (@ 0 Hz)	0.1977	0.2023	0.2001	0.2001	pass
DCV AC/DC:		Tolerance:		Reading:		
Range:	Applied:	Minimum	Maximum	As found	As left	
(V)	(V)	(V)	(V)	(V)	(V)	
5	2.0000 (@ 5 kHz)	1.9640	2.0360	2.0004	2.0004	pass
Capacitance:		Tolerance:		Reading:		
Range:	Applied:	Minimum	Maximum	As found	As left	
(nF)	(nF)	(nF)	(nF)	(nF)	(nF)	
10	5.00	4.90	5.10	5.05	5.05	pass
Diode Test:		Tolerance:		Reading:		
Range:	Applied:	Minimum	Maximum	As found	As left	
(V)	(kΩ)	(V)	(V)	(V)	(V)	
3.1	3.5	2.0000	3.1000	2.8279	2.8279	pass
Verify the beeper sounds with 0 ohms applied.				pass	pass	
AC Current:		Tolerance:		Reading:		
Range:	Applied:	Minimum	Maximum	As found	As left	
(μA)	(μA)	(μA)	(μA)	(μA)	(μA)	
500	500.00 (@ 60 Hz)	496.80	503.20	499.74	499.74	pass
	500.00 (@ 10 kHz)	492.85	507.15	499.40	499.40	pass
5000	5000.0 (@ 10 kHz)	4928.5	5071.5	4999.7	4999.7	pass
(mA)	(mA)	(mA)	(mA)	(mA)	(mA)	
50	4.000 (@ 20 Hz)	3.940	4.060	3.978	3.978	pass
	30.000 (@ 10 kHz)	29.375	30.625	29.968	29.968	pass
400	300.00 (@ 10 kHz)	284.60	315.40	300.09	300.09	pass
	400.00 (@ 60 Hz)	397.55	402.45	400.18	400.18	pass
(A)	(A)	(A)	(A)	(A)	(A)	
5	5.0000 (@ 1 kHz)	4.9580	5.0420	4.9991	4.9991	pass
10	5.000 (@ 1 kHz)	4.955	5.045	5.002	5.002	pass
DC Current:		Tolerance:		Reading:		
Range:	Applied:	Minimum	Maximum	As found	As left	
(μA)	(μA)	(μA)	(μA)	(μA)	(μA)	
500	500.00	499.42	500.58	499.95	499.95	pass
5000	5000.0	4996.0	5004.0	4999.4	4999.4	pass



Land & Sea



Calibration Data Results

Instrument Information

Certificate # 2017121-1
Work Order : 2017121
Manufacturer : Fluke
Model: 289

Description: Multimeter
Serial: 36750150
Asset: N/A

DC Current:(cont.)		Tolerance:		Reading:		
Range:	Applied:	Minimum	Maximum	As found	As left	
(mA)	(mA)	(mA)	(mA)	(mA)	(mA)	
50	0.100	0.090	0.110	0.102	0.102	pass
	50.000	49.965	50.035	49.995	49.995	pass
400	400.0	399.38	400.62	399.95	399.95	pass
(A)	(A)	(A)	(A)	(A)	(A)	
5	5.0000	4.9840	5.0160	4.9995	4.9995	pass
10	10.000	9.968	10.032	10.001	10.001	pass
AC Voltage: (LoZ)		Tolerance:		Reading:		
Range:	Applied:	Minimum	Maximum	As found	As left	
(V)	(V)	(V)	(V)	(V)	(V)	
1000	120.0 (@ 60 Hz)	113.6	126.4	120.6	120.6	pass

Appendix E Arbin Calibration Sheets

Current - Initial Validation

Channel	Calibration Type	Current Setting	Setpoint (A)	Arbin Measurement(A)	Fuke Measurement(A)	Difference in Measurement	Difference from Setpoint	Percentage Error (Measurement)	Abs Percentage Error (Measurement)	Percentage Error (Setpoint)	Abs Percentage Error (Setpoint)	Percentage Error (SetpointTon)	Abs Percentage Error (SetpointTon)
1	CC(A)	High	-90	-89.99	-89.95	0.04	0.05	-0.0445%	0.0445%	0.0556%	0.0556%	-0.0111%	0.0111%
1	CC(A)	High	-25	-24.9996	-24.996	0.0036	0.004	-0.0144%	0.0144%	0.0160%	0.0160%	-0.016%	0.016%
1	CC(A)	Med	-2	-1.9981	-2.007	-0.0089	-0.007	0.4434%	0.4434%	0.3500%	0.3500%	-0.050%	0.050%
1	CC(A)	Med	-2	-1.9999	-1.9987	0.0012	0.0013	-0.0600%	0.0600%	0.0650%	0.0650%	-0.0650%	0.0650%
1	CC(A)	Med	-1	-0.9999	-1.9988	0.0011	0.0012	-0.0550%	0.0550%	0.0600%	0.0600%	-0.060%	0.060%
1	CC(A)	Med	-1	-0.9999	-0.9994	0.000514	0.0006	-0.0516%	0.0516%	0.0550%	0.0550%	-0.055%	0.055%
1	CC(A)	Med	-1	-0.10003	-0.1001	-7E-05	-1E-04	0.0699%	0.0699%	0.1000%	0.1000%	0.0300%	0.0300%
1	CC(A)	Low	-0.1	-0.0999908	-0.09975	0.0002408	0.00025	-0.2414%	0.2414%	0.2500%	0.2500%	-0.025%	0.025%
1	CC(A)	Low	-0.025	-0.0249989	-0.024771	0.0002279	0.000229	-0.9200%	0.9200%	0.9160%	0.9160%	-0.044%	0.044%
1	CC(A)	Low	-0.005	-0.0049989	-0.004776	0.0002215	0.000224	-4.6378%	4.6378%	4.4800%	4.4800%	-0.050%	0.050%
1	CC(A)	Low	0.005	0.0049933	0.00522	0.0002267	0.00022	-4.3423%	4.3423%	4.4000%	4.4000%	0.050%	0.050%
1	CC(A)	Low	0.025	0.0249446	0.025213	0.0002184	0.000213	-0.8662%	0.8662%	0.8520%	0.8520%	-0.016%	0.016%
1	CC(A)	Med	0.1	0.09988	0.0997	-0.00018	-0.0003	0.1805%	0.1805%	0.3000%	0.3000%	-0.030%	0.030%
1	CC(A)	Med	0.1	0.099998	0.10019	0.0001902	0.00019	0.1898%	0.1898%	0.1900%	0.1900%	-0.002%	0.002%
1	CC(A)	Med	1	0.999998	0.999	-0.00084	-0.001	-0.0841%	0.0841%	0.1000%	0.1000%	-0.010%	0.010%
1	CC(A)	Med	1	0.99984	0.999	-0.00084	-0.001	-0.0841%	0.0841%	0.1000%	0.1000%	-0.010%	0.010%
1	CC(A)	High	2	1.9936	1.99	-0.0036	-0.01	-0.1809%	0.1809%	0.5000%	0.5000%	-0.050%	0.050%
1	CC(A)	High	25	24.9951	24.98	-0.0151	-0.02	-0.0604%	0.0604%	0.0800%	0.0800%	-0.080%	0.080%
1	CC(A)	High	90	90.0044	89.93	-0.0744	-0.07	-0.0827%	0.0827%	0.0778%	0.0778%	-0.007%	0.007%
2	CC(A)	High	-90	-89.937	-89.92	0.0737	0.08	-0.0820%	0.0820%	0.0889%	0.0889%	-0.008%	0.008%
2	CC(A)	High	-25	-24.9978	-25.002	-0.0042	-0.002	0.0168%	0.0168%	0.02%	0.02%	-0.002%	0.002%
2	CC(A)	High	-2	-2.0023	-2.011	-0.0087	-0.011	0.4326%	0.4326%	0.5500%	0.5500%	0.1150%	0.1150%
2	CC(A)	Med	-2	-1.9999	-1.9985	0.0014	0.0015	-0.0701%	0.0701%	0.0750%	0.0750%	-0.005%	0.005%
2	CC(A)	Med	-2	-1.9999	-1.9986	0.0013	0.0014	-0.0650%	0.0650%	0.0700%	0.0700%	-0.005%	0.005%
2	CC(A)	Med	-1	-0.9999	-0.9993	0.0007	0.0007	-0.0700%	0.0700%	0.0700%	0.0700%	0.000%	0.000%
2	CC(A)	Med	-1	-0.999606	-0.9998	0.0001606	0.0002	-0.1609%	0.1609%	0.2000%	0.2000%	-0.020%	0.020%
2	CC(A)	Low	-0.1	-0.0999663	-0.0997	0.0002963	0.0003	-0.2972%	0.2972%	0.3000%	0.3000%	-0.003%	0.003%
2	CC(A)	Low	-0.025	-0.025001	-0.0248	0.000201	0.0002	-0.8105%	0.8105%	0.81%	0.81%	-0.008%	0.008%
2	CC(A)	Low	-0.005	-0.004998	-0.004807	0.000191	0.000193	-3.9734%	3.9734%	3.8600%	3.8600%	-0.010%	0.010%
2	CC(A)	Low	0.005	0.0049952	0.005189	0.0001938	0.000189	0.7486%	0.7486%	0.75%	0.75%	-0.003%	0.003%
2	CC(A)	Low	0.025	0.0249915	0.02518	0.0001885	0.00018	0.1484%	0.1484%	0.14%	0.14%	-0.001%	0.001%
2	CC(A)	Med	0.1	0.0998516	0.1	0.0001884	0.00019	0.1397%	0.1397%	0.1400%	0.1400%	0.0001%	0.0001%
2	CC(A)	Med	0.1	0.1000001	0.10014	0.0001399	0.00014	-0.0632%	0.0632%	0.06%	0.06%	-0.005%	0.005%
2	CC(A)	Med	1	0.9999319	0.9993	-0.0006319	-0.0007	0.0505%	0.0505%	0.05%	0.05%	-0.005%	0.005%
2	CC(A)	Med	1	1.9919	1.992	1E-04	-0.008	-0.0356%	0.0356%	0.0720%	0.0720%	-0.007%	0.007%
2	CC(A)	High	25	24.9909	24.982	-0.0089	-0.018	-0.0356%	0.0356%	0.0333%	0.0333%	-0.003%	0.003%
2	CC(A)	High	90	89.9713	89.95	-0.0213	-0.05	-0.0237%	0.0237%	0.0256%	0.0256%	-0.002%	0.002%
3	CC(A)	High	-90	-89.985	-89.97	0.015	0.03	-0.0167%	0.0167%	0.0333%	0.0333%	-0.003%	0.003%
3	CC(A)	High	-25	-24.994	-24.999	-0.005	0.001	0.0200%	0.0200%	0.0040%	0.0040%	-0.004%	0.004%
3	CC(A)	High	-2	-1.9992	-1.999	0.0002	0.001	-0.0100%	0.0100%	0.0050%	0.0050%	-0.005%	0.005%
3	CC(A)	Med	-2	-1.9997	-1.9973	0.0024	0.0027	-0.1202%	0.1202%	0.1350%	0.1350%	-0.013%	0.013%
3	CC(A)	Med	-1	-0.999823	-0.9986	0.001223	0.0014	-0.1225%	0.1225%	0.1400%	0.1400%	-0.017%	0.017%
3	CC(A)	Med	-0.1	-0.0999847	-0.0996	0.0003847	0.0004	-0.3862%	0.3862%	0.4000%	0.4000%	-0.013%	0.013%
3	CC(A)	Low	-0.1	-0.0970047	-0.0827	0.0143047	0.0173	-0.073%	0.073%	n/a	n/a	n/a	n/a
3	CC(A)	Low	-0.025	0	0	0	0.025	n/a	n/a	n/a	n/a	n/a	n/a
3	CC(A)	Low	-0.005	0	0	0	0.005	n/a	n/a	n/a	n/a	n/a	n/a
3	CC(A)	Low	0.005	0	0	0	-0.005	n/a	n/a	n/a	n/a	n/a	n/a
3	CC(A)	Low	0.025	0	0	0	-0.025	n/a	n/a	n/a	n/a	n/a	n/a
3	CC(A)	Med	0.1	0.0998571	0.1	0.0001429	0	0.1429%	0.1429%	0.0000%	0.0000%	-0.0029%	0.0029%
3	CC(A)	Med	0.1	0.0998638	0.999	-0.000638	-0.01	-0.0865%	0.0865%	n/a	n/a	n/a	n/a
3	CC(A)	Med	1	0.9998638	2.002	-0.008638	-0.001	-0.0865%	0.0865%	-0.1000%	-0.1000%	-0.0136%	0.0136%
3	CC(A)	High	2	1.9936	2.02	0.0084	0.002	0.4196%	0.4196%	0.10%	0.10%	-0.3200%	0.3200%
3	CC(A)	High	2	2	1.9981	-0.0019	-0.0019	-0.0951%	0.0951%	-0.0950%	-0.0950%	0.0000%	0.0000%
3	CC(A)	High	25	24.9883	24.999	0.0107	-0.001	0.0428%	0.0428%	-0.0468%	-0.0468%	0.0000%	0.0000%
3	CC(A)	High	90	90.0009	89.99	-0.0109	-0.01	-0.0121%	0.0121%	-0.0111%	-0.0111%	0.0010%	0.0010%

Current – Secondary Validation

Calibration		Current	Arbin	Fuke	Difference in		Percentage Error	Abs Percentage Error		Percentage Error		Abs Percentage Error	
Channel	Type	Setting	Measurement(A)	Measurement(A)	Measurement	Setpoint	(Measurement)	Percentage Error(FSR)	(Measurement)	Setpoint	Error (Setpoint)	Setpoint(A)	Setpoint(TN)
1	CC(A)	High	-90	-89.9946	-89.997	0.0266	-0.003	-0.027%	0.030%	0.03%	0.033%	-0.0060%	0.0060%
1	CC(A)	High	-25	-25.9966	-25.003	0.9966	0.0046	-0.23%	0.011%	0.23%	0.0120%	-0.3200%	0.3200%
1	CC(A)	High	2	-1.9936	2.001	0.0064	0.001	0.31%	0.011%	0.32%	0.0500%	-0.2700%	0.2700%
1	DC(A)	High	25	24.9951	24.99	-0.0051	-0.01	-0.020%	0.020%	0.02%	0.0400%	-0.0196%	0.0196%
1	DC(A)	High	90	90.0044	89.96	-0.0444	-0.04	-0.049%	0.049%	0.05%	0.0444%	-0.0049%	0.0049%
1	CC(A)	Low	-0.1	-0.099941	-0.10001	-1.59E-05	-1E-05	0.015%	0.000%	0.02%	0.0100%	-0.0005%	0.0005%
1	CC(A)	Low	-0.025	-0.0249989	-0.025001	-2.1E-06	-1E-06	0.008%	0.000%	0.01%	0.0040%	-0.0004%	0.0004%
1	CC(A)	Low	-0.005	-0.0050008	-0.0050038	2.8E-06	2E-06	-0.05%	0.000%	0.06%	0.0400%	-0.0160%	0.0160%
1	DC(A)	Low	0.005	0.0049933	0.005002	8.7E-06	2E-06	0.17%	0.000%	0.17%	0.0400%	-0.1340%	0.1340%
1	DC(A)	Low	0.025	0.0249946	0.025003	8.4E-06	3E-06	0.034%	0.000%	0.03%	0.0120%	-0.0216%	0.0216%
1	DC(A)	Low	0.1	0.1000031	0.1	-3.1E-06	0	-0.003%	0.000%	0.00%	0.0000%	-0.0003%	0.0003%
1	CC(A)	Med	-2	-1.9999	-2.0002	-0.0003	-0.0002	0.015%	-0.000%	0.01%	0.0100%	-0.0001%	0.0001%
1	CC(A)	Med	-1	-0.9999	-1.0002	-0.0003	-0.0002	0.030%	-0.000%	0.03%	0.0200%	-0.0100%	0.0100%
1	CC(A)	Med	-0.1	-0.100321	-0.100121	0.000121	-0.0002	-0.12%	-0.000%	0.12%	0.0200%	-0.0200%	0.0200%
1	DC(A)	Med	0.1	0.099865	0.0999	1.35E-05	-0.0001	0.013%	-0.000%	0.01%	0.0100%	-0.0100%	0.0100%
1	DC(A)	Med	1	0.9998412	0.9998	-4.12E-05	-0.0002	-0.004%	-0.000%	0.00%	0.0200%	-0.0200%	0.0200%
1	DC(A)	Med	2	2.0001	2	-0.0001	0	-0.005%	0.000%	0.01%	0.0100%	-0.0100%	0.0100%
2	CC(A)	High	-90	-89.9937	-89.95	0.0437	0.05	-0.048%	0.050%	0.01%	0.0555%	-0.0050%	0.0050%
2	CC(A)	High	-25	-25.0013	-25.005	-0.0037	-0.005	0.014%	-0.005%	0.05%	0.0200%	-0.0070%	0.0070%
2	CC(A)	High	-2	-2.0023	-2.008	-0.0057	-0.008	0.28%	0.008%	0.01%	0.0200%	-0.0052%	0.0052%
2	DC(A)	High	2	1.9954	1.997	0.0016	-0.003	0.080%	-0.003%	0.08%	0.0150%	-0.0230%	0.0230%
2	DC(A)	High	25	24.9909	24.995	-0.0049	-0.005	-0.005%	-0.005%	0.02%	0.0200%	-0.0364%	0.0364%
2	DC(A)	High	90	90.0009	89.96	-0.0409	-0.04	-0.045%	-0.040%	0.05%	0.0444%	-0.0044%	0.0044%
2	CC(A)	Low	-0.1	-0.099963	-0.09999	6.3E-06	1E-05	-0.006%	0.000%	0.01%	0.0100%	-0.0003%	0.0003%
2	CC(A)	Low	-0.025	-0.025001	-0.025001	-2E-06	-1E-06	0.000%	0.000%	0.00%	0.0040%	-0.0004%	0.0004%
2	CC(A)	Low	-0.005	-0.004998	-0.005	3.8E-06	-1E-06	0.000%	0.000%	0.04%	0.0000%	-0.0000%	0.0000%
2	DC(A)	Low	0.005	0.0049952	0.0049957	9E-07	-4.3E-06	0.076%	0.000%	0.08%	0.0200%	-0.0960%	0.0960%
2	DC(A)	Low	0.025	0.0249948	0.0249957	-1.01E-05	-1E-05	-0.01%	0.000%	0.00%	0.0100%	-0.0208%	0.0208%
2	DC(A)	Low	0.1	0.100001	0.09999	-1E-04	0.0002	-0.005%	0.000%	0.01%	0.0100%	-0.0050%	0.0050%
2	CC(A)	Med	-2	-1.9999	-1.9998	1E-04	1E-04	-0.010%	0.000%	0.01%	0.0100%	-0.0000%	0.0000%
2	CC(A)	Med	-1	-1	-0.9999	6.06E-05	0.0001	0.24%	0.000%	0.06%	0.1000%	-0.0394%	0.0394%
2	DC(A)	Med	0.1	0.0998616	0.1001	0.0002484	1E-04	0.001%	0.001%	0.25%	0.100%	-0.1484%	0.1484%
2	DC(A)	Med	1	0.9999319	1.0001	0.0001681	1E-04	0.016%	0.000%	0.02%	0.0100%	-0.0068%	0.0068%
2	DC(A)	Med	2	2.0001	1.9999	-0.0002	-1E-04	-0.01%	-0.000%	0.01%	0.0050%	-0.0050%	0.0050%
3	CC(A)	High	-90	-89.9889	-89.97	0.0189	0.03	-0.021%	0.030%	0.02%	0.0333%	-0.0123%	0.0123%
3	CC(A)	High	-25	-25.01	-25.013	-0.003	-0.013	0.012%	-0.013%	0.01%	0.0520%	-0.0400%	0.0400%
3	CC(A)	High	-2	-1.9992	-2.009	-0.0098	-0.009	0.48%	-0.008%	0.10%	0.4000%	-0.5000%	0.5000%
3	DC(A)	High	2	1.99	1.992	0.002	-0.008	0.10%	-0.006%	0.01%	0.0240%	-0.0184%	0.0184%
3	DC(A)	High	25	24.9954	24.994	-0.0014	-0.006	-0.005%	-0.000%	0.01%	0.0240%	-0.0184%	0.0184%
3	DC(A)	High	90	90.0009	90	-0.0009	0	-0.001%	0.000%	0.00%	0.0000%	-0.0010%	0.0010%
3	CC(A)	Low	-0.1	N/A	N/A	N/A	n/a	N/A	N/A	N/A	N/A	N/A	N/A
3	CC(A)	Low	-0.025	N/A	N/A	N/A	n/a	N/A	N/A	N/A	N/A	N/A	N/A
3	CC(A)	Low	-0.005	N/A	N/A	N/A	n/a	N/A	N/A	N/A	N/A	N/A	N/A
3	DC(A)	Low	0.005	N/A	N/A	N/A	n/a	N/A	N/A	N/A	N/A	N/A	N/A
3	DC(A)	Low	0.025	N/A	N/A	N/A	n/a	N/A	N/A	N/A	N/A	N/A	N/A
3	CC(A)	Med	-2	-1.9999	-1.9998	1E-04	0.0002	-0.005%	0.000%	0.01%	-0.0100%	-0.0050%	0.0050%
3	CC(A)	Med	-1	-0.9999314	-1	-8.6E-06	-0.0002	0.000%	0.000%	0.00%	0.0000%	-0.0003%	0.0003%
3	CC(A)	Med	-0.1	-0.1000531	-0.1002	-0.0001469	-0.0002	0.146%	-0.000%	0.15%	0.2000%	-0.0531%	0.0531%
3	DC(A)	Med	0.1	0.0997886	0.0998	1.14E-05	-0.0002	0.0114%	-0.000%	0.01%	-0.2000%	-0.0211%	0.0211%
3	DC(A)	Med	1	0.99978638	0.9997	-0.0001638	-0.0003	-0.0003%	-0.000%	0.02%	-0.0300%	-0.0136%	0.0136%
3	DC(A)	Med	2	0.9998638	1.9998	-0.0002	-0.0002	-0.0100%	-0.000%	0.01%	-0.0100%	-0.0000%	0.0000%

Final Auxiliary Voltage Validation

Channel	Calibration Type	Setpoint(V)	Arbin Measurement(V)	Fule Measurement(V)	Difference in Measurement from Setpoint	Difference from Setpoint	Percentage Error (Measurement)	Abs Percentage Error (Measurement)	Percentage Error (Setpoint)	Abs Percentage Error (Setpoint)	Percentage Error (Setpoint)	Abs Percentage Error (Setpoint)
1 DV(V)	1	1.0106	1.0106	1.0104	0.0002	0.0104	<div><div>0.0198%</div></div>	<div><div>0.02%</div></div>	<div><div>1.0400%</div></div>	<div><div>1.04%</div></div>	<div><div>1.0600%</div></div>	<div><div>1.0600%</div></div>
2 DV(V)	1	1.0095	1.0095	1.0104	-0.0006	0.0104	<div><div>-0.0594%</div></div>	<div><div>0.06%</div></div>	<div><div>1.0400%</div></div>	<div><div>1.04%</div></div>	<div><div>0.9500%</div></div>	<div><div>0.9500%</div></div>
3 DV(V)	1	1.0102	1.0102	1.0104	-0.0002	0.0104	<div><div>-0.0198%</div></div>	<div><div>0.06%</div></div>	<div><div>1.0400%</div></div>	<div><div>1.04%</div></div>	<div><div>0.9800%</div></div>	<div><div>0.9800%</div></div>
4 DV(V)	1	1.011	1.011	1.0104	0.0006	0.0104	<div><div>0.0594%</div></div>	<div><div>0.06%</div></div>	<div><div>1.0400%</div></div>	<div><div>1.04%</div></div>	<div><div>1.0200%</div></div>	<div><div>1.0200%</div></div>
5 DV(V)	1	1.0106	1.0106	1.0104	0.0002	0.0104	<div><div>0.0198%</div></div>	<div><div>0.02%</div></div>	<div><div>1.0400%</div></div>	<div><div>1.04%</div></div>	<div><div>1.0000%</div></div>	<div><div>1.0000%</div></div>
6 DV(V)	1	1.0103	1.0103	1.0104	-1E-04	0.0104	<div><div>-0.0099%</div></div>	<div><div>0.04%</div></div>	<div><div>1.0400%</div></div>	<div><div>1.04%</div></div>	<div><div>1.0300%</div></div>	<div><div>1.0300%</div></div>
7 DV(V)	1	1.01	1.01	1.0104	-0.0004	0.0104	<div><div>-0.0396%</div></div>	<div><div>0.04%</div></div>	<div><div>1.0400%</div></div>	<div><div>1.04%</div></div>	<div><div>1.0000%</div></div>	<div><div>1.0000%</div></div>
8 DV(V)	1	1.0096	1.0096	1.0104	-0.0008	0.0104	<div><div>-0.0792%</div></div>	<div><div>0.08%</div></div>	<div><div>1.0400%</div></div>	<div><div>1.04%</div></div>	<div><div>0.9600%</div></div>	<div><div>0.9600%</div></div>
9 DV(V)	1	1.0097	1.0097	1.0104	-0.0007	0.0104	<div><div>-0.0693%</div></div>	<div><div>0.07%</div></div>	<div><div>1.0400%</div></div>	<div><div>1.04%</div></div>	<div><div>0.9700%</div></div>	<div><div>0.9700%</div></div>
10 DV(V)	1	1.01	1.01	1.0104	-0.0004	0.0104	<div><div>-0.0396%</div></div>	<div><div>0.04%</div></div>	<div><div>1.0400%</div></div>	<div><div>1.04%</div></div>	<div><div>1.0000%</div></div>	<div><div>1.0000%</div></div>
11 DV(V)	1	1.0098	1.0098	1.0104	-0.0006	0.0104	<div><div>-0.0594%</div></div>	<div><div>0.06%</div></div>	<div><div>1.0400%</div></div>	<div><div>1.04%</div></div>	<div><div>0.9800%</div></div>	<div><div>0.9800%</div></div>
12 DV(V)	1	1.0103	1.0103	1.0104	-1E-04	0.0104	<div><div>-0.0099%</div></div>	<div><div>0.01%</div></div>	<div><div>1.0400%</div></div>	<div><div>1.04%</div></div>	<div><div>1.0300%</div></div>	<div><div>1.0300%</div></div>
13 DV(V)	1	1.0095	1.0095	1.0104	-0.0009	0.0104	<div><div>-0.0891%</div></div>	<div><div>0.09%</div></div>	<div><div>1.0400%</div></div>	<div><div>1.04%</div></div>	<div><div>0.9500%</div></div>	<div><div>0.9500%</div></div>
14 DV(V)	1	1.0095	1.0095	1.0104	-0.0009	0.0104	<div><div>-0.0891%</div></div>	<div><div>0.09%</div></div>	<div><div>1.0400%</div></div>	<div><div>1.04%</div></div>	<div><div>0.9500%</div></div>	<div><div>0.9500%</div></div>
15 DV(V)	1	1.0094	1.0094	1.0104	-0.001	0.0104	<div><div>-0.0990%</div></div>	<div><div>0.10%</div></div>	<div><div>1.0400%</div></div>	<div><div>1.04%</div></div>	<div><div>0.9400%</div></div>	<div><div>0.9400%</div></div>
16 DV(V)	1	5.0505	5.0505	5.0493	0.0012	0.0493	<div><div>0.0238%</div></div>	<div><div>0.02%</div></div>	<div><div>0.9860%</div></div>	<div><div>0.99%</div></div>	<div><div>1.0100%</div></div>	<div><div>1.0100%</div></div>
1 DV(V)	5	5.0496	5.0496	5.0493	0.0003	0.0493	<div><div>0.0059%</div></div>	<div><div>0.01%</div></div>	<div><div>0.9860%</div></div>	<div><div>0.99%</div></div>	<div><div>0.9920%</div></div>	<div><div>0.9920%</div></div>
2 DV(V)	5	5.0506	5.0506	5.0493	0.0013	0.0493	<div><div>0.0257%</div></div>	<div><div>0.03%</div></div>	<div><div>0.9860%</div></div>	<div><div>0.99%</div></div>	<div><div>1.0120%</div></div>	<div><div>1.0120%</div></div>
3 DV(V)	5	5.0496	5.0496	5.0493	0.0003	0.0493	<div><div>0.0059%</div></div>	<div><div>0.01%</div></div>	<div><div>0.9860%</div></div>	<div><div>0.99%</div></div>	<div><div>0.9920%</div></div>	<div><div>0.9920%</div></div>
4 DV(V)	5	5.0507	5.0507	5.0493	0.0014	0.0493	<div><div>0.0277%</div></div>	<div><div>0.03%</div></div>	<div><div>0.9860%</div></div>	<div><div>0.99%</div></div>	<div><div>1.0140%</div></div>	<div><div>1.0140%</div></div>
5 DV(V)	5	5.0501	5.0501	5.0493	0.0008	0.0493	<div><div>0.0158%</div></div>	<div><div>0.02%</div></div>	<div><div>0.9860%</div></div>	<div><div>0.99%</div></div>	<div><div>1.0020%</div></div>	<div><div>1.0020%</div></div>
6 DV(V)	5	5.0488	5.0488	5.0493	-0.0005	0.0493	<div><div>-0.0099%</div></div>	<div><div>0.01%</div></div>	<div><div>0.9860%</div></div>	<div><div>0.99%</div></div>	<div><div>0.9760%</div></div>	<div><div>0.9760%</div></div>
7 DV(V)	5	5.0491	5.0491	5.0493	-0.0002	0.0493	<div><div>-0.0040%</div></div>	<div><div>0.00%</div></div>	<div><div>0.9860%</div></div>	<div><div>0.99%</div></div>	<div><div>0.9820%</div></div>	<div><div>0.9820%</div></div>
8 DV(V)	5	5.0479	5.0479	5.0493	-0.0014	0.0493	<div><div>-0.0279%</div></div>	<div><div>0.03%</div></div>	<div><div>0.9860%</div></div>	<div><div>0.99%</div></div>	<div><div>0.9780%</div></div>	<div><div>0.9780%</div></div>
9 DV(V)	5	5.0489	5.0489	5.0493	-0.0004	0.0493	<div><div>-0.0040%</div></div>	<div><div>0.01%</div></div>	<div><div>0.9860%</div></div>	<div><div>0.99%</div></div>	<div><div>0.9820%</div></div>	<div><div>0.9820%</div></div>
10 DV(V)	5	5.0491	5.0491	5.0493	-0.0002	0.0493	<div><div>-0.0040%</div></div>	<div><div>0.00%</div></div>	<div><div>0.9860%</div></div>	<div><div>0.99%</div></div>	<div><div>0.9820%</div></div>	<div><div>0.9820%</div></div>
11 DV(V)	5	5.0491	5.0491	5.0493	-0.0002	0.0493	<div><div>-0.0040%</div></div>	<div><div>0.01%</div></div>	<div><div>0.9860%</div></div>	<div><div>0.99%</div></div>	<div><div>0.9840%</div></div>	<div><div>0.9840%</div></div>
12 DV(V)	5	5.0497	5.0497	5.0493	0.0004	0.0493	<div><div>0.0079%</div></div>	<div><div>0.01%</div></div>	<div><div>0.9860%</div></div>	<div><div>0.99%</div></div>	<div><div>0.9960%</div></div>	<div><div>0.9960%</div></div>
13 DV(V)	5	5.0498	5.0498	5.0493	0.0005	0.0493	<div><div>0.0099%</div></div>	<div><div>0.01%</div></div>	<div><div>0.9860%</div></div>	<div><div>0.99%</div></div>	<div><div>0.9620%</div></div>	<div><div>0.9620%</div></div>
14 DV(V)	5	5.0481	5.0481	5.0493	-0.0012	0.0493	<div><div>-0.0238%</div></div>	<div><div>0.02%</div></div>	<div><div>0.9860%</div></div>	<div><div>0.99%</div></div>	<div><div>0.9660%</div></div>	<div><div>0.9660%</div></div>
15 DV(V)	5	5.0483	5.0483	5.0493	-0.001	0.0493	<div><div>-0.0198%</div></div>	<div><div>0.02%</div></div>	<div><div>0.9860%</div></div>	<div><div>0.99%</div></div>	<div><div>0.9660%</div></div>	<div><div>0.9660%</div></div>
16 DV(V)	5											

Final Auxiliary temperature Validation

Calibration			Difference in		Percentage Error		Abs Percentage Error		Percentage Error		Abs Percentage Error	
Channel	Type	Setpoint(C)	Arbin Measurement(C)	Bath Measurement(C)	Measurement from Setpoint	(Measurement)	(Measurement)	(SetpointToF)	Error (SetpointToF)	(SetpointToN)	(SetpointToN)	
1 D(V/V)	100	100	98.9101	100.01	-1.0999	-1.098%	1.10%	0.0100%	0.01%	-1.0899%	1.0899%	
2 D(V/V)	100	100	100.68	100.01	0.67	0.669%	0.67%	0.0100%	0.01%	0.6800%	0.6800%	
3 D(V/V)	100	100	100.799	100.01	0.789	0.788%	0.79%	0.0100%	0.01%	0.7990%	0.7990%	
4 D(V/V)	100	100	100.55	100.01	0.54	0.539%	0.54%	0.0100%	0.01%	0.5500%	0.5500%	
5 D(V/V)	100	100	100.06	100.01	0.05	0.050%	0.05%	0.0100%	0.01%	0.0600%	0.0600%	
6 D(V/V)	100	100	99.594	100.01	-0.416	-0.416%	0.42%	0.0100%	0.01%	-0.4060%	0.4060%	
7 D(V/V)	100	100	100.01	100.01	0	0.000%	0.00%	0.0100%	0.01%	0.0100%	0.0100%	
8 D(V/V)	100	100	100.51	100.01	0.5	0.500%	0.50%	0.0100%	0.01%	0.5100%	0.5100%	
9 D(V/V)	100	100	99.19	100.01	-0.82	-0.818%	0.82%	0.0100%	0.01%	-0.8100%	0.8100%	
10 D(V/V)	100	100	99.52	100.01	-0.49	-0.490%	0.49%	0.0100%	0.01%	-0.4800%	0.4800%	
11 D(V/V)	100	100	99.4881	100.01	-0.5219	-0.521%	0.52%	0.0100%	0.01%	-0.5119%	0.5119%	
12 D(V/V)	100	100	88.85	100.01	-11.16	-11.158%	11.16%	0.0100%	0.01%	-11.1500%	11.1500%	
13 D(V/V)	100	100	100.15	100.01	0.14	0.140%	0.14%	0.0100%	0.01%	0.1500%	0.1500%	
14 D(V/V)	100	100	99.82	100.01	-0.19	-0.190%	0.19%	0.0100%	0.01%	-0.1800%	0.1800%	
15 D(V/V)	100	100	100.01	100.01	0	0.000%	0.00%	0.0100%	0.01%	0.0100%	0.0100%	
16 D(V/V)	100	100	100.07	100.01	0.06	0.060%	0.06%	0.0100%	0.01%	0.0700%	0.0700%	
1 D(V/V)	50	50	49.51	49.98	-0.47	-0.940%	0.94%	-0.0200%	0.04%	-0.9800%	0.9800%	
2 D(V/V)	50	50	50.22	49.98	0.24	0.480%	0.48%	-0.0200%	0.04%	0.4400%	0.4400%	
3 D(V/V)	50	50	50.32	49.98	0.34	0.680%	0.68%	-0.0200%	0.04%	0.6400%	0.6400%	
4 D(V/V)	50	50	49.98	49.98	0.32	0.640%	0.64%	-0.0200%	0.04%	0.6000%	0.6000%	
5 D(V/V)	50	50	50.02	49.98	0.04	0.080%	0.08%	-0.0200%	0.04%	0.0400%	0.0400%	
6 D(V/V)	50	50	49.79	49.98	-0.19	-0.380%	0.38%	-0.0200%	0.04%	-0.4200%	0.4200%	
7 D(V/V)	50	50	50.33	49.98	0.35	0.700%	0.70%	-0.0200%	0.04%	0.6600%	0.6600%	
8 D(V/V)	50	50	50.56	49.98	0.58	1.160%	1.16%	-0.0200%	0.04%	1.1200%	1.1200%	
9 D(V/V)	50	50	50.0919	49.98	0.1119	0.223%	0.22%	-0.0200%	0.04%	0.183%	0.1838%	
10 D(V/V)	50	50	49.97	49.98	-0.01	-0.020%	0.02%	-0.0200%	0.04%	-0.0600%	0.0600%	
11 D(V/V)	50	50	49.86	49.98	-0.12	-0.240%	0.24%	-0.0200%	0.04%	-0.2800%	0.2800%	
12 D(V/V)	50	50	50.3179	49.98	0.3379	0.676%	0.68%	-0.0200%	0.04%	0.635%	0.6358%	
13 D(V/V)	50	50	50.66	49.98	0.68	1.360%	1.36%	-0.0200%	0.04%	1.320%	1.3200%	
14 D(V/V)	50	50	50.48	49.98	0.5	1.000%	1.00%	-0.0200%	0.04%	0.9600%	0.9600%	
15 D(V/V)	50	50	50.35	49.98	0.37	0.740%	0.74%	-0.0200%	0.04%	0.7000%	0.7000%	
16 D(V/V)	50	50	50.76	49.98	0.78	1.560%	1.56%	-0.0200%	0.04%	1.520%	1.5200%	
1 D(V/V)	25	25	25.219	24.97	0.249	0.997%	1.00%	-0.0200%	0.12%	0.876%	0.8760%	
2 D(V/V)	25	25	25.34	24.97	0.37	1.481%	1.48%	-0.0200%	0.12%	1.360%	1.3600%	
3 D(V/V)	25	25	25.48	24.97	0.51	2.042%	2.04%	-0.0200%	0.12%	1.920%	1.9200%	
4 D(V/V)	25	25	25.16	24.97	0.19	0.760%	0.76%	-0.0200%	0.12%	0.640%	0.6400%	
5 D(V/V)	25	25	25.06	24.97	0.09	0.360%	0.36%	-0.0200%	0.12%	0.240%	0.2400%	
6 D(V/V)	25	25	25.1071	24.97	0.1371	0.549%	0.55%	-0.0200%	0.12%	0.428%	0.4280%	
7 D(V/V)	25	25	25.2156	24.97	0.2456	0.989%	0.98%	-0.0200%	0.12%	0.862%	0.8620%	
8 D(V/V)	25	25	25.47	24.97	0.5	2.002%	2.00%	-0.0200%	0.12%	1.880%	1.8800%	
9 D(V/V)	25	25	24.57	24.97	-0.4	-1.609%	1.60%	-0.0200%	0.12%	-1.720%	1.7200%	
10 D(V/V)	25	25	24.52	24.97	-0.45	-1.802%	1.80%	-0.0200%	0.12%	-1.920%	1.9200%	
11 D(V/V)	25	25	24.6	24.97	-0.37	-1.480%	1.48%	-0.0200%	0.12%	-1.600%	1.6000%	
12 D(V/V)	25	25	24.5	24.97	-0.47	-1.880%	1.88%	-0.0200%	0.12%	-2.000%	2.0000%	
13 D(V/V)	25	25	25.02	24.97	0.05	0.200%	0.20%	-0.0200%	0.12%	0.080%	0.0800%	
14 D(V/V)	25	25	25.11	24.97	0.14	0.560%	0.56%	-0.0200%	0.12%	0.440%	0.4400%	
15 D(V/V)	25	25	24.86	24.97	-0.11	-0.440%	0.44%	-0.0200%	0.12%	-0.560%	0.5600%	
16 D(V/V)	25	25	25.19	24.97	0.22	0.881%	0.88%	-0.0200%	0.12%	0.760%	0.7600%	

Appendix F MATLAB scripts

Import Script:

```
%The purpose of this script is to import.xlsx files to matlab
clear;
close all;

%absolute path on the local computer to the folder containing the files to
%import and their names.
Path = "C:\Users\rando\Dalhousie University\RESL Jaza Batt Chg Mdl -
General\David Thesis\RawData\PS_NCA";
FileNames = ["DT_PS_NCR18650B_P2_T30_Deg_1S_3P";
              "DT_PS_NCR18650B_P2_T31_RPT_1S_3P";
              "DT_PS_NCR18650B_P2_T32_Deg_1S_3P"];
              "DT_PS_NCR18650B_P2_T33_VRvsSOC_1S_3P"];

i=0;
while(i < size(FileNames,1))
    %increment cycle count
    i=i+1;
    % Full path for file indexed i
    FullPath = Path + "\" + FileNames(i,1);

    %headers and variable types of each column
    Names =
    ["DateTime","Test_Times","Cycle_Index","Step_Index","Step_Times","CurrentA","V
oltageV","PowerW","Discharge_CapacityAh","Charge_CapacityAh","Discharge_Energy
Wh","Charge_EnergyWh","AuxTemp1C","AuxTemp2C"];
    VarTypes =
    ["datetime","double","double","double","double","double","double","double","do
uble","double","double","double","double","double"];
    %making the spreadsheet the table t
    opts =
    spreadsheetImportOptions('VariableNames',Names,'Sheet','Data','VariableTypes',
    VarTypes,'DataRange','A:N','ImportErrorRule','omitrow');
    t = readtable(FullPath,opts);

    %Saving each of the columns individually, this could probably be done
    %better but it works
    clearvars -except t Path FileNames i ;
    DateTime = t.DateTime;
    Test_Times = t.Test_Times;
    Cycle_Index = t.Cycle_Index;
    Step_Index = t.Step_Index;
    Step_Times = t.Step_Times;
    CurrentA = t.CurrentA;
    VoltageV = t.VoltageV;
    PowerW = t.PowerW;
    Discharge_CapacityAh = t.Discharge_CapacityAh;
    Charge_CapacityAh = t.Charge_CapacityAh;
    Discharge_EnergyWh = t.Discharge_EnergyWh;
```

```

Charge_EnergyWh = t.Charge_EnergyWh;
AuxTemp1C = t.AuxTemp1C;
AuxTemp2C = t.AuxTemp2C;

clearvars t;
%Saving it in the local directory with the same name
save(FileNames(i,1)+".mat", '-mat');
%setting up for next loop
clearvars -except Path FileNames i ;

end

Data Slicer script:

%The purpose of this script is to separate VR periods into individual
%datafiles
clear all;
close all;
%Input from operator
DataFile = "DT_PS_NCR18650B_P2_T24_VRvsSOC_1S_3P";
load (DataFile);
% loop variables
i=0;
loopsz = size(Cycle_Index,1);

restCount = zeros(25,1); % how many datapoints are in a rest
restIndex = []; % value of those data points

RN = 0; % Number of rests that have occurred

%Getting each rest and the data index that they occur at
while(i< loopsz)
    i=i+1;
    if((Step_Index(i,1) == 14) || (Step_Index(i,1) == 15))
        if (Step_Index(i-1,1) == 13)
            %updating rest number
            RN = RN+1;
        end
        restCount(RN,1) = restCount(RN,1)+1;
        restIndex(restCount(RN,1),RN) = i;
    end
end

%Altering Loop variables for next loop
i = 0;
loopsz = RN;

%Populating the rest variables and saving them
while (i < loopsz)
    %Iterating for each rest
    i = i + 1;
    j = 0;

```

```

    %Creating a value table based off how many data points there are
    size = restCount(i,1);
    ValueTable = zeros(size,2);

    %Populating the Value Table
    while(j < size)
        j=j+1;
        %Voltage at index
        ValueTable(j,1) =abs(VoltageV(restIndex(j,i),1)-
VoltageV(restIndex(1,i),1));
        %Time at index
        ValueTable(j,2) = Test_Times(restIndex(j,i),1) -
Test_Times(restIndex(1,i),1);

    end
    %Ah Value for the rest
    ValueTable(1,3) = abs(Charge_CapacityAh(restIndex(j,i),1) /
Discharge_CapacityAh(restIndex(j,i),1));
    %Saving full data invloved with calcs
    save(DataFile + "_Rest_" + string(i))
end
%Cleaning up the Rest data files

%Only keeping the vars required for looping
clearvars -except DataFile RN;
i = 0;
loopsz = RN;

%Removing excess data from the .mat files
while (i<loopsz)
    i=i+1;
    load(DataFile + "_Rest_" + string(i))
    clearvars -except i loopsz DataFile ValueTable
    save(DataFile + "_Rest_" + string(i))
end

```

Curve Fitting script:

```

%The purpose of this script is to curve fit every VR period with a 4RC model
clear;
close all;

%-----Required Input from operator-----%
DataFile = "DT_PS_NCR18650B_P2_T24_VRvsSOC_1S_3P";
Type = "PS";
% initial values
x0 = [0, 0.03,1.35,0.02,17.5, 0.053,125,0.005,1000];
%-----%

%Selecting for Cap Variable
switch Type
    case "PS"
        capIndex = 1;
    case "LG"

```

```

        capIndex = 2;
    case "LW"
        capIndex = 3;
    end
%Cap Variable
% 1 -> PS; 2 -> LG; 3 -> LW
CapAh = [3.2*3; 2.6*3; 1.1*3];

>Loading first rest
load(DataFile+"_Rest_1");

%Function for curve fitting
fun = @(x,xdata) x(1) + x(2)*(1-exp(-(xdata/x(3)))) + x(4)*(1-exp(-(xdata/x(5)))) + x(6)*(1-exp(-(xdata/x(7))))+ x(8)*(1-exp(-(xdata/x(9))));

% bounds on the fitting
ub = [ 0.00000001, 0.1, 50, 0.07, 200, 0.05,1000, 0.100, 20000];
lb = [-0.00000001, 0, 0, 0, 0, 0, 0, 0, 0];
%initiate Vars
vars = [];

k = 0;

while (i <= loopsize) %loopsize is from the data file
load(DataFile + "_Rest_" + string(i));

[xa,ra] = lsqcurvefit(fun,x0,ValueTable(:,2),ValueTable(:,1),lb,ub);
%Not including the failure that occurs each test
    %Populating the vars
    vars(i+1-k,[1:9]) = xa;
    vars(i+1-k,(size(xa,2)+1)) = ra;
    vars(i+1-k,(size(xa,2)+2)) = ValueTable(1,3);
    %Showing the curve
    semilogx(ValueTable(:,2),fun(xa,ValueTable(:,2)));
    hold on;
    ylim([0,0.15]);
    i=i+1;
end

clearvars -except vars DataFile ub lb
save (DataFile+"_SimOut");

```

IR analysis Script:

```

% the purpose of this script is to analyse IR from a .mat file
clear all;
close all;
% For operations these are the only things that need to be changed.
FileName = "DT_LW_APR18650M1B_P2_T27_IR_1S_3P";
Type = "LW";
%-----
switch Type
case "PS"
    currIndex = 1;

```

```

        case "LG"
            currIndex = 2;
        case "LW"
            currIndex = 3;
    end
    load (FileName);
    %converting the seconds timeseries to hours
    Hours = Test_Times/3600;

    %loopvars
    loopsize = size(CurrentA,1);
    i = 0;
    b = 0;
    c = 0;

    %outputs initialization
    inits_Chg = [];
    finals_Chg = [];
    AhT_Chg = [];
    inits_Dis = [];
    finals_Dis = [];
    AhT_Dis = [];

    %Current Variable
    % 1 -> PS; 2 -> LG; 3 -> LW
    DeltaI = [2.4; 3.9; 1.65];

    %Getting correct data point for Delta V to calc IR
    while(i<loopsize)
        i = i + 1;
        %Discharge IR
        if(Step_Index(i,1) == 7 )
            % Delta V at start of pulse
            if( Step_Index(i-1,1) == 6 )
                b = b + 1;
                inits_Dis(b,1) = VoltageV(i-1,1);
                % Delta V at end of pulse
            end
            finals_Dis(b,1) = VoltageV(i,1);
            AhT_Dis(b,1) = abs(Discharge_CapacityAh(i,1) -
            Charge_CapacityAh(i,1));

            %Charge IR
        elseif(Step_Index(i,1) == 10)
            % Delta V at start of pulse
            if( Step_Index(i-1,1) == 9 )
                c = c + 1;
                inits_Chg(c,1) = VoltageV(i-1,1);
                % Delta V at end of pulse
            end
            finals_Chg(c,1) = VoltageV(i,1);
            AhT_Chg(c,1) = abs(Discharge_CapacityAh(i,1) -
            Charge_CapacityAh(i,1));
        end
    end

```

```

    end
end

%Calcs
deltaV_Dis = abs(inits_Dis - finals_Dis);
deltaV_Chg = abs(inits_Chg - finals_Chg);

SoC_Dis = 1 - (AhT_Dis ./ abs(max(Discharge_CapacityAh)));
SoC_Chg = 1 - (AhT_Chg ./ abs(max(Discharge_CapacityAh)));

% Delta V / Delta I = mOhms
R_Dis = 1000* deltaV_Dis/DeltaI(currIndex,1); %currIndex is dependant on the
type variable
R_Chg = 1000* deltaV_Chg/DeltaI(currIndex,1);

%Showing Results
plot(SoC_Chg,R_Chg);
hold on;
plot(SoC_Dis,R_Dis);

xlim([0,1]);
xlabel("State of Charge");
ylabel("Resistance (m\Omega) ");

clearvars -except FileName R_Chg R_Dis SoC_Chg SoC_Dis;
save(FileName + "_RESULTS")

```